Multi-Constellation Satellite Navigation: Precise Orbit Determination and Point Positioning

Satellittnavigasjon med flere systemer: Beregning av presise baner og nøyaktig punktbestemmelse

Philosophiae Doctor (PhD) Thesis

Javier Tegedor

Department of Mathematical Sciences and Technology (IMT)

Norwegian University of Life Sciences (NMBU)

Ås (2015)

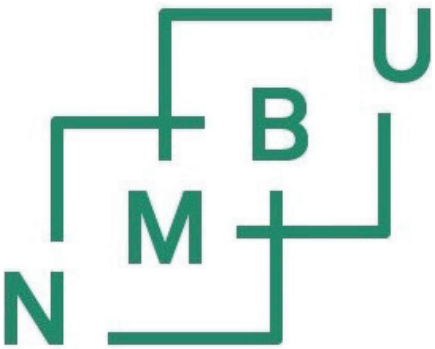

Thesis number 2015:24
ISSN 1894-6402
ISBN 978-82-575-1276-7

Multi-Constellation Satellite Navigation: Precise Orbit Determination and Point Positioning
Philosophiae Doctor (PhD) Thesis, 2015
Javier Tegedor
Department of Mathematical Sciences and Technology (IMT)
Norwegian University of Life Sciences (NMBU), Ås (Norway)

Supervisors
Prof. Dr. Ola Øvstedal
Department of Mathematical Sciences and Technology (IMT)
Norwegian University of Life Sciences (NMBU), Ås (Norway)

Erik Vigen
Fugro Satellite Positioning AS, Oslo (Norway)

Evaluation Committee
Prof. Dr-Ing. Matthias Becker
Institute for Physical Geodesy (PSGD)
Technical University Darmstadt (Germany)

Prof. Dr. Anna Jensen
KTH Royal Institute of Technology, Stockholm (Sweden)

Prof. Dr. Jon Glenn Gjevestad
Department of Mathematical Sciences and Technology (IMT)
Norwegian University of Life Sciences (NMBU), Ås (Norway)

To observe without thinking is as dangerous as to think without observing.

Santiago Ramón y Cajal

Executive Summary

Satellite positioning is evolving rapidly. Thanks to the deployment of new Global Navigation Satellite Systems (GNSS), such as Galileo or BeiDou, as well as the modernization programmes for the traditional systems, such as GPS and Glonass, navigation users can use today as many satellites and signals as never before. Satellite navigation is therefore evolving from dual-frequency GPS and Glonass to a multi-frequency multi-GNSS scenario. The optimal use of all new signals and systems for precise geodetic applications is an on-going research task.

In particular, this thesis focuses on the Precise Point Positioning (PPP) technique, which makes use of precise satellite orbits and clocks for GNSS satellites to obtain centimeter-level absolute positioning. Thanks to the precise products delivered by the International GNSS Service (IGS), the technique has been widely used since its introduction in the late nineties, initially for GPS and later also for Glonass.

In the context of GNSS modernization, the existing products need to be enhanced in order to serve multi-frequency PPP. Regarding the newest GPS L5 signal, this thesis describes the limitations of the current clock products based on GPS L1/L2, which cannot be directly applied to PPP using GPS L5, due to the existence of frequency dependent clock differences.

For the new constellations Galileo and BeiDou, precise orbits and clocks need to be generated before the new systems can be combined in PPP estimation. This thesis presents orbit estimation results making use of the initial tracking data for the new systems. The limits on orbit accuracy for the new systems are described, as well as the contribution of multi-GNSS to the PPP technique. The positioning performance results are promising, but the contribution to PPP accuracy is somehow reduced due to the existing model limitations for Galileo and BeiDou, that need further improvement until they can reach the accuracy level achieved today by GPS and Glonass. Additionally, BeiDou-standalone PPP results have been presented during this research, both real-time and post-processed.

On the other hand, previous studies have shown the feasibility of achieving carrier-phase integer ambiguity resolution in GPS-based PPP, thanks to the estimation of Uncalibrated Hardware Delays (UHDs). The same concept can be applied to new systems, provided the method is adapted to the new signals. This thesis includes an study on ambiguity-fixing for Galileo in PPP, making use of the first four In-Orbit Validation (IOV) satellites.

Finally, the above concepts developed for multi-constellation positioning have been tested in a dynamic positioning test, where two multi-GNSS receivers were installed on board a vessel navigating in Oslo fjord, in Norway. Using this setup, multi-GNSS ambiguity-fixed PPP has been demonstrated in a representative field experiment, and the performance of multi-constellation ambiguity-fixed PPP has been compared to RTK.

In summary, this thesis presents the first results on the evolution from ambiguity-float GPS and Glonass PPP to multi-constellation ambiguity-fixed positioning.

Contents

1 Introduction

Contents

1.1 Principles of satellite navigation

When the first GPS satellite was launched in 1978, it could not be envisaged the impact that satellite navigation has today in our lives. Although GPS was originally designed for military purposes, the civil applications of the system have largely exceeded the original expectations. Location-based services have been continuously growing for the benefit of the overall society. The position delivered by satellite navigation is used in many fields, such as transport systems, civil aviation, precision farming or surveying, just to mention a few. Satellite navigation also gives access to high-accuracy time synchronization which is used in telecommunications or banking applications, for example.

Satellite navigation has been recognized as an strategic asset for national governments and, as a consequence, several Global Navigation Satellite Systems (GNSS) have been developed in the last decades. In addition to the American Global Positioning System (GPS), Russia has developed Glonass, Europe is in the process of deploying Galileo, and China is building the BeiDou system. In addition, there are a number of regional navigation systems, such as the Japanese Quasi Zenit Satellite System (QZSS) or the Indian Regional Navigation Satellite System (IRNSS). As a result of this process, satellite navigation users can use nowadays as many satellites as never before for Position, Navigation and Timing (PNT) applications.

Satellite navigation is based on the principle of trilateration. Time-stamped signals are sent from the GNSS satellites to the ground. The user receiver measures the time of arrival of the signals, and therefore gets an approximate measurement of the distance to each satellite (pseudorange). Satellites are also transmitting their position (orbital parameters) and clock synchronization errors, in so-called *broadcast ephemeris*. A detailed analysis of broadcast ephemeris errors for multiple navigation systems is described in [Warren and Raquet, 2003]. With this information, the receiver can estimate its own position and its local clock synchronization error. Therefore, for three-dimensional positioning, a minimum of four satellites available are needed.

The standard accuracy delivered by standalone GNSS is insufficient for the most demanding applications. As an example, typical accuracy delivered by GPS for single-frequency users is 9 meters horizontally, and 15 meters vertically (95%), [GPS Directorate, 2008]. The user position accuracy depends heavily on the quality of the broadcast ephemeris, the disturbances impacting the signal between transmission and reception, such as atmospheric delays, as well as local effects, such as multipath, interferences or line of sight obstructions.

A number of solutions have been developed to enhance GNSS positional accuracy for different applications. Satellite-Based Augmentation Systems (SBAS) have been implemented to support civil aviation, which not only requires higher accuracy but also integrity, a boundary to the user position error. SBAS achieve better accuracy making use of additional orbit and clock corrections and an enhanced ionosphere model, allowing meter level accuracy for single-frequency users. Examples of SBAS systems are US WAAS (Wide-Area Augmentation System) or the European EGNOS (European Geostationary Overlay System).

An alternative is to exploit the temporal and spatial correlations of GNSS errors. This is the fundamental idea behind Differential GNSS (DGNSS), which makes use of reference stations at known locations to compute corrections for mobile users. Using a data link, reference stations send observation data (pseudorange measurements) to the mobile users on the field. Under the assumption of very similar errors between the reference and mobile receivers, the latter can compensate most of the errors (orbit/clock errors, atmospheric delays, etc). This typically leads to a position accuracy around meter level, which is bounded by the precision of the pseudorange measurements and the presence of uncorrelated errors, such as multipath. As an example, the Nationwide Differential GPS (NDGPS) is the US differential GPS service, operated by the US Coast Guard since 1999.

A further evolution towards higher accuracy is represented by Real-Time Kinematic (RTK) services. The principle is the same as DGNSS, but RTK exploits the precision of carrier-phase measurements. In addition to the removal of correlated errors as DGNSS, the resolution of the so-called carrier-phase integer ambiguity, i.e. the number of carrier-phase cycles between receiver and satellite, allows to obtain centimeter-level accuracy in real-time. Corrections can be derived from a single reference station (single-site RTK), or from a combination of them (Network-RTK), increasing robustness and accuracy [Vollath et al., 2002]. The method works as long as the distance between mobile and reference receivers (baseline) is small (few tenths of kilometers). As a result, RTK networks tend to require a high density of reference stations. As an example, the RTK network of the Satellite Positioning Service of the German *Landesvermessung* (SAPOS) consists of about 270 reference stations distributed in Germany. The extensive infrastructure needed is one of the main drawbacks of the RTK technique, as well as the dependence to a nearby reference station, which imposes limitations for certain applications. For example, offshore maritime positioning cannot rely on RTK due to lack of reference stations far away from the coastline.

A cost-effective alternative to RTK is the Precise Point Positioning (PPP) tecnique, which delivers absolute positioning. The method is based on the estimation of precise orbits and clocks for GNSS satellites, as well as the accurate modeling or estimation of remaining effects impacting user position, such as tropospheric/ionospheric delays, ocean and solid tides, ocean loading, phase wind-up, etc. Similar to RTK, PPP also exploits the precision of

carrier-phase measurements. However, the main advantage of PPP is that orbits and clocks can be accurately estimated for all GNSS satellites using a relatively small network. A global station network between 40 and 60 stations is sufficient to estimate orbits and clock errors with less than 10 centimeters accuracy in real-time. One of the main advantages of PPP is the provision of homogeneous worldwide coverage independent of the distance to the reference stations that were used for computing the orbit and clock solution.

The International GNSS Service (IGS) is generating precise orbits and clock products routinely, that can be used for PPP. IGS is maintaining a global tracking network and coordinating several contributing Analysis Centers (AC). Using different processing strategies and software packages, each AC generates an independent solution. The solutions for all ACs are then combined by the Analysis Center Coordinator (ACC) to generate the official IGS products, that are made publicly available via Internet. There are several types of orbits and clock products with different accuracies and timeliness characteristics, summarized in table 1.1. As can be observed in figure 1.1, the quality of the products has continuously increased over the last 20 years, thanks to the improvement in the models involved in satellite geodesy. Nowadays, IGS products represent the highest level of accuracy available. PPP users can make use of these orbit and clock products to estimate receiver position accuracy at sub-centimeter level for static applications. IGS does not only generate routinely orbit and clocks, but also other GNSS-derived products, such as Earth Rotation Parameters (ERPs), ionospheric maps or calibrated signal biases. A complete guide of the usage of IGS products for PPP can be found in [Kouba, 2009].

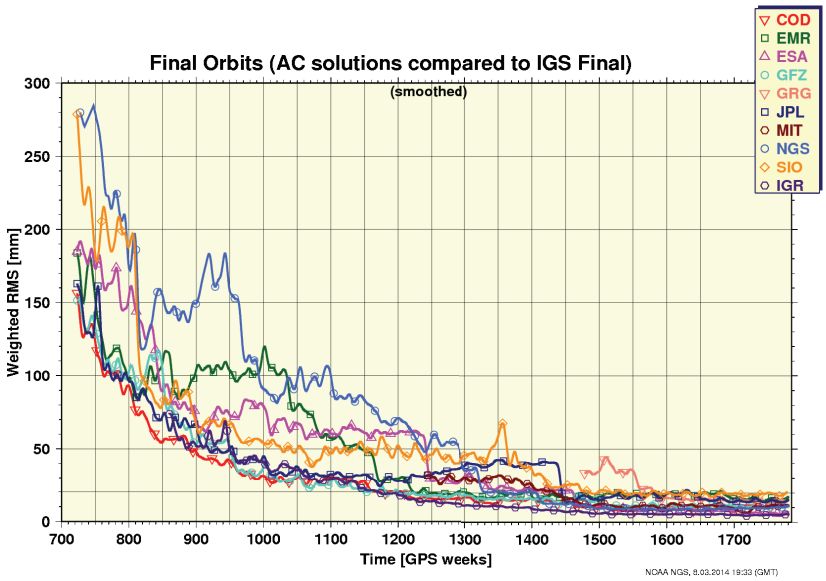

Fig. 1.1: Evolution of the quality of IGS Final Orbit products. Time span is 1993-2014. Source: www.igs.org

Additionally, there are several online PPP services available, where users can upload GNSS data collected from mobile receivers and a post-processed PPP solution is computed. Some examples of PPP services and their main characteristics are listed in table 1.2.

Product Type	Constellations	Orbit Accuracy	Clock Accuracy	Latency	Update rate
Real-time	GPS	5cm	70ps	real-time	real-time
Ultra-Rapid (predicted)	GPS/Glonass[1]	5cm	2.5ns	realtime	Every 6 hours
Ultra-Rapid (observed)	GPS/Glonass[1]	3cm	50ps	3-9 hours	Every 6 hours
Rapid	GPS	2.5cm	25ps	17-41 hours	Daily
Final	GPS/Glonass[2]	2.5cm	20ps	12-28 days	Weekly

[1] The Glonass Ultra-Rapid product is experimental.
[2] There is no combined clock product for Glonass, only orbits are combined.

Tab. 1.1: Summary of IGS orbit and clock products delivered by IGS. Accuracies are approximate.

Name	Organisation	URL	Characteristics
CSRS-PPP	Natural Resources Canada (NRCan)	http://www.geod.nrcan.gc.ca/service_e.php	Single+Dual frequency GPS+Glonass Static+Kinematic
GPS Analysis and Positioning Software (GAPS)	University of New Brunswick (UNB)	http://gaps.gge.unb.ca	Dual-frequency GPS Static+Kinematic
Automatic Precise Point Positioning Service (APPS)	Jet Propulsion Laboratory (JPL)	http://apps.gdgps.net	Single+Dual frequency GPS Static+Kinematic
magicGNSS	GMV	http://magicgnss.gmv.com/ppp	Dual-frequency GPS+Glonass Static+Kinematic

Tab. 1.2: Summary of online PPP services available.

PPP has also drawn the attention of commercial service providers for professional applications. Generally, orbit and clock corrections are computed in real-time using a proprietary reference station network, and sent to the users in the field via a data link (either using geostationary satellites or an Internet connection). As an example, Fugro's G2 [Melgard et al., 2010], Veripos' APEX [Rocken et al., 2011] or C&C's C-NAV [Wert et al., 2004] offer decimeter-level accuracy for maritime applications, all of them using GPS and Glonass. Similar services exists for land applications, such as Trimble's RTX [Chen et al., 2011], Terrastar-D or Navcom's Starfire [Hatch et al., 2006].

Typical PPP accuracies in real-time are at decimeter-level when carrier-phase ambiguities are not resolved to their integer values, known as *float PPP*. Recent research has demonstrated the feasibility of resolving integer carrier-phase ambiguities in PPP (*fixed PPP*), bringing the accuracy closer to RTK, as explained in detail in [Rizos et al., 2012]. Ambiguity-fixed PPP solutions are typically known as PPP-RTK or PPP-AR (PPP with Ambiguity Resolution), and represent the state-of-the-art absolute positioning using GNSS.

1.2 Motivation of the research

As described in the previous section, the popularity of PPP has steadily increased since its introduction in the late 1990s. When this research started in 2011, state-of-the-art PPP was mainly based on dual-frequency processing of GPS and Glonass observations, for which accurate orbit/clock estimates were readily available from IGS.

However, the GNSS landscape is evolving rapidly, with the deployment of new systems, such as Galileo and BeiDou, and the modernization of the current systems GPS and Glonass, which are including new signals and frequencies for the benefit of navigation users.

Following this GNSS modernization, the future of positioning will be based on multi-frequency and multi-constellation PPP. Multi-constellation positioning is attractive in order to obtain higher level of accuracy and availability, particularly under marginal satellite visibility conditions. Additionaly, the usage of multiple satellite systems increases robustness and reliability and protects the user agains single-system failures.

However, there are a number of challenges to address before the benefits of multi-GNSS can be fully achieved. The research presented in this dissertation has been driven by the usage of new systems and signals in precise point positioning. In particular the following topics have been covered:

- Extension of dual-frequency GPS PPP to triple-frequency PPP
- Precise orbit and clock estimation for Galileo and BeiDou
- Contribution of Galileo and BeiDou to PPP performance
- Real-time and post-processed PPP using BeiDou standalone, and in combination with GPS
- Multi-constellation ambiguity resolution in PPP (PPP-AR)
- Comparison of PPP-AR and RTK in a maritime environment

1.3 Outline of the thesis

This dissertation is divided in 10 chapters. Chapter 1 provides a general overview of status of GNSS positioning and describes the motivation for the research.

Chapter 2 gives an overview the current status of satellite navigation systems, focusing also on their modernization plans with the introduction of new frequencies and signals, that were used during the research.

Chapter 3 focuses on the theory of ambiguity-resolution for GNSS. PPP does not only benefit from the availability of more satellites and signals, but also on a more accurate modeling of the GNSS observables. Integer ambiguity resolution in PPP has been extensively studied in recent years, mainly for GPS, in order to increase positional accuracy. One of the problems of the existing literature on this topic is the usage of different observation equations and nomenclature by different authors. The aim of this chapter is to provide a comprehensive overview of the different methods, following a common notation, and putting special emphasis on the extension to other frequencies and systems.

The research results presented in this thesis have been published in a number of peer-reviewed scientific articles. These are reproduced in chapters 4 to 8.

In particular, chapter 4 addresses multi-frequency PPP. GPS IIF satellites were the first operational satellites transmitting more than two frequencies, with the new signals on L5, on top of the legacy on L1 and L2. However, the usage of the third frequency in PPP was found to be challenging, due to the existence of time-variant interfrequency-biases that were already described by other authors [Montenbruck et al., 2011]. The study presented in chapter 4 provides with a rigorous incorporation of L1/L5 ionosphere-free linear combination observables, on top of the traditional L1/L2 observables. Additionally, time-variant interfrequency-biases are handled by estimating a separate set of L1/L5 satellite clocks for the IIF satellites. The result of this work was published in *Survey Review* in 2013.

Regarding multi-GNSS PPP, new satellite systems can bring a significant contribution to precise positioning, thanks to increased availability and accuracy. For example, BeiDou, the Chinese navigation system, has been significantly developed in last years. In 2013, an operational constellation of 14 satellites allowed to obtain standalone positioning in China and neighboring regions. The usage of BeiDou in standalone Precise Point Positioning in real-time was demonstrated in the study presented in chapter 5. For the first time, real-time precise orbit, clock and positioning results for BeiDou were presented. The study includes a validation versus post-processed solutions, both for the orbit and the PPP estimates. This work was presented in the International Association of Geodesy (IAG) Scientific Assembly in July 2013, and accepted for publication in the *IAG Symposia Series* as peer-reviewed paper.

Multi-constellation PPP will become a reality once the new systems, such as Galileo and BeiDou, are fully deployed. However, we can already anticipate today the contribution of the new systems on top of the legacy GPS/Glonass solutions, using the initial satellites available. In particular, chapter 6 presents orbit estimation results for the new systems, and their contribution to PPP accuracy and availability. It is of particular interest the analysis of intersystem biases that need to be taken into account for the integration of all GNSS systems. The outcome of this research was published in the *Journal of Geodetic Science* in 2014.

Ambiguity-resolution in PPP has become increasing popular in scientific studies, as a successful method in increasing the accuracy in GPS-based PPP. It is challenging to apply the same approach to Glonass, due to the existence of frequency-dependent biases, but the approach can be also used to other systems such as Galileo and BeiDou. In particular, chapter 7 presents the work done to apply the method to Galileo. This study was presented in the *International Technical Meeting of the Institute of Navigation (ION GNSS 2014)*, and accepted

after peer-review process for publication in the conference proceedings. The paper has been invited for publication in *Navigation*, and is under peer-review process at the time of writing this thesis.

Finally, ambiguity-fixed multi-GNSS positioning has been demonstrated in the maritime environment. A ferry navigating on the Oslo fjord has been equipped with state-of-the-art GNSS receivers and antennas, in order to assess ambiguity-fixed multi-constellation PPP in a truly dynamic environment. A comparison between PPP-AR and RTK accuracies is presented. The paper has been accepted for publication in the *Journal of Applied Geodesy*.

Conclusions of the research are described in chapter 9.

Chapter 10 contains a list of non peer-review publications, oral presentations and conference posters that have been produced during the PhD programme.

2 Current Status of Satellite Navigation Systems

Contents

2.1 Scope

Global Navigation Satellite System (GNSS) have constantly developed since the launch of the first GPS satellite in the late 1970s. Currently, the navigation landscape is changing dramatically, and new global and regional systems are being deployed for the benefit of navigation users. In this chapter, we look at how GNSS history has developed during the last decades and we describe the current status of global positioning systems, such as GPS, Glonass, Galileo and BeiDou, whose main characteristics are summarized in 2.1. Regional (QZSS and IRNSS) and augmentation systems (WAAS, EGNOS, etc) will also be described for completeness.

	GPS	**GLONASS**	**Galileo**	**BeiDou**
Constellation Type	MEO	MEO	MEO	MEO / IGSO / GEO
Number of satellites (nominal)	27	24	30	27 / 3 / 5
Satellite Altitude (km)	20180	19130	23220	21150 / 36000 / 36000
Orbital Period (hours)	11.97	11.26	14.08	12.63/24/24

Tab. 2.1: Main characteristics of Global Navigation Satellite Systems (GNSS), when fully deployed.

2.2 Global Navigation Systems

2.2.1 GPS

Originally known as Navigation System Using Timing And Ranging (NAVSTAR), the American Global Positioning System (GPS) was the first satellite navigation system available. Its origins date back to 1973, when the US Military took the decision to develop a new positioning system based on its predecessors, *Transit* and *Timation*. The first satellite (GPS-I) was launched in 1978, and the system steadily grew till it reached Full Operational Capability (FOC), declared on July 17th, 1995.

The space segment is composed of a nominal 24 satellite constellation, which was expanded in 2011 to a 27 satellite constellation. Satellites are deployed in six orbital planes. Typically, the US Air Force, in charge of the system operation, keeps a constellation of up to 32 operational satellites, in order to increase redundancy and availability.

(a) GPS IIF

(b) GPS III

Fig. 2.1: GPS satellites (source: US Air Force).

GPS offers two kind of positioning services. The Standard Positioning Service (SPS) is based on the C/A (Coarse/Acquisition) code that is transmitted on the L1 carrier frequency (1575.42 MHz) [GPS Directorate, 2008], while the Precise Positioning Service (PPS) is based on the P-code which is transmitted in both L1 and L2 carriers (1276.42 MHz) frequencies [GPS Directorate, 2007]. The P code can be encrypted in order to allow access to authorized users only. The encrypted P code is known as the P(Y) code.

The constellation is made of several generation (blocks) of satellites, which are summarized in table 2.2. The evolution of the constellation over time is depicted in figure 2.2. Block II was the first generation of operational satellites, launched in 1989-1990. Block IIA (*advanced*) followed with 19 additional satellites (1990-1997). Although Block-IIA satellites were designed with a 7.5 years life-span, there are still 5 operational satellites from this generation in 2014. Block IIR (*replenishment*) (1997-2004, 12 satellites) included additional on-board clock monitoring. Block IIR-M (*modernized*) satellites (2005-2009, 8 satellites) included for the first time an additional civil signal (L2C) in the L2 carrier frequency, together with two military M-code signals with enhanced jamming resistance (flexible power). One satellite of this generation (SVN-49) included the first experimental payload on the L5

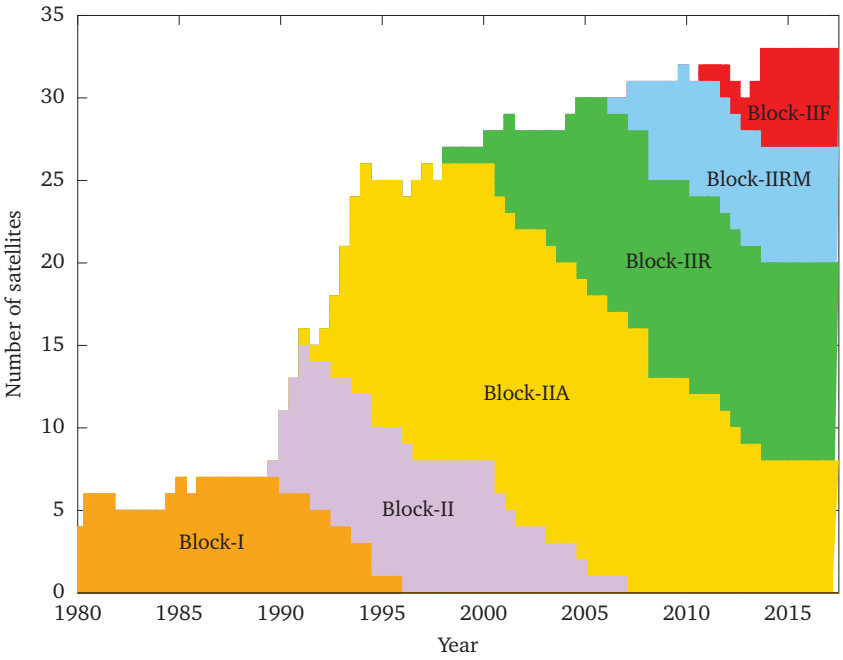

Fig. 2.2: Evolution of GPS constellation.

(1176.45 MHz) carrier, which introduced an undesired anomaly on the operational L1/L2 signals [Springer and Dilssner, 2009], and was never declared healthy.

At the time of writing, the IIF (*follow-on*) block is being deployed. This generation includes the operational version of the new civil signal in L5 carrier (1175.45 MHz) [GPS Directorate, 2011a]. Block IIF satellites deliver improved navigation accuracy thanks to enhanced Rubidium atomic clocks [Dupuis et al., 2008]. 12 IIF satellites have been manufactured, 8 of them were launched till December 2014.

The new generation of satellites (GPS-III) will provide additional signal accuracy and integrity, including a new civil signal in the L1 carrier (L1C) [GPS Directorate, 2012], designed to improve compatibility with Galileo signals. The satellites will also carry a Laser Retroreflector Array (LRA) and a Search And Rescue (SAR) payload. The Next Generation Operational Control System (OCX) is being developed to be able to fully support and control the first signals that will be implemented in the frame of the GPS modernization programme [GPS Directorate, 2011a].

GPS has implemented a transmission scheme based on Code Division Multiple Access (CDMA), where all satellites transmit in the same carrier-frequency, and the signals can be distinguished by the receivers using different PRNs (Pseudo-Random Codes), which is unique per satellite.

Block	Launch Years	Satellites	L1 C/A	L1 P(Y)	L2 P(Y)	L2C	L5	L1C
I	1978-1985	10	✓	✓	✓			
II	1989-1990	9	✓	✓	✓			
IIA	1990-1997	19	✓	✓	✓			
IIR	1997-2004	12	✓	✓	✓			
IIR-M	2005-2009	8	✓	✓	✓	✓		
IIF	Since 2010	8*	✓	✓	✓	✓	✓	
III	Expected 2016	-	✓	✓	✓	✓	✓	✓

*Until December 2014

Tab. 2.2: GPS space segment characteristics (source: www.gps.gov).

The scientific use of GPS has brought important advances in the field of satellite geodesy, providing a better understanding of Earth dynamics, such as Earth rotation or plate motion [Herring, 1999], and it is an important contributor to the realization of International Terrestrial Reference Frame (ITRF) [Altamimi et al., 2011], in combination with other geodetic techniques, such as Very Large Baseline Interferometry (VLBI) or Doppler Orbitography and Radiopositioning Integrated by Satellite (DORIS). Other scientific applications of GPS are atmospheric sounding [Kursinski and Hajj, 1997], orbit determination of Low Earth Orbit (LEO) observation satellites [Montenbruck et al., 2005] or soil moisture estimation [Larson et al., 2008], just to mention a few.

2.2.2 Glonass

Glonass (GLObalnaya NAvigatsionnaya Sputnikovaya Sistema) is the satellite navigation system developed by the Soviet Union during the 1970s. The constellation is deployed in three orbital planes, with eight satellites per plane. The first generation of Glonass satellites were launched between 1985 and 1990, and the system was first declared operational in 1993, with 12 satellites in orbit, that was increased to a full constellation with the nominal 24 satellites in 1995. Due to financial difficulties, the constellation could not be properly maintained, and in 2001 there were only 6 operational satellites in orbit. At that point, a new Russian Federal programme was started aiming at restoring the full service. New Glonass-M (*modernized*) satellites were developed, with a lifespan of 7 years, and the first one put into orbit in 2001. The full constellation of 24 satellites was restored in 2010, as shown in figure2.4.

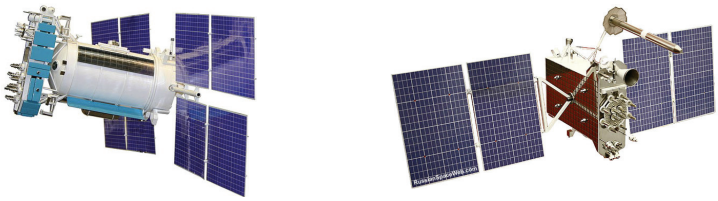

(a) Glonass-M **(b)** Glonass-K

Fig. 2.3: Glonass satellites (source: Anatoly Zak/ RussianSpaceWeb.com).

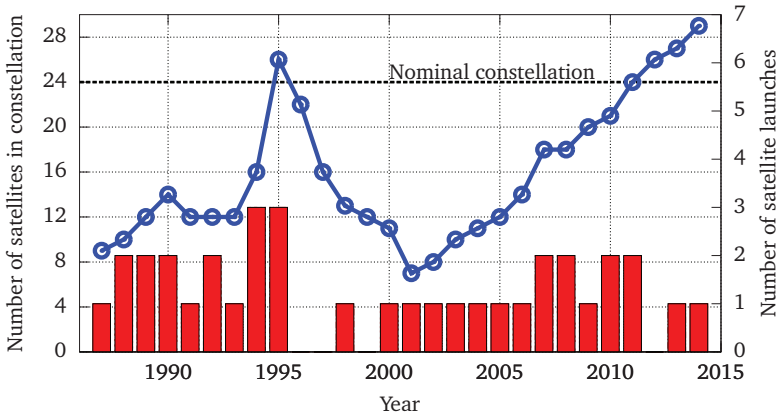

Fig. 2.4: Evolution of Glonass constellation.

The system is transmitting high- (HP) and standard (SP) precision signals, transmitting on L1 and L2 bands [Russian Institute of Space Device Engineering, 2008]. Contrary to GPS, Glonass has implemented the Frequency Division Multiple Access (FDMA) scheme, in which all satellites are transmitting the same PRN code, but in slightly different carrier frequencies for each satellite. The Glonass carrier-frequencies are:

$$f_1(n) = 1602 + n \cdot 0.5625 \ MHz \tag{2.1}$$

$$f_2(n) = 1246 + n \cdot 0.4375 \ MHz \tag{2.2}$$

where n is the channel number, that can vary from -7 to 6. In Glonass, two antipodal satellites use the same channel number in order to save radio frequency spectrum.

In a similar way to GPS, Glonass has also started a modernization programme, with the production of new generation satellites Glonass-K [Urlichich et al., 2011]. These new satellites have a longer lifespan of 10 years, include a Search And Rescue (SAR) payload, and include for the first time a CDMA signal on the L3 carrier (1202.25 MHz). Glonass is also planning to transmit a new signals also in the L5 carrier, same as GPS. The first Glonass-K1 was launched in February 2011, and the first CDMA signal was received in April 2011 [Willems and Sleewaegen, 2011]. The second Glonass-K1 satellite was launched in November 2014.

For precise geodetic applications, it has been demonstrated that the inclusion of Glonass on top of GPS improves positioning accuracy [Bruyninx, 2006] and reduces convergence time in kinematic applications [Li and Zhang, 2013]. Glonass also delivers better coverage at high latitudes, thanks to the higher orbit inclination, compared to GPS. As described in [Weber and Springer, 2001], this higher inclination has also benefits for the estimation of the Length of Day (LOD). Additionally, the fact that Glonass orbit period (11h 15 minutes) is shorter than for GPS, has the benefit that GPS+Glonass solutions avoid problems derived from the 2:1 resonance of the GPS orbital period with the gravity field, as the GPS orbital period is half sidereal day (11h 58 minutes).

2.2.3 Galileo

Galileo, the European satellite navigation system, is currently under development. The first two experimental GIOVE (Galileo In-Orbit Validation Element) satellites were launched in 2005 and 2008 (Giove-A and Giove-B, respectively), in order to test critical technologies for the later deployment of the system. In particular, signal generation modules, initial ground infrastructure and the on-board atomic clocks, such as the Rubidium Atomic Frequency Standard (RAFS) and the Passive Hydrogen Maser (PHM), were tested. A characterization of the clocks on-board Galileo satellites can be found in [Droz and Mosset, 2006]. Another innovation of Galileo is the introduction on an Alternate Binary Offset Carrier (AltBOC) signal, which is attractive thanks to its large bandwidth, that delivers smaller psedurorange noise than other GNSS signals. As an example, the benefits of the usage of the AltBOC signal for single-frequency positioning were presented in [Diessongo et al., 2012].

The first two In Orbit Validation (IOV) satellites were launched in October 2011, followed by two more in October 2012. The first Galileo-only position fix using these four satellites was achieved in March 2013, where the initial broadcast ephemeris in all four satellites were transmitted simultaneously.

In August 2014, the first two Full Operational Capability (FOC) were launched, but an anomaly in the Soyuz-upper stage caused the satellites to be delivered to a non-nominal orbit, with an inclination of 49.8 degrees (instead of the nominal 56 degrees) and an eccentricity of 0.23 (instead of 0 for circular orbits). In November 2014, the perigee of the FOC-1 satellite was raised, resulting in an orbit with an eccentricity of 0.15. This is illustrated in figure 2.5. At the time of writing this thesis, it is unclear whether these satellite will be part of the final operational constellation. Two additional FOC satellites were launched in March 2015, and are under commissioning at the time of writing this thesis.

Galileo Early Services are expected to start in 2015, and the Full Operational Capability is scheduled for 2020.

Galileo is offering different types of services. On top of the freely available Open Service (OS), the Public Regulated Service (PRS) has been designed for protected users with stringent requirements on accuracy, integrity and continuity. Additionally, Galileo will provide a Commercial Service (CS), which includes a data channel for the provision of additional information, such as corrections for high accuracy or integrity.

Galileo has implemented a CDMA frequency scheme, including open-signals in E1 and E5 band [European Commision, 2010] and the commercial-service signal in E6, as shown in figure 2.6. Galileo satellites are also equipped with a Search and Rescue payload [Lewandowski, 2008].

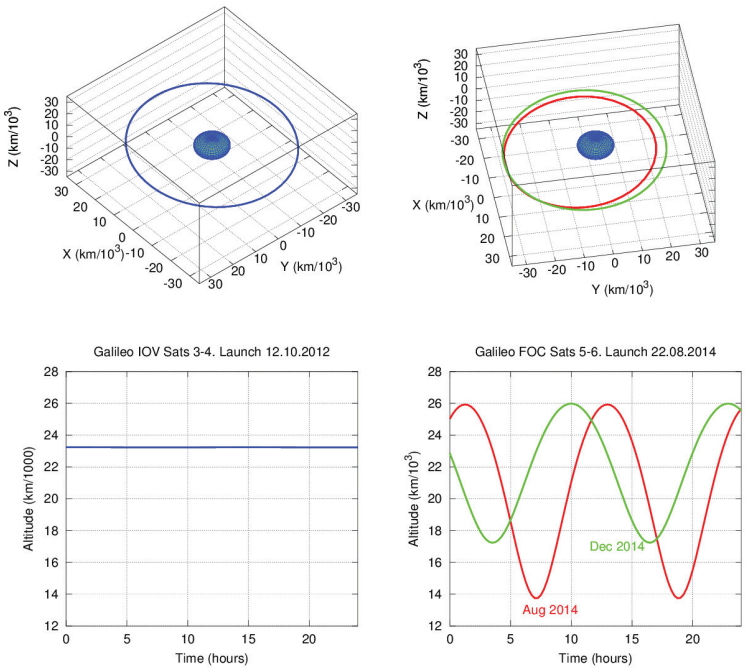

Fig. 2.5: Galileo orbits for IOV (left) and FOC-1/2 (right).

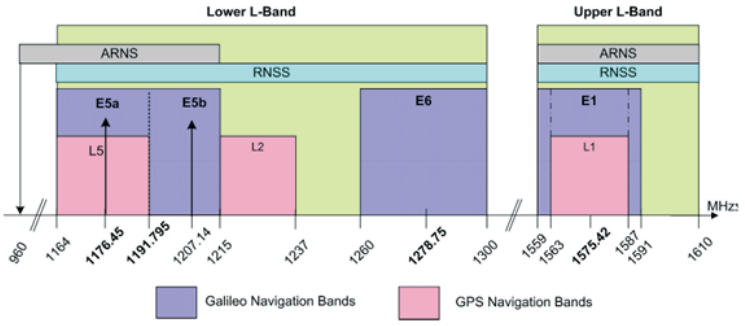

Fig. 2.6: Galileo signal plan [European Commision, 2010].

2.2.4 BeiDou

Also known as Compass, BeiDou is the Chinese contribution to GNSS. The satellite constellation is composed of Geostationary Orbit (GEO), Inclined Geosynchronous Orbit (IGSO) and Medium Earth Orbit (MEO) satellites. This constellation design has allowed the system to provide early positioning services around China, making use of a reduced initial GEO and IGSO constellation. At the time of writing, the system consists of 5 GEO satellites, 5

IGSO satellites and 4 MEO satellites. It is expected that the MEO constellation will be fully deployed by 2020, providing global coverage.

An Interface Control Document has been released, describing the signal in the B1 frequency at 1561.098 MHz [CSNO, 2012]. The system is also transmitting in the B2 and B3 carrier frequencies, at 1207.14 MHz and 1268.52 MHz respectively.

As a new navigation system, BeiDou has attracted scientific research in the last years. From the characterization and analysis of the new signals [Grelier, 2007, Wilde et al., 2007, Gao et al., 2009], to the first attempts of orbit determination using laser measurements. [Hauschild et al., 2011a]. The availability of GNSS tracking data has made possible the estimation of precise orbits, as presented in this dissertation in chapters 5 and 6. Similar analysis have been presented in parallel by different authors. In particular, [Steigenberger et al., 2013, Lou et al., 2014] presented an analysis of the orbit accuracies, using different orbit arc lengths and solar radiation pressure models. The usage of BeiDou in Precise Point Positioning has been also addressed in [He et al., 2013b].

BeiDou has been applied to relative positioning as well. For example, [Teunissen et al., 2013] and [He et al., 2013a] presented the benefits of adding BeiDou to GPS-based RTK. Additionally, phase-biases have been detected for BeiDou, which prevents fixing ambiguities in RTK positioning, when mixing GEO with IGSO/MEO satellites, in the case when two different receiver types are used. This has been studied in detail in [Nadarajah et al., 2014].

2.3 Regional Positioning Systems

2.3.1 QZSS

The Quasi Zenith Satellite System (QZSS) is a regional navigation system deployed by the Japanese Aerospace Exploration Agency (JAXA). QZSS is not an autonomous navigation system, but it is intended to enhance the civil service offered by GPS. QZSS is transmitting GPS-like signals as C/A L1, L1C, L2C and L5. The signal specification is fully described in QZSS Interface Control Document [JAXA, 2013]. Additionally, the system is delivering a L1-SAIF (Sub-meter Augmentation with Integrity Function) [Sakai et al., 2009] with additional correction data to enhance GPS-standalone positioning, in a SBAS-like system. Finally, the LEX (L-band Experimental) signal transmits a high data rate for performing real-time PPP.

QZSS is following Quasi Zenith Orbits (QZO), inclined excentric orbits with the apogee over Japan, so that the satellite is visible at high-elevation from that location an extended amount of time.

The first QZSS satellite (QZS-1) was launched in September-2010. Its ground track is depicted in figure 2.7. It is expected that the system will be followed by two more QZO satellites and a GEO satellite in the 2016-2017 timeframe.

A detailed assessment of signal characteristics and first orbit estimation for QZS-1 was presented in [Hauschild et al., 2011b]. One particularity of QZSS is the use of two different attitude modes, depending on the elevation of the Sun over the orbital plane, so-called the β angle. For $|\beta| > 20^o$, the satellite follows the nominal *yaw-steering* mode, similar to GPS and Glonass, steering the spacecraft around the nadir axis, in order to point the solar panels to the Sun, while keeping the L-band antenna pointing towards the Earth. However, for $|\beta| < 20^o$, the satellite enters into so-called *orbit-normal* mode, where solar panels are kept perpendicular to the orbital plane [Inaba et al., 2009, Ishijima et al., 2009], in order to avoid high-rate yaw steering maneuvers, as further described by [Hauschild et al., 2012].

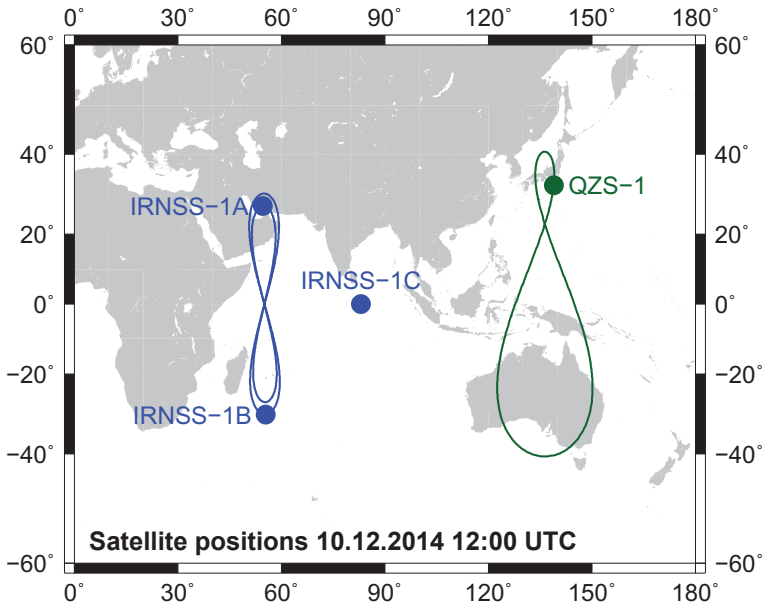

Fig. 2.7: Ground track for IRNSS 1A, 1B and 1C, and QZS-1 satellites.

2.3.2 IRNSS

The Indian Regional Navigation Satellite System (IRNSS) is being developed by the Indian Space Research Organisation (ISRO), for providing navigation services to India. The first satellite (IRNSS-1A) was launched in July 2013, followed by IRNSS-1B in April 2014, IRNSS-1C in October 2014 and IRNSS-1D in March 2015. [Thoelert et al., 2013] presented the signal characteristics in L5 (1176.45 MHz) and S-band (2492.028 MHz), using a high gain antenna and advanced signal processing techniques. The Interface Control Document has been released in 2014 [ISRO, 2014], describing a final configuration of 3 GEO satellites and 4 IGSO satellites. The ground track for the current constellation is depicted in figure 2.7.

2.4 Satellite-based augmentation systems

Satellite-based augmentation systems (SBAS) have been developed in order to increase the accuracy of standard positioning systems, by delivering additional information via geostationary satellites, such as orbit/clock corrections and ionospheric-information. Using SBAS, single-frequency users can compensate the ionospheric-delay and obtain higher accuracy (typically around meter-level) [Oliveira and Tiberius, 2008].

Additionally, SBAS systems have been designed to provide integrity monitoring, i.e. a boundary for the user position error and timely warnings when GNSS signals cannot be trusted for a given accuracy, which is critical for Safety-of-Life applications, such as civil aviation. Several SBAS systems have been developed in parallel, as the US Wide Area Augmentation System (WAAS), the European Geostationary Navigation Overlay System (EGNOS), the Japanese Multi-functional Satellite Augmentation System (MSAS), the Russian System for Differential Corrections and Monitoring (SDCM) or the Indian GPS Aided Geo-Augmented Navigation (GAGAN). A list of existing SBAS satellites is presented in table 2.3. The fact that SBAS corrections are transmitted as GPS-like signals can be exploited to use

System	Satellite	Launch date	Longitude	PRN	signals
WAAS	Inmarsat 4F3	Aug 18, 2008	98°W	133	L1/L5
	Galaxy 15	Oct 13, 2005	133 W	135	L1/L5
	Telesat Anik F1R	Sep 9, 2005	107.3 °W	138	L1/L5
EGNOS	Inmarsat 3F2 (AOR)	Sep 6,1996	15.5°W	120	L1
	Artemis	Jul 12, 2001	21.5°E	124	L1
	Inmarsat 3F5 (IOR-W)	Jan 22, 1998	25.0°E	126	L1
	SES-5	Jul 10, 2012	5 °E	136	L1/L5
MSAS	MTSAT-1R	Feb 26, 2002	140°E	129	L1
	MTSAT-2	Feb 18, 2006	145°E	129	L1
SCDM	Luch-5A	Dec 11, 2011	167°E	140	L1
	Luch-5B	Nov 2, 2012	16°W	125	L1
GAGAN	GSAT-8	May 20, 2011	55°E	127	L1/L5
	GSAT-10	Sep 28, 2012	83°E	128	L1/L5

Tab. 2.3: List of SBAS Geostationary satellites (source: http://igs.org/mgex/Status_SBAS.htm)

pseudorange and carrier-phase measurements for user positioning using the geostationary satellites (geo-ranging). Although this can be used to increase GNSS availability, one of the main difficulties is to compute with high-accuracy the orbit of the geostationary satellites, as attempted in [Beutler et al., 2005]. An alternative use of SBAS systems for PPP is to make use of the satellite orbit/clock corrections to correct ephemeris errors from other GNSS satellites. The initial results in this direction were presented in [Hesselbarth and Wanninger, 2012], where corrections from EGNOS, WAAS and MSAS were used to compute PPP solution using GPS observation data.

3 Ambiguity resolution strategies for Precise Point Positioning

Contents

3.1 Introduction

Geodetic GNSS receivers provide mainly two kind of observables for the GNSS satellites, namely pseudorange and carrier-phase. The Precise Point Positioning (PPP) technique is based on the accurate modeling of these observables and their corresponding errors, in order to obtain an accuracy of the receiver location from decimeter to centimeter level, depending on the type of application (real-time versus post-processed, kinematic versus static).

The carrier-phase measurements are of particular interest for precise applications due to their high precision. Observation noise for carrier-phase is at sub-centimeter level, whereas the noise of pseurorange observations is around meter level. Therefore, in parameter estimation for PPP, carrier-phase observations are given higher relative weight compared to pseudorange observations. However, phase measurements are biased by an arbitrary number of integer cycles, so-called integer-ambiguity, which is initially estimated as a float parameter. When the highest accuracy is required, the recovery of the ambiguity integer value (so-called integer ambiguity resolution) is necessary to fully benefit from the precision of the carrier-phase observables.

Several approaches have been presented during the last years to achieve ambiguity resolution in PPP for GPS L1/L2 measurements. The aim of this chapter is to present the different techniques proposed, following a common notation, and with particular focus on the extension of the method to multi-frequency and multi-GNSS.

3.2 Observation equations

The observation equations, for pseudorange P and carrier-phase L, between receiver r and satellite s, for frequency f_i read [Teunissen and Kleusberg, 1996]:

$$P_i^{r,s} = \rho^{r,s} + T^{r,s} + I_i^{r,s} + c(\delta t^r - \delta t^s) + c(p_i^r - p_i^s) + \varepsilon_{P_i} \quad (3.1)$$

$$L_i^{r,s} = \rho^{r,s} + T^{r,s} - I_i^{r,s} + c(\delta t^r - \delta t^s) + c(l_i^r - l_i^s) + \lambda_i N_i^{r,s} + \varepsilon_{L_i} \quad (3.2)$$

where:

- ρ is the geometric distance between station and satellite, assuming that relevant corrections have been accounted for. These corrections include antenna phase corrections for transmitting and receiving antennas, ocean loading, solid tides, phase wind-up, etc. A comprehensive study of the state-of-the-art corrections for PPP can be found in [Hesselbarth, 2011], and will not be repeated here for simplicity. Let $X^r = (x^r, y^r, z^r)$ and $X^s = (x^s, y^s, z^s)$ be the receiver and satellite cartesian coordinates, then the term $\rho^{r,s}$ reads:

  $$\rho^{r,s} = \| X^r - X^s \| = \sqrt{(x^r - x^s)^2 + (y^r - y^s)^2 + (z^r - z^s)^2} \quad (3.3)$$

  In Precise Point Positioning, satellite coordinates X^s are considered known, i.e. derived from precise orbit estimates from the International GNSS Service (IGS)[Kouba, 2009]. Receiver coordinates X^r are estimated in the PPP algorithm. All coordinates are here specified in the International Terrestrial Reference System (ITRS).

- c is the speed of light.

- δt^r and δt^s are receiver and satellite clock biases, respectively. Satellite clock biases are considered known (i.e. derived from IGS products), while the receiver clock bias needs to be estimated in PPP.

- $T^{r,s}$ is the tropospheric delay between station and satellite, which can be expressed as follows [Teke et al., 2011]:

  $$T^{r,s} = T(a,e) = m_d(e)\, T_d + m_w(e)\, T_w + m_g(e)\, cot(e)\, [G_N cos(a) + G_E sin(a)] \quad (3.4)$$

  Where a and e are azimuth and elevation of the path between station and satellite, T_d is the zenith hydrostatic (dry) delay, T_w is the zenith wet delay, and m_d and m_w are the dry and wet elevation-dependent mapping functions, respectively. G_N and G_E are the North and East tropospheric gradients, respectively, with the corresponding mapping function m_g. The zenith hydrostatic delay T_d can be accurately computed using a-priori models, such as the Saastamoinen model [Saastamoinen, 1972] or the Global Pressure and Temperature (GPT) model [Boehm et al., 2007]. The wet-component T_w cannot be accurately modeled, and is usually estimated included as a parameter in the PPP adjustment. Several dry and wet mapping functions have been proposed by different authors, such as the Niell Mapping Function (NMF) [Niell, 1996], the Vienna Mapping Function (VMF) [Boehm, 2004] or the Global Mapping

Function (GMF) [Boehm et al., 2006]. Studies on the impact of tropospheric-gradients in GNSS processing can be found in [Bar-Sever et al., 1998] and [Ghoddousi-Fard et al., 2009].

- $I_i^{r,s}$ is slant ionospheric delay between receiver and satellite at frequency f_i. The first order ionospheric effect accounts for 99.9% of the ionospheric refraction [Hernandez-Pajares et al., 2007], and follows the next frequency relation:

$$\frac{I_i^{r,s}}{I_j^{r,s}} = \frac{f_j^2}{f_i^2} \tag{3.5}$$

  Higher-order ionospheric terms will not be considered here for simplicity. A detailed study of the second-order ionospheric delay on GPS signals can be found in [Hernandez-Pajares et al., 2007].

- p_i^r and p_i^s are the pseudorange hardware delays for receiver and satellite, respectively, at frequency f_i.

- l_i^r and l_i^s are the phase hardware delays for receiver and satellite, respectively, at frequency f_i.

- $\lambda_i N_i^{r,s}$ is the carrier-phase ambiguity term for frequency f_i, where $N_i^{r,s}$ is the integer ambiguity and λ_i is the associated wavelength:

$$\lambda_i = \frac{c}{f_i} \tag{3.6}$$

- ε_{P_i} and ε_{L_i} are observation errors for pseudorange and carrier-phase, respectively, including thermal noise and multipath. It is assumed that these errors follow a normal distribution, such as $\varepsilon_{P_i} \sim \mathcal{N}(0, \sigma_{P_i}^2)$, $\varepsilon_{L_i} \sim \mathcal{N}(0, \sigma_{L_i}^2)$, and precision of carrier-phase is significantly higher than for pseudorange: $\sigma_{L_i} << \sigma_{P_i}$.

3.3 Traditional ionosphere-free PPP

The traditional PPP technique makes use of dual-frequency measurements to remove the first-order ionospheric delay [Zumberge et al., 1997],[Kouba and Héroux, 2001]. The ionospheric-free (IF) observations for frequencies f_i, f_j are derived as:

$$P_{IF}^{r,s} = \alpha_{ij} P_i^{r,s} + \beta_{ij} P_j^{r,s} \tag{3.7}$$

$$L_{IF}^{r,s} = \alpha_{ij} L_i^{r,s} + \beta_{ij} L_j^{r,s} \tag{3.8}$$

Where combination coefficients α_{ij} and β_{ij} are chosen to remove the frequency-dependent ionospheric error ($\alpha_{ij}/\beta_{ij} = -f_i^2/f_j^2$), with the additional condition of preserving geometry ($\alpha_{ij} + \beta_{ij} = 1$). The resulting coefficients read:

$$\alpha_{ij} = \frac{f_i^2}{f_i^2 - f_j^2} \tag{3.9}$$

$$\beta_{ij} = \frac{-f_j^2}{f_i^2 - f_j^2} \tag{3.10}$$

The ionosphere-free observation equations can be written as:

$$P_{IF}^{r,s} = \rho_r^s + T^{r,s} + c(\delta t_{IF}^r - \delta t_{IF}^s) + \varepsilon_{P_{IF}} \tag{3.11}$$
$$L_{IF}^{r,s} = \rho_r^s + T^{r,s} + c(\delta t_{IF}^r - \delta t_{IF}^s) + T^{r,s} + a_{IF}^{r,s} + \varepsilon_{L_{IF}} \tag{3.12}$$

Where the new ionosphere-free clocks are derived as:

$$\delta t_{IF}^r = \delta t^r + \alpha_{ij} p_i^r + \beta_{ij} p_j^r \tag{3.13}$$
$$\delta t_{IF}^s = \delta t^s + \alpha_{ij} p_i^s + \beta_{ij} p_j^s \tag{3.14}$$

And the new ambiguity term reads:

$$a_{IF}^{r,s} = \alpha_{ij}\lambda_i N_i^{r,s} + \beta_{ij}\lambda_j N_j^{r,s} + b_{IF}^r - b_{IF}^s \tag{3.15}$$

Where new hardware delays b_{IF}^r and b_{IF}^s are a combination of pseudorange and carrier-phase delays:

$$b_{IF}^r = c(\alpha_{ij} l_i^r + \beta_{ij} l_j^r - \alpha_{ij} p_i^r - \beta_{ij} p_j^r) \tag{3.16}$$
$$b_{IF}^s = c(\alpha_{ij} l_i^s + \beta_{ij} l_j^s - \alpha_{ij} p_i^s - \beta_{ij} p_j^s) \tag{3.17}$$

$a_{IF}^{r,s}$ is in general non-integer due to the non-integer nature of α_{ij} and β_{ij} and the presence of the hardware delay terms.

The resulting pseudorange and carrier-phase observation errors are $\varepsilon_{P_{IF}} \sim \mathcal{N}(0, \sigma_{P_{IF}}^2)$, $\varepsilon_{L_{IF}} \sim \mathcal{N}(0, \sigma_{L_{IF}}^2)$. According to the error propagation law, and assuming same observation noise in both carriers:

$$AF = \frac{\sigma_{P_{IF}}}{\sigma_P} = \frac{\sigma_{L_{IF}}}{\sigma_L} = \sqrt{(\alpha_{ij}^2 + \beta_{ij}^2)} \tag{3.18}$$

As derived from equations 3.9 and 3.10, for all pairs of GNSS frequencies f_i, f_j, $|\alpha_{ij}| > 1$, $|\beta_{ij}| > 1$, and therefore $AF > 1$. This means that the observation noise of the linear combination will be always higher than the noise from the uncombined observations. AF is known as the noise amplification factor of the linear combination, and depends only on the frequency separation between the two carriers. Table 3.1 represents the combination coefficients and the noise amplification factor for all possible dual-frequency combinations for GPS, Galileo and BeiDou. As derived from this analysis, not all ionosphere-free linear combinations are favorable for PPP, as the noise amplification factor degrades significantly the precision of the observations, when the frequency separation is too small, such as GPS L2/L5, Galileo E5/E5a/E5b, or BeiDou B2/B3 combinations. It is also noticeable that the noise standard GPS L1/L2 combination is around three times larger than the original uncombined measurements. Galileo E1/E5 or BeiDou B1/B2 combinations have a noise amplification factor of the same order of magnitude.

Constellation	f_i/f_j	α_{ij}	β_{ij}	AF
GPS	L1/L2	2.55	-1.55	2.98
	L1/L5	2.26	-1.26	2.59
	L2/L5	12.26	-11.26	16.64
Galileo	E1/E5a	2.26	-1.26	2.59
	E1/E5	2.34	-1.34	2.69
	E1/E5b	2.42	-1.42	2.81
	E1/E6	2.93	-1.93	3.51
	E6/E5a	6.51	-5.51	8.53
	E6/E5	7.61	-6.71	10.08
	E6/E5b	9.19	-8.19	12.30
	E5a/E5	39.08	-38.08	54.57
	E5b/E5	39.58	-38.58	55.28
	E5a/E5b	19.92	-18.92	27.47
BeiDou	B1/B2	2.49	-1.49	2.90
	B1/B3	2.94	-1.94	3.53
	B2/B3	10.59	-9.59	14.29

Tab. 3.1: Ionosphere-free coefficients (α_{ij},β_{ij}) and noise amplification factors (AF) for GPS, Galileo and BeiDou frequencies

In traditional parameter estimation for PPP, equations 3.11 and 3.12 are used as observation equations. Accurate satellite positions X^s and clocks δ^s_{IF} are routinely provided by the International GNSS Service [Kouba, 2009]. Estimated parameters are the station coordinates $X_r = (x^r, y^r, z^r)$, wet tropospheric zenith delay T_w, the receiver clock error δ^r_{IF}, and ambiguity term $a^{r,s}_{IF}$. For a given epoch with n satellites in view, there are $2n$ observations (pseudorange and carrier-phase), and 5+n epoch-wise parameters to be estimated (all except carrier-phase ambiguities, which are considered constant in absence of cycle slips). Therefore the degree of freedom is n-5, meaning that a minimum of 5 satellites in view are required to compute the user position.

3.4 Wide/Narrow Lane methods

As discussed in previous section, the integer property of the ambiguity is not preserved in the traditional PPP model due to the introduction of the linear combination and the presence of hardware delays, which generate a non-integer term $a^{r,s}_{IF}$. In order to overcome that limitation, so-called Wide/Narrow lane approaches have recently been developed by different authors. These include the Decoupled Clock model [Collins et al., 2008] and the Integer Clock method [Laurichesse et al., 2009], both at zero-difference level. [Ge et al., 2007] developed between-satellites differences for resolving the integer ambiguities in PPP. It has been proven that these approaches are effectively slightly different implementations

of the same method [Shi and Gao, 2013], which will be reproduced here without loss of generality.

The method is based on the introduction of a new Wide-Lane ambiguity $N_w^{r,s} = N_i^{r,s} - N_j^{r,s}$, so that the ambiguity term $a_{IF}^{r,s}$ can be rewritten as:

$$a_{IF}^{r,s} = (\alpha_{ij}\lambda_i + \beta_{ij}\lambda_j)N_i^{r,s} - \beta_{ij}\lambda_j N_w^{r,s} + b_{IF}^r - b_{IF}^s \quad (3.19)$$

$$= \frac{c}{f_i + f_j}N_i^{r,s} - \frac{f_j c}{f_i^2 - f_j^2}N_w^{r,s} + b_{IF}^r - b_{IF}^s \quad (3.20)$$

The Wide-Lane ambiguity $N_w^{r,s}$ can be resolved using the Melbourne-Wübbena (MW) linear combination ([Melbourne, 1985], [Wübbena, 1985]), which is both geometry- and ionosphere-free. This linear combination is actually a wide-lane combination of phase and a narrow-lane combination of pseudorange measurements in two carrier frequencies:

$$MW^{r,s} = \alpha_{ij}^w L_i^{r,s} + \beta_{ij}^w L_j^{r,s} + \alpha_{ij}^n P_i^{r,s} + \beta_{ij}^n P_j^{r,s} \quad (3.21)$$

Where the combination coefficients are:

$$\alpha_{ij}^w = \frac{f_i}{f_i - f_j} \quad (3.22)$$

$$\beta_{ij}^w = \frac{-f_j}{f_i - f_j} \quad (3.23)$$

$$\alpha_{ij}^n = \frac{f_i}{f_i + f_j} \quad (3.24)$$

$$\beta_{ij}^n = \frac{f_j}{f_i + f_j} \quad (3.25)$$

Applying equation 3.21 to equations 3.1 and 3.2 results in:

$$MW^{r,s} = \frac{c}{f_i - f_j}N_w^{r,s} + b_{WL}^r - b_{WL}^s \quad (3.26)$$

$$b_{WL}^r = c(\alpha^n p_i^r + \beta^n p_j^r + \alpha^w l_i^r + \beta^w l_j^r) \quad (3.27)$$

$$b_{WL}^s = c(\alpha^n p_i^s + \beta^n p_j^s + \alpha^w l_i^s + \beta^w l_j^s) \quad (3.28)$$

As shown in equation 3.26, the Melbourne-Wübbena observations include the integer Wide-Lane ambiguity $N_w^{r,s}$, plus additional hardware delays terms b_{WL}^r and b_{WL}^s, for receiver and satellite, respectively. These delays have been known in the existing literature as Wide-Lane Fractional Cycle Biases (FCBs) or Uncalibrated Phase Delays (UPDs). As observed in equations 3.27 and 3.28, these terms contain both pseudo-range and carrier-phase biases. Therefore, a more appropriate nomenclature is Uncalibrated Hardware Delays (UHDs), as suggested in [Geng et al., 2009].

The associated Wide- and Narrow-Lane wavelengths λ^w and λ^n are derived from equations 3.26 and 3.20, respectively:

$$\lambda^w = \frac{c}{f_i - f_j} \quad (3.29)$$

$$\lambda^n = \frac{c}{f_i + f_j} \quad (3.30)$$

Constellation	f_i/f_j	$\lambda^w(cm)$	$\lambda^n(cm)$
GPS	L1/L2	86.25	10.70
	L1/L5	75.19	10.90
	L2/L5	586.51	12.48
Galileo	E1/E5a	75.19	10.90
	E1/E5	78.20	10.84
	E1/E5b	81.46	10.78
	E1/E6	101.12	10.51
	E6/E5a	293.26	12.22
	E6/E5	345.01	12.14
	E6/E5b	418.94	12.07
	E5a/E5	1955.03	12.67
	E5b/E5	1955.03	12.51
	E5a/E5b	977.52	12.59
BeiDou	B1/B2	84.76	10.84
	B1/B3	102.54	10.60
	B2/B5	488.76	12.12

Tab. 3.2: Wide- and narrow-lane wavelengths for different signal combinations

Table 7.1 shows wide- and narrow-lane wavelengths for all GPS/Galileo/BeiDou signal combinations. Although there are significant variations in the wide-lane wavelength, the narrow-lane wavelengths are in the range 10-12 cm for all frequency combinations. Galileo E1/E5a, E1/E5b, E1/E5 and BeiDou B1/B2 combinations offer similar wavelengths to GPS L1/L2, for which the method was originally developed.

The extra wide combinations, such as Galileo E5a/E5 or E5b/E5 ($\lambda^w = 19.55$ m), might appear interesting due to the very high wavelength, which allows to easily resolve the wide-lane ambiguity. However, narrow-lane ambiguity resolution becomes very challenging due to the high noise amplification factor for these combinations.

3.4.1 Wide-Lane ambiguity resolution

Network solution

Wide-lane ambiguity resolution is achieved using a geometry-free approach using the Melbourne-Wübbena observations. However, due to the meter-level noise of pseudorange-observations, an accurate estimate of the wide-lane ambiguity cannot be generally achieved

using a single epoch, except for very wide-lane combinations, as previously explained. This is typically solved averaging the K observations of a satellite pass:

$$\overline{MW^{r,s}} = \frac{1}{K}\sum_{k=1}^{K} MW^{r,s}(k) \tag{3.31}$$

Undifferenced approach For the estimation of the UHDs, in a network solution with S satellites and R receivers, the following normal system of equations needs to be solved.

$$\langle\overline{MW^{r,s}}\rangle = b^r_{WL} - b^s_{WL} \qquad r = 1,..,R \quad s = 1,..,S \tag{3.32}$$

Where $\langle x\rangle$ is the fractional part of x. The equation system is singular, and therefore a reference satellite or receiver needs to be selected, such as $b^{ref}_{WL} = 0$. Then, all remaining satellite WL-UHDs terms b^s_{WL} are obtained. The station WL-UHDs b^s_{WL} are obtained as a by-product.

Single-difference approach The single-difference approach is based on building single-diference between satellites observed from the same receiver, with the objective of removing the receiver terms b^r_{WL}, and estimate only b^s_{WL}:

$$\overline{MW^{s1,s2}} = \overline{MW^{r,s1}} - \overline{MW^{r,s2}} \tag{3.33}$$

Therefore, the equation system becomes:

$$\langle\overline{MW^{s1,s2}}\rangle = b^{s1}_{WL} - b^{s2}_{WL} \qquad s1 = 1..S \quad s2 = 1..S \quad s1 \neq s2 \tag{3.34}$$

This equation system is also singular, requiring to select a reference satellite $b^{ref}_{WL} = 0$ for obtaining a unique solution for the satellite biases.

PPP solution

Undifferenced approach In PPP, the wide-lane ambiguities can be resolved taking as input the b^s_{WL} from the network solution, and estimating the remaining receiver term b^r_{WL}. Taking the mean as estimator, and with the S satellites in view, the receiver bias can be obtained as:

$$b^r_{WL} = \frac{1}{S}\sum_{s=1}^{S}(\overline{\langle\overline{MW^{r,s}}\rangle} + b^s_{WL}) \tag{3.35}$$

Once b^r_{WL} is known, the integer wide-lane ambiguities can be resolved directly as:

$$\widehat{N^{r,s}_w} = \left[\frac{MW^{r,s} + b^s_{WL} - b^r_{WL}}{\lambda_w}\right] \qquad s = 1..S \tag{3.36}$$

Where $[x]$ is the closest integer value of x.

Single-difference approach In the single-difference approach, the receiver term is cancelled and the single-difference ambiguities can be solved directly:

$$\widehat{N_w^{s1,s2}} = \left[\frac{MW^{s1,s2} + b_{WL}^{s1} - b_{WL}^{s2}}{\lambda_w} \right] \qquad s1 = 1..S \quad s2 = 1..S \quad s1 \neq s2 \tag{3.37}$$

3.4.2 Narrow-Lane ambiguity resolution

The remaining narrow-lane ambiguity N_i can be solved using a geometry-based approach, once wide-lane ambiguity resolution has been performed. Equation 3.20 can be rewritten as:

$$a_{IF}^{r,s} + \frac{f_j c}{f_i^2 - f_j^2} \widehat{N_w^{r,s}} = \lambda_n (N_i^{r,s} + b_{NL}^r - b_{NL}^s) \tag{3.38}$$

Where $a_{IF}^{r,s}$ is already known from the float solution, $\widehat{N_w^{r,s}}$ is known after wide-lane ambiguity resolution, and the remaining unknowns are the integer narrow-lane ambiguity $N_i^{r,s}$, and the associated Narrow-Lane Uncalibrated Hardware delays (NL-UHDs) terms for receiver and satellite, b_{NL}^r and b_{NL}^s, defined as:

$$b_{NL}^r = b_{IF}^r / \lambda_n \tag{3.39}$$

$$b_{NL}^s = b_{IF}^s / \lambda_n \tag{3.40}$$

Network solution

Undifferenced approach In the network solution, parameters b_{NL}^r and b_{NL}^s are resolved following system of equations:

$$\left\langle \frac{a_{IF}^{r,s} + \frac{f_j c}{f_i^2 - f_j^2} \widehat{N_w^{r,s}}}{\lambda_n} \right\rangle = b_{NL}^r - b_{NL}^s \qquad r = 1..R \quad s = 1..S \tag{3.41}$$

The equation system is singular, and therefore a reference satellite or receiver needs to be selected, such as $b_{NL}^{ref} = 0$. Then, all remaining satellite NL-UHDs terms b_{NL}^s are obtained. The station NL-UHDs b_{NL}^s are obtained as a by-product.

A variation of this method is to assimilate the NL-UHD into the clock terms, in order to generate so-called the Integer Phase Clocks ([Laurichesse et al., 2009]), δ_{IC}^r, δ_{IC}^r, so that equations 3.11 and 3.12 become:

$$P_{IF}^{r,s} = \rho_r^s + c(\delta t_{IF}^r - \delta t_{IF}^s) + T^{r,s} + \varepsilon_{P_{IF}} \tag{3.42}$$

$$L_{IF}^{r,s} = \rho_r^s + c(\delta t_{IC}^r - \delta t_{IC}^s) + T^{r,s} + a_{IC}^{r,s} + \varepsilon_{L_{IF}} \tag{3.43}$$

Where:

$$a_{IC}^{r,s} = a_{IF}^{r,s} - b_{IF}^r + b_{IF}^s \tag{3.44}$$

$$\delta_{IC}^r = \delta_{IF}^r + b_{IF}^r / c \tag{3.45}$$

$$\delta^s_{IC} \quad = \quad \delta^s_{IF} + b^r_{IF}/c \tag{3.46}$$

Using this notation, the network solution needs to estimate the Integer Clock terms δ_{IC} instead of the NL-UHDs. It is to be noted that the observation equations include now a different clocks δ_{IF} and δ_{IC} for pseudorange or carrier-phase, respectively. This is the basis of the Decoupled Clock model introduced by [Collins et al., 2008]. The Integer Clocks fulfill the condition that the derived Narrow-Lane ambiguities are already integer, without having to estimate additional narrow-lane delays:

$$\left\langle \frac{a^{r,s}_{IC} + \frac{f_j c}{f_i^2 - f_j^2}\widehat{N^{r,s}_w}}{\lambda_n} \right\rangle = 0 \quad r = 1..R \quad s = 1..S \tag{3.47}$$

Single-difference approach In the single-difference approach, the following equation systems needs to be solved.

$$\left\langle \frac{a^{s1,s2}_{IF} + \frac{f_j c}{f_i^2 - f_j^2}\widehat{N^{s1,s2}_w}}{\lambda_n} \right\rangle = b^{s1}_{NL} - b^{s2}_{NL} \quad s1 = 1..S \quad s2 = 1..S \quad s1 \neq s2 \tag{3.48}$$

With:

$$a^{s1,s2}_{IF} = a^{r,s1}_{IF} - a^{r,s2}_{IF} \tag{3.49}$$

PPP solution

Undifferenced-approach In the undifferenced approach, the remaining receiver Narrow-lane UHDs b^r_{NL} needs to be estimated using the S satellites in view:

$$b^r_{NL} \quad = \quad \frac{1}{S}\sum_{s=1}^{S}\left\langle \frac{a^{r,s}_{IF} + \frac{f_j c}{f_i^2 - f_j^2}\widehat{N^{r,s}_w}}{\lambda_n} + b^s_{NL} \right\rangle \tag{3.50}$$

Then the narrow-lane ambiguities for all satellites can be resolved as:

$$\widehat{N^{r,s}_i} \quad = \quad \left[\frac{a^{r,s}_{IF} + \frac{f_j c}{f_i^2 - f_j^2}\widehat{N^{r,s}_w}}{\lambda_n} - b^r_{NL} + b^s_{NL} \right] \quad s = 1..S \tag{3.51}$$

Once both wide-and narrow-lane ambiguities have been fixed, the ionosphere-free ambiguity term can be reconstructed using the integer-ambiguities and the estimated satellite and hardware delays:

$$\widehat{a^{r,s}_{IF}} \quad = \quad \lambda_n \left[\widehat{N^{r,s}_i} + b^r_{NL} - b^s_{NL} \right] - \frac{f_j c}{f_i^2 - f_j^2}\widehat{N^{r,s}_w} \tag{3.52}$$

Finally, $\widehat{a^{r,s}_{IF}}$ is re-introduced in the observation equations as a known amount and the float ambiguity term $a^{r,s}_{IF}$ is no longer estimated as a parameter.

Single-difference approach In the single-difference approach, the single-difference narrow-lane ambiguity $N_i^{s1,s2}$ can be obtained directly as:

$$\widehat{N_i^{s1,s2}} = \left[\frac{a_{IF}^{s1,s2} + \frac{f_j c}{f_i^2 - f_j^2} \widehat{N_w^{s1,s2}}}{\lambda_n} - b_{NL}^{s1,s2} + b_{NL}^{s1,s2} \right] \quad s1 = 1..S \quad s2 = 1..S \quad (3.53)$$

Once the narrow-lane ambiguity is resolved, the reconstructed single-difference ionosphere-free ambiguity reads:

$$\widehat{a_{IF}^{s1,s2}} = \lambda_n \left[\widehat{N_i^{s1,s2}} + b_{NL}^{s1} - b_{NL}^{s2} \right] - \frac{f_j c}{f_i^2 - f_j^2} \widehat{N_w^{s1,s2}} \quad s1 = 1..S \quad s2 = 1..S \quad (3.54)$$

The single-difference ambiguities can be then introduced as additional constrain equations in the PPP parameter estimation, such as:

$$\widehat{a_{IF}^{s1,s2}} = a_{IF}^{r,s1} - a_{IF}^{r,s2} \quad s1 = 1..S \quad s2 = 1..S \quad (3.55)$$

3.5 Raw method

Although ionosphere-free PPP has become increasingly popular since its introduction, it has the main drawback of the increased observation noise. An alternative is to process directly the original uncombined observations. This approach is known in the literature as the *raw method*.

The processing of original uncombined observations has been extensively studied for single-frequency positioning applications [Øvstedal, 2002], [Bree and Tiberius, 2011], [Le and Tiberius, 2006], [Chen and Gao, 2005]. The ionospheric error can be removed to some extent from the single-frequency observations making use of ionospheric maps, which are made available by IGS [Hernández-Pajares et al., 2009]. However, the accuracy of global ionospheric maps is limited to 5-10 Total Electron Content Units (TECUs). 1 TECU is approximately equivalent to 16 centimeters in GPS L1 frequency.

In order to remove more accurately the ionospheric delay, multi-frequency processing is needed. The raw method is based on the estimation of the ionospheric delay from multi-frequency observations [Schönemann et al., 2011]. Ambiguity resolution for the raw method in PPP is also of interest to fully benefit from the precision of the carrier-phase observations, this has been proposed by several authors, such as [Zhang et al., 2011, Li et al., 2013]. The method proposed in will be extended here deriving all the terms from the original observation equations:

$$P_i^{r,s} = \rho^{r,s} + T^{r,s} + I_i^{r,s} + c(\delta t^r - \delta t^s) + c(p_i^r - p_i^s) + \varepsilon_P \quad (3.56)$$

$$L_i^{r,s} = \rho^{r,s} + T^{r,s} - I_i^{r,s} + c(\delta t^r - \delta t^s) + c(l_i^r - l_i^s) + \lambda_i N_i^{r,s} + \varepsilon_L \quad (3.57)$$

When using satellite clocks as input, these are typically derived using the ionosphere-free approach in frequencies f_n and f_m (i.e. IGS clocks), therefore:

$$\delta t^s = \delta t^s_{IF} - \alpha_{nm} p^s_n - \beta_{nm} p^s_m \tag{3.58}$$

So that equations 3.56 and 3.57 are rewritten as:

$$P^{r,s}_i = \rho^{r,s} + T^{r,s} + I^{r,s}_i + c(\delta t^r - \delta t^s_{IF}) + DCB^r_i - DCB^s_i + \varepsilon_P \tag{3.59}$$
$$L^{r,s}_i = \rho^{r,s} + T^{r,s} - I^{r,s}_i + c(\delta t^r - \delta t^s_{IF}) + DCB^r_i - DCB^s_i + a^{r,s}_i + \varepsilon_L \tag{3.60}$$

Where the Differential Code Biases (DCBs) are derived as:

$$DCB^r_i = c\, p^r_i \tag{3.61}$$
$$DCB^s_i = c(p^s_i - \alpha_{nm} p^s_n - \beta_{nm} p^s_m) \tag{3.62}$$

It is to be noted that, in general, ionosphere-free clocks derived from frequencies f_n and f_m, can be applied to observation in frequency f_i, provided that the satellite biases are properly accounted for as per equation 3.62.

The ambiguity term $a^{r,s}_i$ reads:

$$a^{r,s}_i = \lambda_i (N^{r,s}_i + b^r_i - b^s_i) \tag{3.63}$$

and includes the Uncalibrated Hardware Delay terms b^r_i and b^s_i:

$$b^r_i = f_i(l^r_i - p^r_i) \tag{3.64}$$
$$b^s_i = f_i(l^s_i - p^s_i) \tag{3.65}$$

In the float solution for the raw approach, the parameters that need to be estimated are: station coordinates X^s, receiver clock term δt^r, tropospheric $T^{r,s}$ and ionospheric $I^{r,s}_i$ delays, differential code biases DCB^r_i, DCB^s_i, and float ambiguity terms $a^{r,s}_i$. It needs to be mentioned, that not all parameters in equations 3.59 and 3.60 are observable. In particular, the receiver clock error term δ^r_t and all DCB^r_i cannot be estimated simultaneously, as the system is singular. With N satellites in view, a carrier frequency f_i can be selected as reference, so that $DCB^r_i = 0$, and all remaining $DCB^r_j, j \neq i$ can be estimated. Additionally, instead of estimating a ionospheric-parameter for each frequency, the ionospheric-delay $I^{r,s}_i$ in a reference frequency f_i can be estimated, using the frequency-dependent relation $I^{r,s}_j = I^{r,s}_i \cdot f^2_i / f^2_j$.

Network solution

Undifferenced approach In the network solution, Uncalibrated Hardware Delays b^s_i and b^s_j need to be estimated. This is done taking the fractional part of the ambiguity parameters, and solving the resulting system of equations:

$$\left\langle \frac{a_i^{r,s}}{\lambda_i} \right\rangle = b_i^r - b_i^s \quad r = 1..R \quad s = 1..S \tag{3.66}$$

The system is singular, and a reference satellite or receiver needs to be selected, so that $b_i^{ref} = 0$. Then all the remaining satellite delays b_i^s are determined. The receiver delays b_i^r are obtained as a by product. The same has to be done for each other frequency processed f_j.

Single-difference approach In the single-difference approach, the receiver delays b_i^r cancel out, and the following system of equations needs to be solved.

$$\left\langle \frac{a_i^{r,s1} - a_i^{r,s2}}{\lambda_i} \right\rangle = b_i^{s2} - b_i^{s1} \quad s1 = 1..S \quad s2 = 1..S \tag{3.67}$$

After taking one satellite as reference b_i^{ref}, all remaining satellite delays b_i^s can be estimated.

PPP solution

Undifferenced approach In the undifferenced approach, the receiver delays b_i^r need to be estimated. Taking the mean as estimator, this results in:

$$b_i^r = \frac{1}{S} \sum_{s=1}^{S} \left(\left\langle \frac{a_i^{r,s}}{\lambda_i} \right\rangle + b_i^s \right) \tag{3.68}$$

Then the integer value of the ambiguities can be resolved as:

$$\widehat{N_i^{r,s}} = \left[\frac{a_i^{r,s}}{\lambda_i} + b_i^s - b_i^r \right] \tag{3.69}$$

Finally, the fixed ambiguity term to be replaced in the observation equation reads:

$$\widehat{a_i^{r,s}} = \lambda_i (N_i^{r,s} + b_i^r - b_i^s) \tag{3.70}$$

The same needs to be done for all other frequencies involved.

Single-difference approach In the single-diference approach, the receiver term is not estimated, and the ambiguities can be resolved directly at single-difference level after applying the satellite delays:

$$\widehat{N_i^{r,s1}} - \widehat{N_i^{r,s2}} = \left[\frac{a_i^{r,s1} - a_i^{r,s2}}{\lambda_i} + b_i^{s1} - b_i^{s2} \right] \tag{3.71}$$

3.6 Raw versus ionosphere-free PPP

As described in this chapter, precise point positioning can be implemented by using the original raw observations, or building dual-frequency ionosphere-free observations using a linear combination. From the theoretical point of view these approaches are identical, but in practice there are few aspects that need to be considered.

The raw observation method benefits from a lower observation noise as it avoids building ionosphere-free linear combinations that are noisier. The drawback is the need of a more complex model, where ionospheric-delays and frequency-dependent biases need to be taken into account. A potential benefit is that a-priori ionospheric information can be used to accelerate convergence time, as shown in [Zhang et al., 2013], [Yao et al., 2013], [Juan et al., 2012]. The ionosphere-free model is more simple as these parameters do not have to be estimated.

On the other hand, when attempting ambiguity resolution, there are significant differences between both. The ionosphere-free model has the implication that an additional step with the Melbourne-Wübbena combination needs to be added for the resolution of the wide-lane ambiguity. This additional step is suboptimal due to the inclusion of the noisy pseudorange observations. In fact, one of the main constraints is the need to average the Melbourne-Wübbena measurements over a significant amount of time between wide-lane ambiguity can be attempted. Using empirical data, [Geng et al., 2011] showed that 90% of GPS L1/L2 wide-lane ambiguities could be solved within 10 minutes, 95% within 20 minutes. Narrow-lane ambiguity can be attempted after successful wide-lane fixing, and also when the float solution has reached a good level of accuracy, due to the short narrow-lane wavelength. According to [Bisnath and Gao, 2009], up to 30 minutes are required for a traditional PPP solution to achieve decimeter level accuracy in kinematic applications. Wide-lane ambiguity resolution does not improve accuracy, only narrow-lane ambiguity resolution does.

In the raw-method, ambiguity-fixing can be achieved without this Melbourne-Wübbena step, as the carrier-phase ambiguities in each frequency are available in the first place. Additionally, the raw model can be more naturally extended to multi-frequency PPP, as ambiguity fixing is largely treated in an independent way for each frequency, regardless of the number of frequencies.

The ionosphere-free model, the wide-lane method is a bit limited as it is specifically designed for the dual-frequency case. The extension to multi-frequency makes use of different wide-lane combinations, that allow resolution of ambiguities in all frequencies, once the

narrow-lane ambiguity is resolved. On the contrary, the raw method can be naturally expanded to multi-frequency, as ambiguity fixing is largely treated in an independent way for each frequency.

4 Paper A: Triple-carrier Precise Point Positioning using GPS L5

Paper title: "Triple-carrier Precise Point Positioning using GPS L5"
Authors: Javier Tegedor, Ola Øvstedal[1]
Published in *Survey Review*, Vol 4 Issue 337 Pages 228-297, 2014
DOI: 10.1179/1752270613Y.0000000076
Manuscript Submitted: March 21, 2013
Manuscript Accepted: August 20 2013

Contents

4.1 Abstract

The latest generation of GPS satellites, block IIF, include for the first time a new civil signal on L5 frequency (1176.45 MHz), in addition to the legacy signals on L1 (1575.42 MHz) and L2 (1227.60 MHz). Traditional Precise Point Positioning (PPP) is based on L1/L2 dual-frequency observations to remove the ionospheric delay. However, L5 presents interesting properties, such as more robustness against interference compared to L2, that makes it suitable for critical applications. Therefore, navigation users can already start making use of the L5 signal, to increase reliability and redundancy for the most demanding applications. This article addresses the integration of the new L5 pseudorange and carrier phase observables in PPP, which at the same time allows to perform efficient signal characterization. In particular, ionosphere-free combinations including L5 are explored and their corresponding observation equations introduced. Practical results using IGS MGEX observation data are presented.

Keywords: Biases characterization, GPS L5, Precise Point Positioning

[1]Norwegian University of Life Sciences, Department of Mathematical Sciences and Technology

4.2 GPS evolution: the L5 signal

Traditional GNSS processing is often based on dual-frequency L1/L2 ionosphere-free linear combination, that allows removal of the first-order ionospheric delay that affects navigation signals [Hesselbarth, 2011]. At the same time, in the context of GNSS modernization, there is a trend to make more signals and frequencies available to navigation users. For example, GLONASS is adding a third frequency L3 with the GLONASS-K generation satellites [Urlichich et al., 2011], while Galileo open signals are located in E1/E5a/E5b/E5a+b carriers [European Commision, 2010], in addition to the commercial service on E6.

In particular, GPS is currently deploying the block IIF satellites, with the new civil signals in L5, whose main purpose is to serve Safety of Life (SoL) applications, including civil aviation [Jan, 2010]. Satellite SVN-49 (block IIR-M), launched in 2009, had the first experimental L5 payload. At the time of writing, there are three IIF satellites in operation, SVN-62, SVN-63 and SVN-65, assigned to PRN25, PRN01 and PRN24 respectively (table 4.1).

Satellite ID	SVN	PRN	Launch date	COSPAR ID	NORAD ID	Plane/Slot
IIF-1	62	25	28 May 2010	2010-022A	36585	B/2
IIF-2	63	01	16 Jul 2011	2011-036A	37753	D/2
IIF-3	65	24	04 Oct 2012	2012-053A	38833	A/1

Tab. 4.1: Current[2]GPS IIF satellite characteristics including Satellite Vehicle Number (SVN), Pseudo Random Noise number (PRN), International Designator (COSPAR ID) and Satellite Catalog Number (NORAD ID).

L5 carrier frequency (1176.45 MHz), contrary to L2 (1227.60 MHz), is included in the Aeronautical Radionavigation Service (ARNS) band, meaning that it is more protected against interference. Additionally, the L5 spreading codes have a chipping rate of 10.23 MHz, same as P-code, and 10 times faster than C/A or L2C codes [Montenbruck et al., 2010]. The in-phase carrier component (I) contains the the modernized civil navigation message (CNAV), which is capable of transmitting integrity information. The quadrature component (Q) contains a pilot signal without navigation information [GPS Directorate, 2011a].

The new civil signal in the third frequency opens the door to further research opportunities including new multi-frequency processing approaches [Schönemann et al., 2011], extended linear combinations and new ambiguity resolution techniques ([Odijk, 2003],[Cocard et al., 2008]). The fact that L5 is shared by Galileo E5a will likely improve interoperability between the two systems [Feng, 2003], as they also share the E1/L1 frequency (1575.42 MHz).

At the same time, new challenges arise for processing the new signal, as, for instance, new biases need to properly characterized. This article will focus on the particular challenges of GPS L5 for Precise Point Positioning (PPP).

[2]As in March 2013

4.3 Ionosphere-free measurements

Ionosphere-free linear combination has been widely used in PPP [Zumberge et al., 1997] as it removes the first order ionospheric effect. For two given (pseudo-range or carrier-phase) measurements S_i and S_j at frequencies f_i and f_j, respectively, the geometry-preserving ionosphere-free combination S_{ij} reads:

$$S_{ij} = \alpha_{ij} S_i + \beta_{ij} S_j \tag{4.1}$$

$$\alpha_{ij} = \frac{f_i^2}{f_i^2 - f_j^2} \tag{4.2}$$

$$\beta_{ij} = 1 - \alpha_{ij} = -\frac{f_j^2}{f_i^2 - f_j^2} \tag{4.3}$$

With triple-frequency GPS, the feasible ionosphere-free combinations can be expressed compactly in matrix form as:

$$\mathbf{L_{IF}} = \begin{bmatrix} S_{12} \\ S_{15} \\ S_{25} \end{bmatrix} = \begin{bmatrix} \alpha_{12} & \beta_{12} & 0 \\ \alpha_{15} & 0 & \beta_{15} \\ 0 & \alpha_{25} & \beta_{25} \end{bmatrix} \cdot \begin{bmatrix} S_1 \\ S_2 \\ S_5 \end{bmatrix} = \mathbf{F} \cdot \mathbf{L_0} \tag{4.4}$$

Under the assumption of uncorrelated observations and same a-priori noise in all carriers ($\sigma_1 = \sigma_2 = \sigma_5 = \sigma_0$), the variance-covariance matrix $\mathbf{\Sigma_0}$ of the original uncombined observations can be expressed as:

$$\mathbf{\Sigma_0} = \begin{bmatrix} \sigma_1^2 & 0 & 0 \\ 0 & \sigma_2^2 & 0 \\ 0 & 0 & \sigma_5^2 \end{bmatrix} = \sigma_0^2 \cdot \mathbf{I} \tag{4.5}$$

Making use of the error propagation law, the resulting covariance matrix of the combined iono-free measurements $\mathbf{\Sigma_{IF}}$ is:

$$\mathbf{\Sigma_{IF}} = \mathbf{F} \cdot \mathbf{\Sigma_0} \cdot \mathbf{F^T} = \sigma_0^2 \cdot \begin{bmatrix} \alpha_{12}^2 + \beta_{12}^2 & \alpha_{12}\alpha_{15} & \beta_{12}\alpha_{25} \\ \alpha_{12}\alpha_{15} & \alpha_{15}^2 + \beta_{15}^2 & \beta_{15}\beta_{25} \\ \beta_{12}\alpha_{25} & \beta_{15}\beta_{25} & \alpha_{25}^2 + \beta_{25}^2 \end{bmatrix} \tag{4.6}$$

Applying the GPS frequencies, the transformation matrix $\mathbf{F}$ and the resulting covariance matrix $\mathbf{\Sigma_{IF}}$ read:

$$\mathbf{F} = \begin{bmatrix} 2.55 & -1.55 & 0 \\ 2.26 & 0 & -1.26 \\ 0 & 12.26 & -11.26 \end{bmatrix} \tag{4.7}$$

$$\mathbf{\Sigma_{IF}} = \sigma_0^2 \cdot \begin{bmatrix} 8.87 & 5.76 & -18.94 \\ 5.76 & 6.70 & 14.19 \\ -18.94 & 14.19 & 276.86 \end{bmatrix} \tag{4.8}$$

From these equations, we can derive the coefficients for the iono-free linear combination and noise amplification factors for each combination:

Combination	α_{ij}	βij	σ_{ij}/σ_0
L1/L2	2.55	-1.55	2.98
L1/L5	2.26	-1.26	2.59
L2/L5	12.26	-11.26	16.64

Tab. 4.2: Ionosphere-free coefficients and noise amplification factors for GPS frequencies

As shown in table 4.2, the L2/L5 linear combination brings a high noise amplification factor which makes it not favorable for high accuracy applications. This is due to the small frequency separation between the two carriers. On the other hand, the L1/L5 combination noise makes it suitable for PPP, and even offers a-priori slightly better performance than the traditional L1/L2 combination.

It is also interesting to look into the correlations introduced by the linear combinations. This can be derived using the correlation matrix $\mathbf{R_{IF}}$, obtained from the variance-covariance matrix as:

$$R_{IF_{ij}} = \frac{\Sigma_{IF_{ij}}}{\sqrt{\Sigma_{IF_{ii}} \Sigma_{IF_{jj}}}} \tag{4.9}$$

The correlation matrix for GPS frequencies reads:

$$\mathbf{R_{IF}} = \begin{bmatrix} 1.00 & 0.75 & -0.38 \\ 0.75 & 1.00 & 0.33 \\ -0.38 & 0.33 & 1.00 \end{bmatrix} \tag{4.10}$$

It is worth mentioning the correlation between ionosphere-free linear combinations, represented by the off-diagonal elements of the matrix $\mathbf{R_{IF}}$. This high-correlation detected implies that the off-diagonal elements of the weight matrix used in least-squares should not be neglected in order to perform a correct parameter estimation and to obtain a realistic a-posteriori covariance matrix. For the particular case of L1/L2 and L1/L5, the variance-covariance and correlation matrices read:

$$\mathbf{R_{IF}^{S_{12},S_{15}}} = \begin{bmatrix} 1.00 & 0.75 \\ 0.75 & 1.00 \end{bmatrix} \tag{4.11}$$

$$\mathbf{\Sigma_{IF}^{S_{12},S_{15}}} = \sigma_0^2 \cdot \begin{bmatrix} 8.87 & 5.76 \\ 5.76 & 6.70 \end{bmatrix} \tag{4.12}$$

In parameter estimation using the L1/L2 and L1/L5 linear combinations, the weight matrix $\mathbf{W}$ is the inverse of the variance-covariance matrix $\mathbf{\Sigma}_{\mathbf{IF}}^{\mathbf{S_{12}},\mathbf{S_{15}}}$.

4.4 Observation model

The observation equations for pseudorange P_n^{ij} and carrier-phase L_n^{ij} from station i to satellite j and frequency f_n read [Collins et al., 2008]:

$$P_n^{ij} = \rho^{ij} + \frac{\kappa}{f_n^2} + \upsilon^{ij}\Gamma^i + c(\delta t^i - \delta t^j) + c(\tau_{P_n}^i - \tau_{P_n}^j) + \varepsilon_{P_n}^{ij} \tag{4.13}$$

$$L_n^{ij} = \rho^{ij} - \frac{\kappa}{f_n^2} + \upsilon^{ij}\Gamma^i + c(\delta t^i - \delta t^j) + c(\tau_{L_n}^i - \tau_{L_n}^j) + \frac{c}{f_n}N_n + \varepsilon_{L_n}^{ij} \tag{4.14}$$

where:

- ρ^{ij} is the distance associated to the non-dispersive delay between the station i and satellite j. This term includes geometric distance (assuming relevant corrections have been accounted for):

$$\rho^{ij} = \sqrt{(x^i - x^j)^2 + (y^i - y^j)^2 + (z^i - z^j)^2} \tag{4.15}$$

  In the absence of publicly available L5-specific antenna phase corrections, we apply for this study those of L2, under the assumption of similarity due to the small frequency separation between L2 and L5 carriers.

- κ/f_n^2 is the first-order ionospheric delay. Higher order terms are not considered for this study.

- $\upsilon^{ij}\Gamma^i$ is the wet component of the troposheric delay, where Γ^i is the tropospheric zenith delay and υ^{ij} the associated elevation-dependent mapping function. Troposphere gradients are not considered here for simplicity. The dry component is removed from the observations using a conventional model.

- c is the speed of light.

- δ^i and δ^j are the station and satellite clock biases respectively.

- $\tau_{P_n}^i$ and $\tau_{P_n}^j$ are the pseudorange delays for frequency f_n, for station and satellite, respectively.

- $\tau_{L_n}^i$ and $\tau_{L_n}^j$ are the Uncalibrated Phase Delays [Laurichesse et al., 2009] for frequency f_n, for station and satellite, respectively.

- N_n is the integer carrier phase ambiguity for frequency f_n.

- $\varepsilon_{S_n}^{ij}$ includes unmodelled errors, such as multipath and thermal noise.

Applying equation 4.1, the ionospheric-free observables, for pseudorange and carrier-phase, for frequencies f_n and f_m read:

$$P^{ij}_{nm} = \rho^{ij} + v^{ij}\Gamma^i + c(\delta t^i_{nm} - \delta t^j_{nm}) + \varepsilon^{ij}_{P_{nm}} \quad (4.16)$$

$$L^{ij}_{nm} = \rho^{ij} + v^{ij}\Gamma^i + c(\delta t^i_{nm} - \delta t^j_{nm}) + a^{ij}_{nm} + \varepsilon^{ij}_{L_{nm}} \quad (4.17)$$

where δt^i_{nm} and δt^j_{nm} are station and satellite ionosphere-free clocks:

$$\delta t^i_{nm} = \delta t^i + \alpha_{nm}\tau^i_{P_n} + \beta_{nm}\tau^i_{P_m} = \delta t^i + \tau^i_{P_{nm}} \quad (4.18)$$

$$\delta t^j_{nm} = \delta t^j + \alpha_{nm}\tau^j_{P_n} + \beta_{nm}\tau^j_{P_m} = \delta t^j + \tau^j_{P_{nm}} \quad (4.19)$$

The resulting ambiguity term a^{ij}_{nm} is in general non-integer, due to the non-integer nature of factor α_{nm} and β_{nm}, and the presence of station and satellite hardware delays:

$$a^{ij}_{nm} = \alpha_{nm}\left(\frac{c}{f_n}N_n + c\tau^i_{L_n} - c\tau^i_{P_n}\right) + \beta_{nm}\left(\frac{c}{f_m}N_m + c\tau^i_{L_m} - c\tau^i_{P_m}\right) \quad (4.20)$$

For the particular case of L1/L2 and L1/L5, the observation equations can be written as:

$$P^{ij}_{12} = \rho^{ij} + v^{ij}\Gamma^i + c(\delta t^i_{12} - \delta t^j_{12}) + \varepsilon^{ij}_{P_{12}} \quad (4.21)$$

$$L^{ij}_{12} = \rho^{ij} + v^{ij}\Gamma^i + c(\delta t^i_{12} - \delta t^j_{12}) + a^{ij}_{12} + \varepsilon^{ij}_{L_{12}} \quad (4.22)$$

$$P^{ij}_{15} = \rho^{ij} + v^{ij}\Gamma^i + c(\delta t^i_{12} - \delta t^j_{12}) + b^{ij}_{15} + \varepsilon^{ij}_{P_{15}} \quad (4.23)$$

$$L^{ij}_{15} = \rho^{ij} + v^{ij}\Gamma^i + c(\delta t^i_{12} - \delta t^j_{12}) + b^{ij}_{15} + a^{ij}_{15} + \varepsilon^{ij}_{L_{15}} \quad (4.24)$$

where δt^j_{12} are the satellite clocks associated to the L1/L2 combination, and the new term b^{ij}_{15} contains inter-frequency biases introduced by both station and satellite:

$$b^{ij}_{15} = c(\delta t^i_{15} - \delta t^j_{15} - \delta t^i_{12} + \delta t^j_{12}) = b^i_{15} - b^j_{15} \quad (4.25)$$

Therefore, the addition of L1/L5 to PPP means that new parameters a^{ij}_{15} and b^{ij}_{15} need to be estimated together with the traditional station coordinates (included in the term ρ^{ij}), station clock bias δt^i_{12}, tropospheric zenith delay Γ^i, and phase ambiguity a^{ij}_{12}.

A least-squares kinematic sequential PPP engine has been implemented according to the guidelines given in [Kouba, 2009], as a new module in NAPEOS v3.3.1 software [Springer and Dow, 2009]. In the new implementation, the design matrix has been extended with the partial derivatives of the observations with respect to the new parameters, as shown in table 4.3. With only three IIF satellites it is not yet possible to perform L1/L5 standalone PPP, so L1/L5 combinations are processed together with L1/L2. No significant PPP accuracy improvement can be expected with just three satellites transmitting the L5 signal, but this approach will allow us to look at the particularities of the new signals, that will be addressed in the following sections.

4.5 L5 tracking data: the IGS MGEX network

Following the GNSS systems modernization, the International GNSS Service (IGS) [Dow et al., 2009] has recently started the Multi-GNSS EXperiment (MGEX), which aims at

	P_{12}^{ij}	L_{12}^{ij}	P_{15}^{ij}	L_{15}^{ij}
x^i	$(x^i - x^j)/\rho^{ij}$	$(x^i - x^j)/\rho^{ij}$	$(x^i - x^j)/\rho^{ij}$	$(x^i - x^j)/\rho^{ij}$
y^i	$(y^i - y^j)/\rho^{ij}$	$(y^i - y^j)/\rho^{ij}$	$(y^i - y^j)/\rho^{ij}$	$(y^i - y^j)/\rho^{ij}$
z^i	$(z^i - z^j)/\rho^{ij}$	$(z^i - z^j)/\rho^{ij}$	$(z^i - z^j)/\rho^{ij}$	$(z^i - z^j)/\rho^{ij}$
Γ^i	υ^{ij}	υ^{ij}	υ^{ij}	υ^{ij}
$c \cdot \delta t_{12}^i$	1	1	1	1
a_{12}^{ij}	0	1	0	0
a_{15}^{ij}	0	0	0	1
b_{15}^{ij}	0	0	1	1

Tab. 4.3: Partial derivatives of the observations with respect to the estimated parameters, for triple-frequency PPP.

providing the scientific community with adequate tracking of new systems and signals, using state-of-the-art geodetic equipment. A call for proposals was issued at the end of 2011, and several world-wide organizations joined the experiment, both on the provision of GNSS tracking data and processing analysis.

As shown in figure 4.1, the network deployment started early in 2012 and Rinex3 [Gurtner and Estey, 2009] observation files are being made available for post-processing at Crustal Dynamics Data Information System (CDDIS) and Bundesamt für Kartographie und Geodäsie (BKG) data centers. Real-time users can also access data via real-time RTCM streams.

Figure 4.2 shows a map with the current network status. Almost all MGEX stations provide adequate tracking of GPS L5 signals. Only station WARN (Rostock-Warnemuende), equipped with a JPS Legacy receiver, is not able to provide GPS L5 tracking.

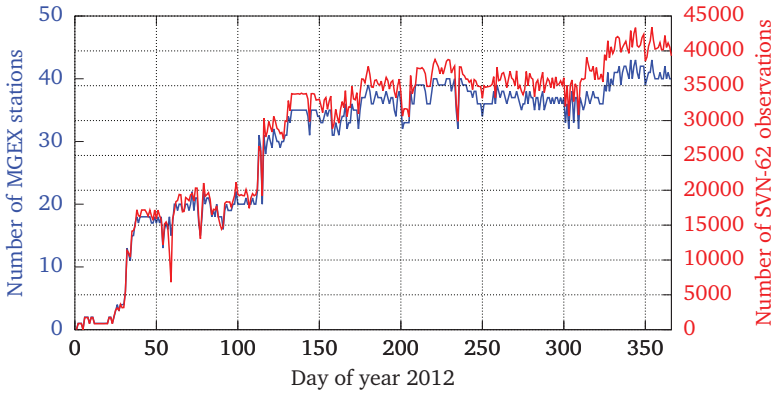

Fig. 4.1: MGEX network evolution, including number of stations available daily at CDDIS data centre, and observations for IIF SVN62 (PRN25), at 30s sampling rate.

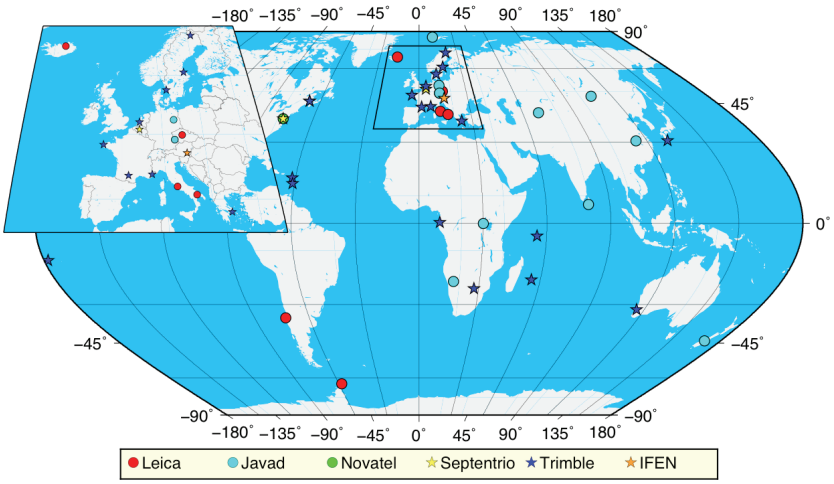

Fig. 4.2: MGEX network including receiver manufacturer distribution (as per DOY 362 2012)

Table 4.4 shows the distribution of receiver types in the MGEX network, together with the Rinex3 observables available from each receiver.

		L1		L2					L5	
Receiver type	Stations	C1C	C1W	C2W	C2D	C2X	C2L	C2P	C5X	C5Q
Trimble NETR9	19	✓		✓		✓			✓	
Javad Delta G3T	10	✓	✓	✓		✓			✓	
Leica GR1200+GNSS	5	✓		✓		✓			✓	
Septentrio PolarRx4	3	✓	✓	✓			✓			✓
Leica GR10	2	✓		✓		✓			✓	
Leica GR25	1	✓		✓		✓			✓	
Javad JPS Legacy	1	✓						✓		
Ifen SX_NSR_RT_800	1	✓			✓	✓			✓	
Novatel OEM6	1	✓			✓					✓

Tab. 4.4: Receivers available in the MGEX network (as per DOY 362 2012). Rinex3 pseudorange tracking modes for each receiver type are included. Rinex3 tracking modes are described in [Gurtner and Estey, 2009].

Focusing on the L5 tracking in particular, figure 4.3 represents the signal to noise ratio (SNR) measurements for PRN01 for station BRUX (equipped with a Septentrio PolarRx4 receiver), as a function of the satellite elevation angle. The signal level for the L5 pilot signal (S5Q) is about 4-5 dB higher than other signals available. This is consistent with the specifications given in the GPS Interface Control Document [GPS Directorate, 2011a], that for L5 states a minimum received power of -157.9 dBW, higher compared to -158.5 dBW for L1 C/A and -160 dBW for L2C [GPS Directorate, 2011b]. Notable is also the increased power level of the L2C signal (S2L) compared to the legacy P-code (S2W). The increased power observed in L5 brings important advantages regarding robustness against interference and signal fading due to, i.e. scintillation. Although SNR is very much receiver-dependent, similar patterns have been observed for other MGEX stations.

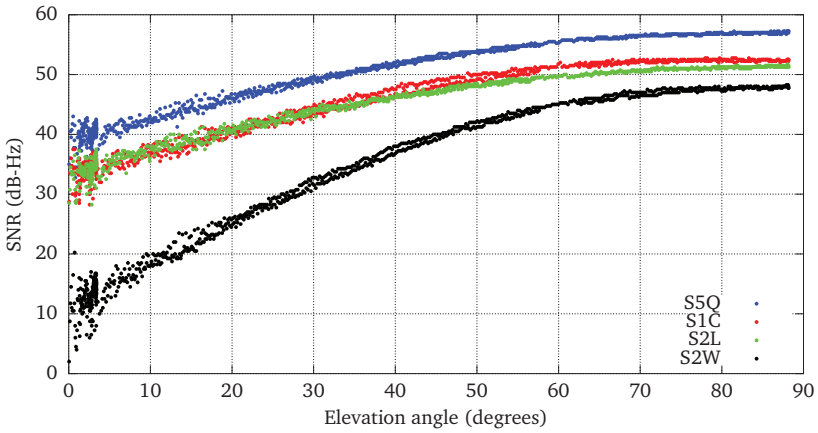

Fig. 4.3: Signal to Noise Ratio for PRN01 as a function of satellite elevation, reported by station BRUX (Septentrio PolarRx4 receiver) on DOY 173 2012

In order to assess the impact of forming ionosphere-free linear combinations including L5, we analyze zero-baseline data from 2 MGEX receivers (WTZZ and WTZR) located at the Wetzell Geodetic Observatory (Germany). Double differenced pseudorange minus phase observables are shown in figure 4.4 (left), together with the equivalent using the iono-free combinations derived from equation 4.4 (right). According to observation equations 4.16 and 4.17, residual observation noise is obtained, as all other effects are cancelled out. It is clearly visible that the L2/L5 combination is not favorable for PPP, because of the high noise amplification factor resulting from the small frequency separation. This is consistent with the theoretical analysis explained in section 4.3. L1/L2 and L1/L5 linear combinations have similar resulting noise level, and will be further analyzed in sections 4.6 and 4.7.

4.6 Interfrequency biases

For PPP processing, IGS Final Orbits and Clock products are taken as input in the PPP engine, which is fed with MGEX daily Rinex3 observation data. In this section we have a look at

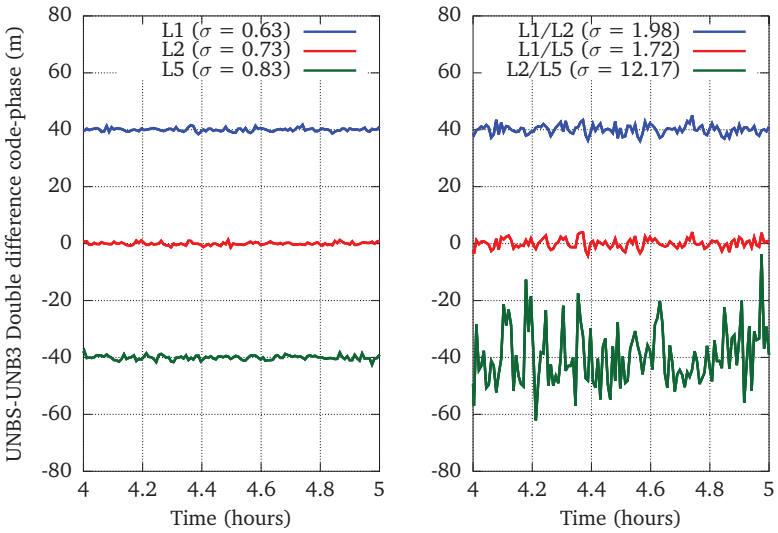

Fig. 4.4: Double-difference code-phase measurements for original measurements in L1, L2 and L5 carriers (left) and ionosphere-free linear combinations (right). Observation data is a zero-baseline configuration located at Wetzell (Germany), corresponding to WTZZ and WTZR receivers. An arbitrary offset has been applied to each signal to improve plot clarity.

the interfrequency bias term b_{15}^{ij} estimated in the PPP process according to the observation equations presented in section 4.3.

As shown in table 4.4, MGEX stations present a variety of different observables, depending on the tracking mode selected by each receiver manufacturer. For our PPP processing, P-code in L1 and L2 measurements are selected, for compatibility with the IGS products. For those receivers that only provide C/A measurements in L1, the P1-C1 biases provided by CODE IGS analysis center are applied. For the L5 signals, each receiver provides one kind of measurement, either the dataless pilot component (C5Q/L5Q) or the combined I+Q component (C5X/L5X). For simplicity, L2C signals are not used in this study. The reader is referred to [Leandro et al., 2008] for a detailed analysis on the impact of L2C in PPP.

The signals selected for PPP processing are summarized in table 4.5. It is important to mention that Sepentrio receivers are reporting pseduranges C1W and C1C, but only report phase as L1C. In principle the L1C and L1W phases are different by a quarter cycle, but the Rinex3.01 format specifies that phase observables have to be aligned, meaning that the receiver is already applying this quarter cycle when generating the Rinex3.01 file. In any case, this phase-offset could be absorbed by the ambiguity term a_{12}^{ij}, and thus does not have further impact in this study.

Receiver Type	L1	L2	L5	P1-C1 bias applied
Trimble	C1C/L1C	C2W/L2W	C5X/L5X	✓
Leica	C1C/L1C	C2W/L2W	C5X/L5X	✓
Septentrio	C1W/L1C	C2W/L2W	C5Q/L5Q	
Javad	C1W/L1W	C2W/L2W	C5X/L5X	
IFEN	C1C/L1C	C2D/L2D	C5X/L5X	✓
Novatel	C1C/L1C	C2D/L2D	C5Q/L5Q	✓

Tab. 4.5: Rinex3 Code and phase observations selected for PPP processing.

Typical PPP performance is shown in figure 4.5, together with the epoch-wise estimates of b_{15}^{ij}, for the three IIF satellites. It can be seen from the plot that there are significant bias differences, and therefore three independent b_{15}^{ij} parameters, one per satellite, are actually needed. It is assumed that these inter-frequency biases are constant over time, at least over the typical 24 hours run length, thus no process noise is added to the variance-covariance matrix between consecutive epochs. The daily estimates of b_{15}^{ij}, for both IIF satellites, observed from several stations, are represented in figure 4.6. The day-to-day repeatability appears to be at decimeter level, taking into account that this interfrequency biases depend on the pseudorange observations.

Figure 4.7 represents the biases observed from each station in the MGEX network, for a particular day. There are significant differences between different receivers, but it can be observed that receivers from the same manufacturer experience similar biases. Station CUT0 (Curtin) is an exception, but no sensible explanation has been found to explain the difference with other Trimble NETR9 receivers. Noticeable also is the big offset value observed by the IFEN receiver at station GRAB (Graz).

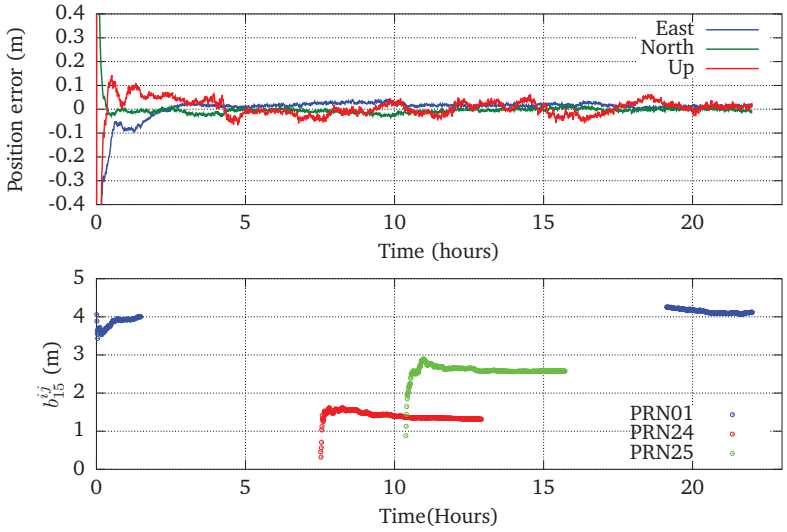

Fig. 4.5: PPP performance for station GMSD (Nakatane, Japan) on DOY 346 2012, including the estimated interfrequency bias parameter b_{15}^{ij}.

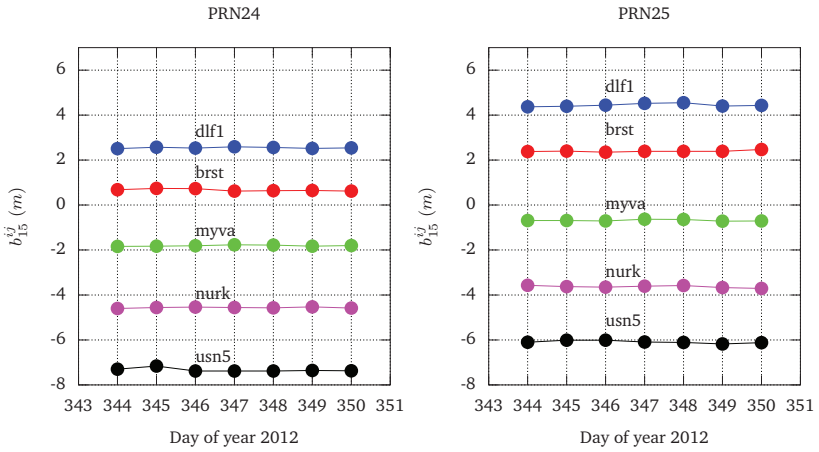

Fig. 4.6: Daily estimates for inter frequency bias parameter b_{15}^{k}, for IIF satellites PRN24 and PRN25, observed from MGEX stations DLF1 (Delft), BRST (Brest), MYVA (Reykjavik), NURK (Kigali), and USN5 (Washington).

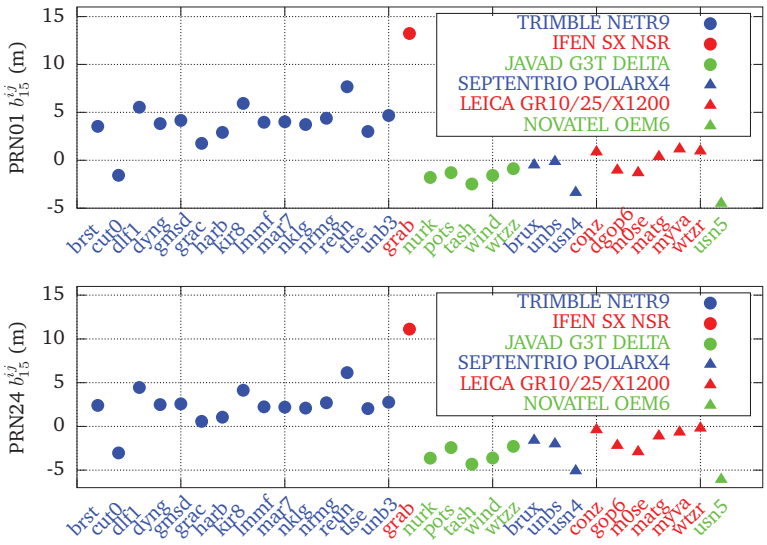

Fig. 4.7: Interfrequency bias estimates for PRN01 and PRN24 for each MGEX station during GPS Week 1718.

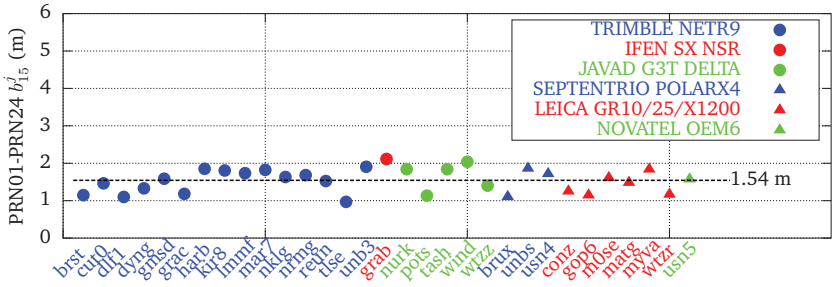

Fig. 4.8: Differential PRN01-PRN24 inter frequency code bias observed from the MGEX station network (GPS week 1718).

Figure 4.8 shows the difference in the estimated biases between PRN01 and PRN24, for each station. The idea here is to remove the station dependent biases (b_{15}^{i} in equation 4.25) and come-up with a satellite-only dependent bias b_{15}^{j}. The agreement obtained from different receivers is very good, and the overall estimated satellite difference bias value is 1.54 meters (5.1 nanoseconds). It is also notable that no visible difference is observed between receivers tracking the pilot Q component (Novatel, Septentrio) and those tracking the combined signal I+Q (Trimble, Leica, Javad and Ifen).

The estimation of the satellite interfrequency biases brings an important advantage for PPP users. As we have seen, in absence of this information, the PPP implementation needs to estimate an additional parameter b_{15}^{ij} for each IIF satellite. However, if the satellite biases are estimated (as described in this section) and provided to an PPP end-user, the algorithm

will be simplified, as a single receiver-dependent b_{15}^{i}, valid for all IIF satellites, could be sufficient to include L1/L5 measurements.

4.7 The phase anomaly

It was first presented in [Montenbruck et al., 2011] that SVN-62 (PRN25) has an abnormal phase behavior, causing an apparent clock anomaly in the L1/L5 ionosphere free phase combination with respect to the L1/L2. This is probably due to uncontrolled thermal effects in the satellite. The phase variations are dependent mainly on the elevation of the Sun over the orbital plane, commonly known as the β angle. This phenomenon reaches the maximum effect during the eclipse seasons ($|\beta| < 14^{o}$). We address in this section how the phase anomaly can impact PPP processing.

Figure 4.9 shows the L1/L5 PPP phase residuals for PRN24 and PRN25. It is clear that the ambiguity term a_{15}^{ij}, which is assumed to be constant over a satellite pass, cannot absorb the time-variant phase anomaly for the satellites. This effect has also been observed in the third IIF satellite PRN01 in a similar way. This L5 phase anomaly is fairly significant, and can cause PPP performance degradation if not properly accounted for, specially when more IIF satellites will become available and the contribution from L5 observables increases.

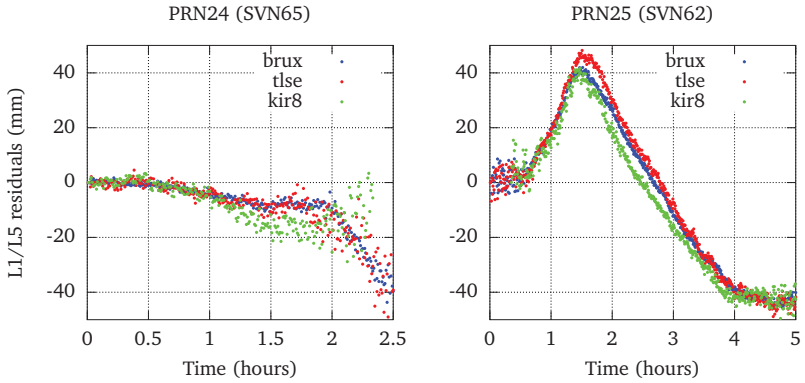

Fig. 4.9: L1/L5 PPP phase residuals for PRN24 (left) and PRN25 (right) for stations BRUX (Brussels), BRST (Brest) and KIR8 (Kiruna).

There are several possibilities to address the phase anomaly in PPP. The first option is to assign stochastic properties to the ambiguity parameters a_{15}^{ij}, so that they can absorb the time variations of the L1/L5 phase measurements. The problem with this approach is the difficulty in assigning an adequate a-priori spectral density to the parameter. Additionally, the approach will limit the contribution of the L1/L5 measurements to the position domain, as the new observations will mainly contribute to the additional time-variant ambiguity.

A second approach is to estimate a different set of satellite clock biases δt_{15}^{j}, using L1/L5 observations only, than can be input to the PPP algorithm together with the traditional L1/L2-

derived clocks δt^j_{12}. The L1/L5-based clocks are able to assimilate the temporal variations, so that a constant ambiguity term a^{ij}_{15} can be estimated for kinematic positioning.

In order to assess the feasibility of this approach, L1/L5-based clocks are generated in a two-step process. In the first step, a static PPP network solution is performed using L1/L2 ionosphere-free observations, that allows the estimation of tropospheric delays Γ^i and station clock biases δt^i_{12} for all stations in the MGEX network. In the second step, these parameters are kept fixed and only the satellite clocks for the IIF satellites are estimated using L1/L5 ionosphere-free observations only. In this case, the observation model can be re-written using a decoupled clock model:

$$P^{ij}_{12} = \rho^{ij} + v^i\Gamma^{ij} + c(\delta t^i_{12} - \delta t^j_{12}) + \varepsilon^{ij}_{P_{12}} \quad (4.26)$$

$$L^{ij}_{12} = \rho^{ij} + v^i\Gamma^{ij} + c(\delta t^i_{12} - \delta t^j_{12}) + a^{ij}_{12} + \varepsilon^{ij}_{L_{12}} \quad (4.27)$$

$$P^{ij}_{15} = \rho^{ij} + v^i\Gamma^{ij} + c(\delta t^i_{12} - \delta t^j_{15}) + b^i_{15} + \varepsilon^{ij}_{P_{15}} \quad (4.28)$$

$$L^{ij}_{15} = \rho^{ij} + v^i\Gamma^{ij} + c(\delta t^i_{12} - \delta t^j_{15}) + b^i_{15} + a^{ij}_{15} + \varepsilon^{ij}_{L_{15}} \quad (4.29)$$

Where δt^{ij}_{12} is the satellite clock corresponding to the L1/L2 observations (as provided in IGS Final clock product), while δt^{ij}_{15} is the new set of estimated L1/L5 satellite clocks. It is to be noted that this clock includes also the satellite-dependent part of the term b^j_{15}, while the remaining receiver-dependent part is noted as b^i_{15}.

Figure 4.10 shows the comparison between L1/L5 clock and the original L1/L2 clocks. It can be clearly seen the more significant sub daily variations for PRN25 during the eclipse season ($\beta = 9^o$), while the variations for PRN01 are much smaller ($\beta = 76^o$). The new δ^j_{15} have been applied to the PPP engine for the L1/L5 measurements. The new residuals shown in figure 4.11 confirm that the anomaly is compensated with this approach.

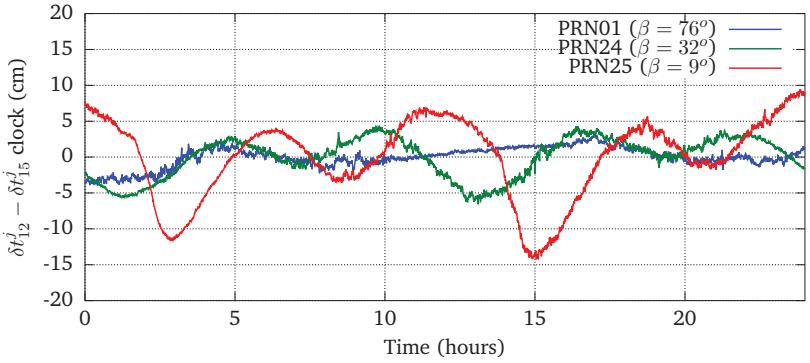

Fig. 4.10: Comparison between L1/L2 and L1/L5 clocks, for all three IIF satellites on DOY 344 2012. The daily bias per satellite has been removed from the time series.

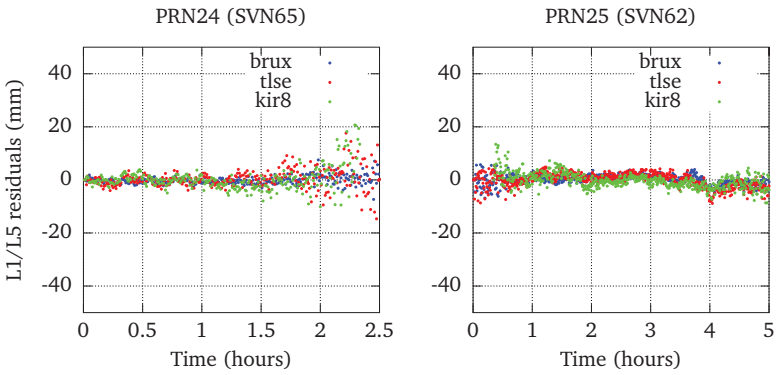

Fig. 4.11: L1/L5 PPP phase residuals for PRN24 (left) and PRN25 (right) after L1/L5-based clocks are applied.

4.8 Conclusions

New GPS signals in L5 present interesting properties that make them attractive for the most precise applications, such as PPP. When forming ionosphere-free linear combinations, however, the observations noise is amplified, and this effect is particularly severe for the L2/L5 combination, because of the reduced frequency separation. However, the amplification noise of L1/L5 combinations is reasonable. The L1/L5 combination is therefore the preferred complement to the traditional L1/L2 observations. This will increase robustness in situations where there is poor L2 tracking due to for example, interferences or ionospheric scintillation.

However, due to the frequency difference, satellite and receiver interfrequency biases arise that need to be taken into account in the PPP engine. An extended design matrix is therefore needed to accommodate the additional parameters. Using this formulation, we can conduct an interfrequency bias analysis. Different groups of values have been observed between several stations depending on the receiver type. Furthermore, if the station component is removed using single differences, the interfrequency bias between the two GPS IIF satellites can be adequately estimated using PPP.

Regarding the phase performance, the known L5 phase anomaly can degrade the PPP accuracy if not properly handled. This can be mitigated by providing the PPP user with an additional set of L1/L5 clocks so that observed phase ambiguity can be actually considered constant. The new L1/L5 clocks absorb the temporal phase variations as well as the interfrequency bias.

Finally, thanks to the efforts of IGS, the MGEX network data is providing routinely adequate tracking for all new signals, which is of great interest for the scientific community. This study would not have been possible without such data.

5 Paper B: Real-time Precise Point Positioning using BeiDou

Paper title: "Real-time Precise Point Positioning using BeiDou"
Authors: Javier Tegedor, Kees de Jong[1], Xianglin Liu[1], Erik Vigen[2], Ola Øvstedal[3]
Accepted for publication in the *International Association of Geodesy Symposia*
Manuscript Submitted: 12 October 2013
Manuscript Accepted: 5 December 2013

Contents

5.1 Abstract

Satellite positioning is evolving rapidly, with the deployment of Galileo and BeiDou systems, in addition to the modernisation programmes for GPS and GLONASS. At the time of writing, the BeiDou constellation consists of 5 Geostationary Orbit (GEO), 5 Geosynchronous Orbit (IGSO) and 4 Medium-Earth Orbit (MEO) satellites. The constellation design is particularly interesting as it allows visibility of a sufficient number of BeiDou satellites over Asia for autonomous positioning. In this paper, possibilities for real-time precise point positioning (PPP) using BeiDou are explored.

For real-time generation of orbit and clock products, observation data from Fugro's proprietary station network are used, together with data from the IGS Multi-GNSS Experiment (MGEX). In order to perform orbit estimation, the NAPEOS (Navigation Package for Earth Orbiting Satellites) software has been extended for processing BeiDou data.

[1]Fugro Intersite BV, Leidschendam (The Netherlands)
[2]Fugro Satellite Positioning AS, Oslo (Norway)
[3]Norwegian University of Life Sciences, Department of Mathematical Sciences and Technology

Satellite orbits are generated every hour and include a predicted part which can be used for real-time positioning. In order to estimate the accuracy of the real-time orbit, a validation with post-processed products is presented.

A Kalman filter has been extended to process BeiDou observation data, in order to estimate satellite clock biases in real-time.

For precise point positioning, Fugro's kinematic PPP engine is used. The engine is fed with real-time orbits and clocks, as well as observation data from test receivers. Kinematic PPP results are presented, in real-time and post-processing, including BeiDou standalone and in combination with GPS.

5.2 Introduction - BeiDou status

BeiDou, the Chinese satellite navigation system, started with the experimental phase from 2000 to 2003. During this period, three geostationary satellites were put in orbit, known as BeiDou 1B, 1C and 1D, which constituted the initial regional phase of the system, known as BeiDou-1.

Tab. 5.1: Operational BeiDou satellites in August 2013 (Source: www.celestrack.org).

PRN	Common Name	Launch date	COSPAR ID	NORAD ID	Position
C01	BeiDou G1	2010-01-16	2010-001A	36287	140.0° East
C02	BeiDou G6	2012-10-25	2012-059A	38953	80.0° East
C03	BeiDou G3	2010-06-02	2010-024A	36590	84.7° East
C04	BeiDou G4	2010-10-31	2010-057A	37210	160.0° East
C05	BeiDou G5	2012-02-24	2012-008A	38091	58.8° East
C06	BeiDou IGSO 1	2010-07-31	2010-036A	36828	
C07	BeiDou IGSO 2	2010-12-17	2010-068A	37256	
C08	BeiDou IGSO 3	2011-04-09	2011-013A	37384	
C09	BeiDou IGSO 4	2011-07-26	2011-038A	37763	
C10	BeiDou IGSO 5	2011-12-01	2011-073A	37948	
C11	BeiDou M3	2012-04-29	2012-018A	38250	Plane B / slot 4
C12	BeiDou M4	2012-04-29	2012-018B	38251	Plane B / slot 3
C13	BeiDou M5	2012-09-18	2012-050A	38774	Plane A / slot 7
C14	BeiDou M6	2012-09-18	2012-050B	38775	Plane A / slot 8

The operational system, known as Compass/BeiDou-2 is well under development. The constellation has been designed to provide augmented navigation services over China, thanks to Inclined Geosynchronous Orbit (IGSO) and Geostationary Orbit (GEO) satellites, in addition to Medium Earth Orbit (MEO) satellites for providing global coverage. At the time of writing, the constellation consists of 14 operational satellites, whose characteristics are detailed in table 5.1. The ground track is depicted in figure 5.1. The second phase of

BeiDou foresees the operation of up to 27 MEO satellites before 2020, offering worldwide positioning coverage.

BeiDou has been designed for transmitting three carrier frequencies: 1561.098 MHz (B1), 1207.14 MHz (B2) and 1268.52 MHz (B3) [Grelier, 2007]. The Interface Control Document for the open-service signals on the B1 carrier was released in December 2012. [CSNO, 2012].

BeiDou has drawn the attention of the scientific community since its very beginning. Shortly after the first MEO M1 satellite was launched in 2007, ranging codes were obtained thanks to the use of high-gain antennas and advanced signal processing techniques [Grelier, 2007, Wilde et al., 2007, Gao et al., 2009]. Initial results for orbit determination of M1 satellite using Satellite Laser Ranging (SLR) were presented in [Hauschild et al., 2011a], together with clock estimates obtained using microwave observations from two GNSS receivers.

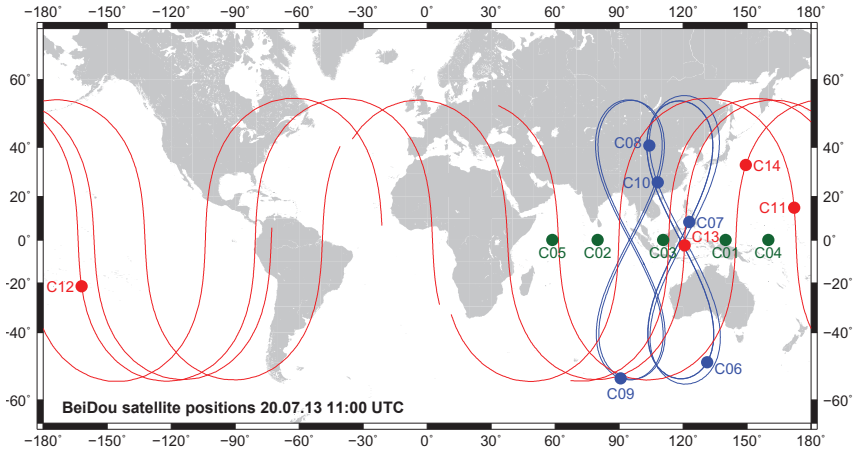

Fig. 5.1: Ground track for BeiDou constellation, as of July 20th 2013. IGSO satellites in blue, MEO satellites in red and GEO satellites in green.

Initial positioning results using a reduced 3-GEO and 3-IGSO constellation were presented in [Shi et al., 2012]. Using experimental broadcast ephemerides, accuracies of tens of meters were achieved with absolute positioning. Regarding relative positioning, accuracy below decimeter level was obtained in a short baseline configuration. A characterization of triple-carrier ionosphere-free linear combination for BeiDou frequencies was presented in [Montenbruck et al., 2012]. In the same study, ambiguity resolution was also attempted in a short baseline configuration making use of the extra wide-lane observations with the signals on the B2 and B3 frequencies.

The first assessment on precise orbit determination using GNSS data for GEO and IGSO satellites was presented in [Steigenberger et al., 2013], where several solar radiation pressure parametrisations were assessed. In that study, the GEO orbit accuracy was limited to few meters due to the reduced size of the tracking network available. Further results using an

extended network are available in [?], where sub-meter orbit errors were achieved for the first time.

In this study, we assess the possibility of real-time navigation with BeiDou, using the Precise Point Positioning technique [Zumberge et al., 1997]. For the generation of satellite orbit and clock estimates, a global GNSS tracking network is used, which is described in section 5.3. Section 5.4 presents the processing strategy for real-time PPP. In section 5.5, BeiDou orbit results are given. BeiDou standalone positioning results are presented in section 5.6, and combined GPS and BeiDou positioning is discussed in section 5.7. Conclusions are summarized in section 5.8.

5.3 BeiDou tracking networks: MGEX and Fugro

In 2010, the International GNSS Service (IGS) [Dow et al., 2009] started the MGEX campaign [Rizos et al., 2013], in order to provide the scientific community with tracking data for the new GNSS signals and systems, using state-of-the art geodetic equipment. At the time of writing, a subset of the stations in the network are equipped with BeiDou-capable equipment, including Trimble NETR9, Javad Delta G3T and Septentrio PolaRx4 geodetic receivers.

In parallel, Fugro has upgraded the Trimble NETR9 receivers in its proprietary reference station network in order to support new constellations, on top of the existing commercial G2 PPP service based on GPS and GLONASS [Melgard et al., 2009].

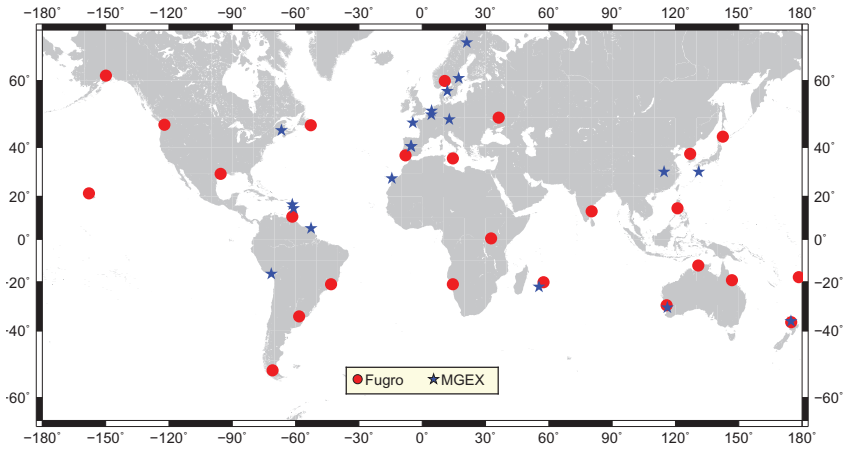

Fig. 5.2: BeiDou tracking network, including Fugro and MGEX stations (August 2013).

In order to obtain the highest possible accuracy in orbit and clock estimation, all available stations from both networks are used. Figure 5.2 shows the combined station network, and the receiver type distribution is summarized in table 5.2. Although many of the stations are located in Europe, the network is still reasonably well distributed, thus providing worldwide tracking of BeiDou with an adequate level of redundancy.

Regarding the observation types available, it has been found that not all MGEX receivers available are tracking BeiDou satellites; this depends not only on the receiver type, but also on particular firmware installed in each receiver. A summary of the receivers available with BeiDou observations is displayed in table 5.2. Regarding observations types, all Trimble NETR9 receivers are providing pseudorange and carrier-phase observables in the three BeiDou carrier frequencies, B1 B2 and B3. However, Javad Delta G3T and Septentrio PolaRx4 receivers are not providing tracking data in B3, due to a current limitation in the receiver hardware and/or firmware. In order to maximize data availability for the orbit computation, B1 and B2 frequencies are used in this study, which are processed using the well-known ionosphere-free linear combination.

Tab. 5.2: BeiDou-capable receivers available from Fugro and MGEX networks.

Receiver Type	Fugro	MGEX	B1	B2	B3
Trimble NETR9	25	13	✓	✓	✓
Septentrio PolaRx4	0	7	✓	✓	
Javad Delta G3T	0	1	✓	✓	

5.4 Processing strategy

The processing strategy for real-time PPP is depicted in figure 5.3, where BeiDou data is processed together with GPS. The NAPEOS software package [Springer and Dow, 2009] is used to generate an orbit prediction suitable for real-time applications. The software has been enhanced in order to process BeiDou observation data via RINEX3 format [IGS and RTCM-SC104, 2013]. For the orbit estimation, hourly observation files from both Fugro and MGEX stations are used. MGEX station data is downloaded from the CDDIS data centre (ftp://cddis.nasa.gov). The Fugro data arriving in real-time via Trimble's RT27 format is converted to RINEX3 using a specific converter. The predicted orbit, based on NAPEOS batch-runs using 48 hours of observation data, is updated every hour, in order to ensure short prediction times and thus avoiding large orbit errors for real-time PPP. For generation of real-time satellite clocks, a Kalman filter has been developed where both BeiDou- and GPS-data are processed using the predicted orbits as fixed values. The Kalman filter also estimates ancillary parameters, such as station clock biases, wet tropospheric delays and carrier-phase ambiguities. GPS-BeiDou intersystem biases are estimated as part of the orbit adjustment, and kept fixed for real-time clock estimation. The Kalman filter is fed with observation data coming from the Fugro network, which is available in real-time with few seconds latency.

Finally, orbit prediction and real-time clock estimates are injected into Fugro proprietary PPP engine, together with observation data from the RT27 streams, in order to obtain station coordinates in real-time making use of BeiDou satellites.

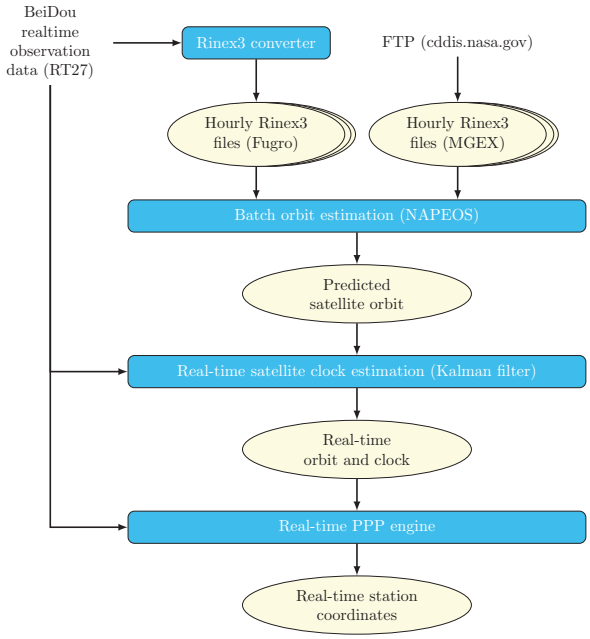

Fig. 5.3: Processing strategy for real-time PPP.

5.5 Orbit results

In an attempt to assess the accuracy of the BeiDou orbits, the real-time estimates are compared against a post-processed product stemming from 24 hours of observation data. It is assumed that the post-processed orbit has higher accuracy, therefore this comparison is a good assessment of the accuracy of the real-time orbit, which is later used in PPP.

Daily statistics of the orbit comparison are presented in figure 5.4. The accuracy of IGSO and MEO satellites is very good, down to sub-decimeter level. However, the orbit accuracy of GEO satellites is worse, at decimeter level, including some meter-level outliers, specially for the along-track orbit component. The reason for the lower orbit accuracy for GEO satellites is mainly the lack of geometry variation for these satellites, as they appear static in the sky observed from each reference station. These poor geometry conditions weaken the observability of the orbit dynamics, affecting the estimated orbit parameters. These results are consistent with the analysis previously presented in [**?**]. The radial and cross-track orbit components are still very good, and the GEO satellites can be used in PPP.

It should be noted that there are still a number of factors limiting the orbit quality in the network adjustment. These are mainly due to modeling uncertainties, such as precise satellite antenna phase center corrections for BeiDou satellites, which are available for GPS [Schmid et al., 2005]. For the BeiDou satellites, the antenna phase center offsets proposed in the MGEX campaign have been used, namely [0.6 0.0 1.1] meters in XYZ in the satellite body-fixed reference frame. For the BeiDou frequencies, antenna phase center corrections

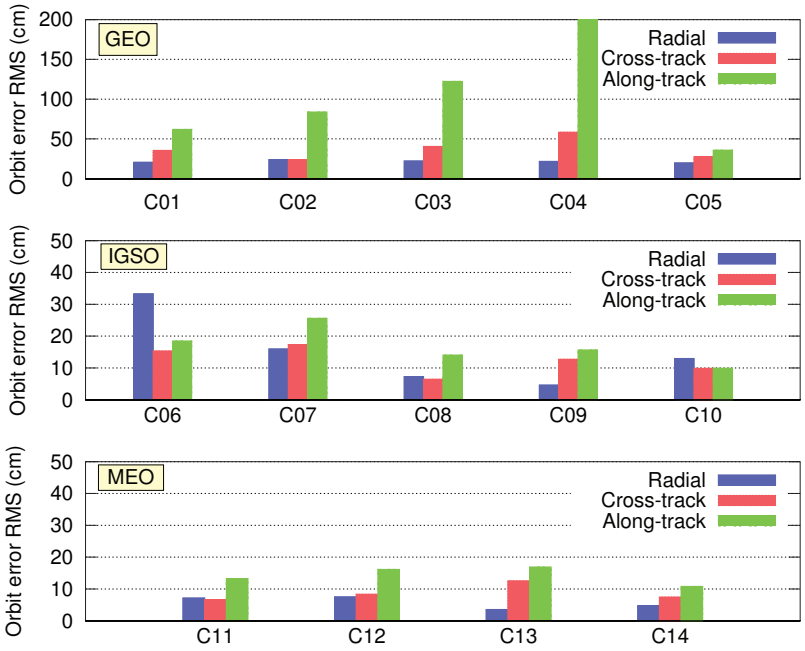

Fig. 5.4: Orbit comparison results (real-time vs post-processed) on August 17th, 2013.

are not yet publicly available for receiver antennas. Furthermore, BeiDou satellite modeling needs to be improved, in particular regarding solar radiation pressure and attitude modeling. In this study, CODE empirical model with 5 parameters has been used for solar radiation pressure. Finally, ambiguity resolution is a promising way to improve the orbit quality, in the same way as it can be done for GPS [Ge et al., 2005]. The assessment of ambiguity resolution for BeiDou goes beyond the scope of this article, as it needs an extensive characterization of BeiDou signals.

5.6 BeiDou standalone PPP

In order to assess PPP performance, several Fugro reference stations in the Asia-Pacific region are selected, as they have full visibility of the BeiDou constellation, including also GEO and IGSO satellites, and data can be processed in real-time via data streams in RT27 format.

In particular, stations located in Chennai (India), Manila (Philipines), Darwin and Perth (Australia) are selected for this analysis. Polar visibility plots for these stations are depicted in figure 5.5.

Precise point positioning results for station Perth are represented in figure 5.6, where the PPP engine is run in kinematic mode using 10 seconds observation sampling. These results were obtained in real-time using BeiDou-standalone PPP on August 17th, 2013. The good visibility of the BeiDou constellation allows to have enough satellites in view for continuous

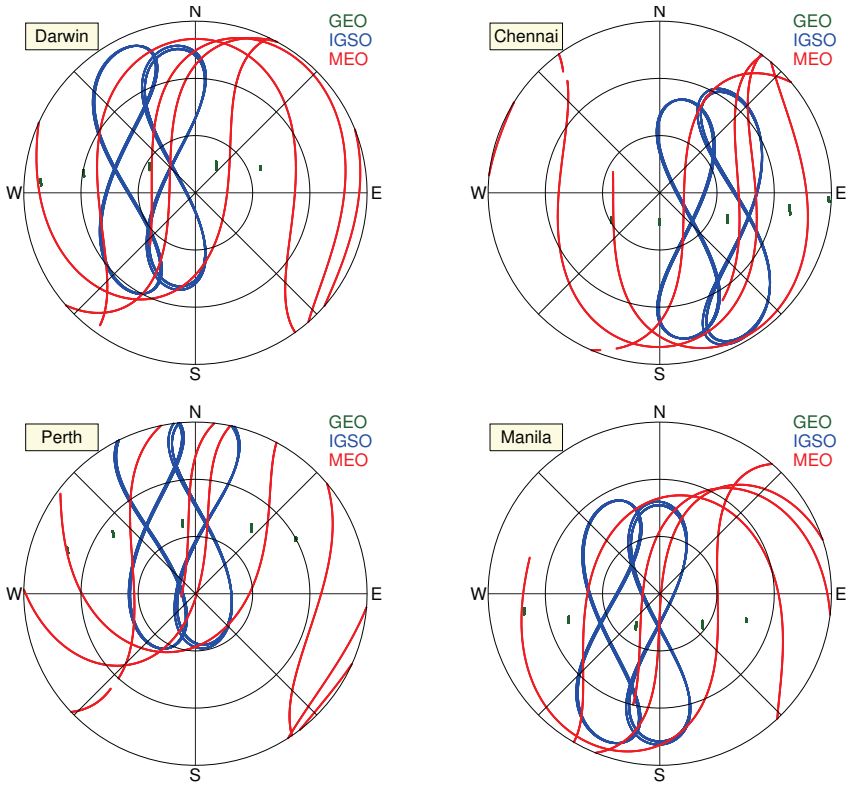

Fig. 5.5: Polar visibility plots for Fugro stations in Darwin, Chennai, Perth and Manila.

positioning. However, the satellite geometry is occasionally suboptimal as can be observed in the increased values for horizontal and vertical dilution of precision (HDOP and VDOP) in the second half of the day. Horizontal positioning errors for the three other stations are presented in figure 5.7. In order to compare real-time versus post-processed solutions, the

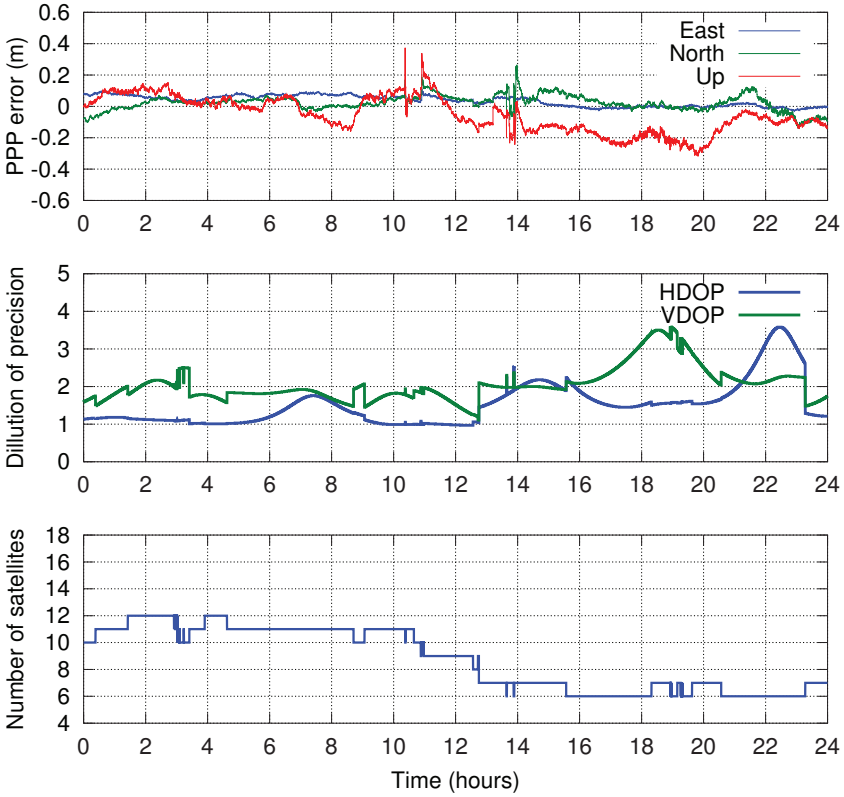

Fig. 5.6: Real-time BeiDou-standalone PPP results for Perth, on August 17th, 2013.

PPP engine has also been run using the post-processed orbit and clock solution mentioned in section 5.5. The PPP configuration between the real-time and the post-processed solution is identical, the only difference is the source of orbit and clocks. Positioning statistics for the four stations are summarized in table 5.3. The post-processed solution is significantly more accurate than the real-time one; the reason is mainly the higher quality of the post-processed orbit and clock estimates.

Tab. 5.3: BeiDou standalone PPP statistics (RMS), on August 17th 2013.

Station	Real-time			Post-processing		
	East (cm)	North (cm)	Up (cm)	East (cm)	North (cm)	Up (cm)
Darwin	6.09	5.88	16.14	4.24	4.40	7.81
Perth	4.73	5.27	12.63	1.31	3.75	4.44
Chennai	8.68	5.90	15.25	3.41	1.63	8.02
Manila	7.60	4.68	13.60	3.38	1.59	8.71

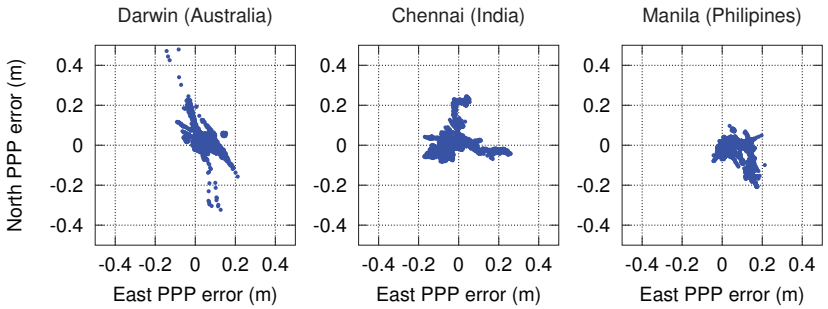

Fig. 5.7: Real-time horizontal results for BeiDou PPP, on August 17th, 2013.

5.7 GPS + BeiDou PPP

In this section, the contribution of BeiDou on top of GPS-based PPP is addressed. In order to obtain positioning statistics in different configurations, the PPP engine is run in post-processing using the satellite orbit and clocks obtained in real-time, as described in section 5.4. Additionally, the PPP engine is restarted every hour, in order to observe the improvement in convergence time when adding BeiDou on top of GPS. Figure 5.8 represents average position error as a function of time since PPP start, for all four stations from 18th to 22nd of August 2013. A total of 480 independent PPP runs have been performed for this analysis.

It is interesting to observe that adding BeiDou on top of GPS systematically improves PPP position accuracy and reduces convergence time by several minutes. These results are very encouraging, taking into account the current limitations on BeiDou tracking data and satellite modelling.

5.8 Conclusions

In this article, the first real-time PPP results using BeiDou have been presented. Using a well distributed station network, real-time orbit accuracy can be achieved at decimeter level for MEO and IGSO satellites, and around meter-level for GEO satellites. The accuracy of GEO

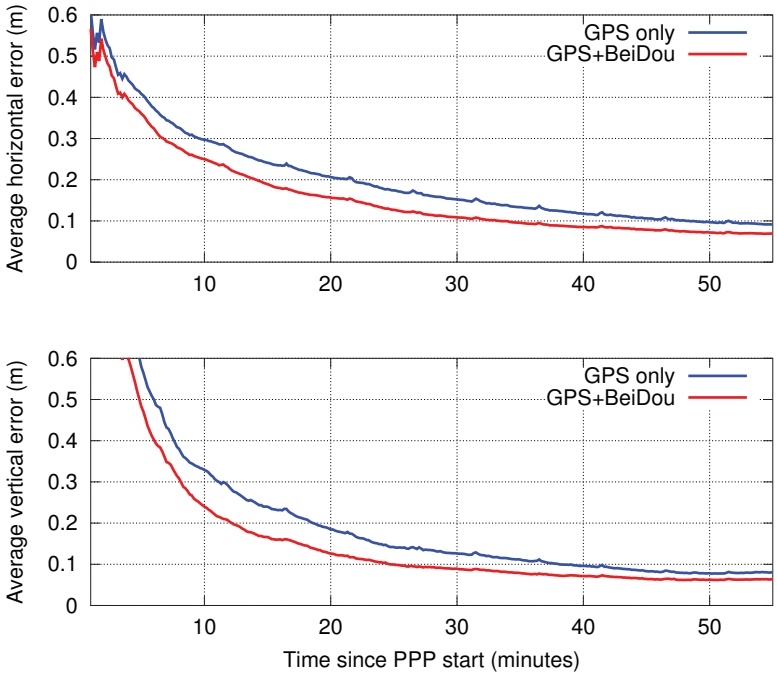

Fig. 5.8: Convergence time analysis for GPS standalone and BeiDou+GPS.

orbits is mainly limited due to lack of geometry change, resulting in poor observability of the orbit dynamic parameters.

The real-time positioning accuracy using BeiDou PPP standalone is around 5 cm horizontal and 15 cm vertical, for stations with good visibility of IGSO and GEO satellites. Post-processed PPP results are significantly better thanks to the higher quality of post-processed orbits and clocks. Regarding convergence time, it has been observed that combined GPS and BeiDou PPP converges faster than GPS standalone, thanks to the enhanced visibility and satellite geometry when adding the new constellation.

The overall BeiDou accuracy is currently limited by the number of receivers with BeiDou tracking capability, as well as modeling limitations for BeiDou, such as antenna phase center corrections, solar radiation pressure and attitude modelling. Taking these limitations into account, the positioning results are very promising and will likely improve following the further development of the BeiDou constellation, as well as further improvements in the processing models for these satellites.

6 Paper C: Muti-constellation Orbit Determination and PPP using GPS, Glonass, Galileo and BeiDou

Paper title: "Multi-constellation Precise Orbit Determination and Point Positioning using GPS, Glonass, Galileo and BeiDou"
Authors: Javier Tegedor, Erik Vigen[1], Ola Øvstedal[2]
Published in *Journal of Geodetic Science*, Vol 4, Issue 1, Pages 65-73, 2014
DOI: 10.2478/jogs-2014-0008
Manuscript Submitted: January 20, 2014
Manuscript Accepted: April 3, 2014

Contents

6.1 Abstract

State of the art Precise Point Positioning (PPP) is currently based on dual-frequency processing of GPS and Glonass navigation systems. The International GNSS Service (IGS) is routinely providing the most accurate orbit and clock products for these constellations,

[1]Fugro Satellite Positioning AS, Oslo (Norway)
[2]Norwegian University of Life Sciences, Department of Mathematical Sciences and Technology

allowing point positioning at centimeter-level accuracy. At the same time, the GNSS landscape is evolving rapidly, with the deployment of new constellations, such as Galileo and BeiDou. The BeiDou constellation currently consists of 14 operational satellites, and the 4 Galileo In-Orbit Validation (IOV) satellites are transmitting initial Galileo signals. This paper focuses on the integration of Galileo and BeiDou in PPP, together with GPS and Glonass. Satellite orbits and clocks for all constellations are generated using a network adjustment with observation data collected by the IGS Multi-GNSS Experiment (MGEX), as well as from Fugro proprietary reference station network. The orbit processing strategy is described, and orbit accuracy for Galileo and BeiDou is assessed via orbit overlaps, for different arc lengths. Kinematic post-processed multi-GNSS positioning results are presented. The benefits of multi-constellation PPP are discussed in terms of enhanced availability and positioning accuracy.

Keywords: BeiDou, Galileo, Intersystem-biases, Multi-constellation Precise Point Positioning

6.2 Introduction

The Precise Point Positioning (PPP) technique [Zumberge et al., 1997] has become increasingly significant in high-precision positioning applications during recent years [Kanzaki et al., 2011, Geng et al., 2010], as it allows the estimation of accurate receiver coordinates, without the need of a nearby reference station. PPP has other interesting applications, such as time-transfer [Defraigne et al., 2008], ionospheric [Leandro et al., 2007a] and tropospheric characterization [Kjørsvik et al., 2006], or biases calibration [Leandro et al., 2010].

The International GNSS Service (IGS) is routinely generating the most accurate orbit and clock estimates, for GPS and Glonass satellites, by means of a dense global network and several contributing analysis centers [Dow et al., 2009]. Making use of these products and precise observation modeling [Kouba and Héroux, 2001], static absolute positioning can be achieved at centimeter level accuracy in post-processing. Sub-decimeter level accuracy can be achieved in kinematic applications [Hesselbarth, 2011]. Real-time users can also access orbit and clock corrections via RTCM streams, enabling decimeter-level accuracy in real-time [Caissy et al., 2012]. In addition, there are several commercial PPP services making use of GPS and Glonass, such as Fugro‘s G2 [Melgard et al., 2009] or Trimble‘s RTX [Leandro et al., 2011], which also supports the Japanese QZSS (Quasi-Zenith Satellite System).

The current development of BeiDou and Galileo constellations offers new prospects for precise navigation, when combined with traditional GPS and Glonass PPP, thanks to the increased number of satellites available. At the time of writing, the BeiDou constellation consists of 5 Geostationary Orbit (GEO), 5 Inclined Geosynchronous Orbit (IGSO) and 4 Medium-Earth Orbit (MEO) satellites, providing regional coverage around China for continuous positioning. The constellation deployment is expected to resume in 2014, with the further development of the MEO constellation, in order to achieve global coverage before the end of this decade. The Galileo constellation is currently composed of 4 initial

In-Orbit-Validation (IOV) satellites. The Full Operational Capability (FOC) phase is expected to start also in 2014 with the launch of the first operational satellites.

This article focuses on the contribution of Galileo and BeiDou to PPP. A prerequisite is the generation of precise satellite orbits and clocks for the new constellations. This is done using a network least-squares adjustment, making use of observation data from the IGS Multi-GNSS Experiment (MGEX), as well as from Fugro's proprietary network, which has been made available for this study. The network and the observables available are described in section 6.3.

Ionosphere-free observation equations for multi-GNSS PPP are presented in section 6.4, where constellation-dependent intersystem biases are introduced, for Galileo and BeiDou. The processing strategy for orbit and clock estimation is presented in section 6.5, together with an assessment of the orbit accuracy. The estimated intersystem biases are presented in section 6.6. Kinematic multi-GNSS positioning results are presented in section 6.7, where the benefits of adding Galileo and BeiDou to PPP are discussed. Conclusions are summarized in section 6.8.

6.3 Tracking data

For GPS and Glonass, the International GNSS Service (IGS) has been providing observation data for scientific purposes during the last twenty years. With the development of new navigation systems, IGS started in 2011 the Multi-GNSS Experiment (MGEX) [Rizos et al., 2013], aiming at upgrading the current station network to support new constellations. Most of the stations in the MGEX campaign are Galileo-capable, and a subset of them are also tracking BeiDou. The Japanese QZSS system is also observed by the network, but this system has not been included in this study, as the contribution to PPP is still relatively small, with only one satellite (QZSS-1) available at the moment.

At the same time, Fugro is operating a worldwide reference station network for supporting its commercial positioning services, mainly for maritime applications. A subset of the stations in the network have been upgraded to Galileo and BeiDou capability.

A map of the stations available in both networks is depicted in figure 6.1. It can be observed that, although there is a concentration of stations in Europe, the network still provides a fairly good global coverage. Particularly relevant are the stations located in Asia-Pacific area, for the tracking of BeiDou IGSO and GEO satellites.

Regarding the frequency plan for the new constellations, BeiDou is broadcasting signals in three carrier frequencies: 1568.091 MHz (B1), 1207.14 MHz (B2) and 1268.52 MHz (B3) [Grelier, 2007], whereas Galileo is transmitting open signals in E1 (1575.42 MHz), E5a (1176.45 MHz), E5b (1207.14 MHz) and E5a+b (1195.795 MHz) [European Commision, 2010], in addition to the future commercial service in the E6 carrier (1278.75 MHz). It is to be noted that BeiDou and Galileo are sharing the B2/E5b carrier, while Galileo and GPS are sharing both L1/E1 and L5/E5a carriers. This opens the door to interoperability applications,

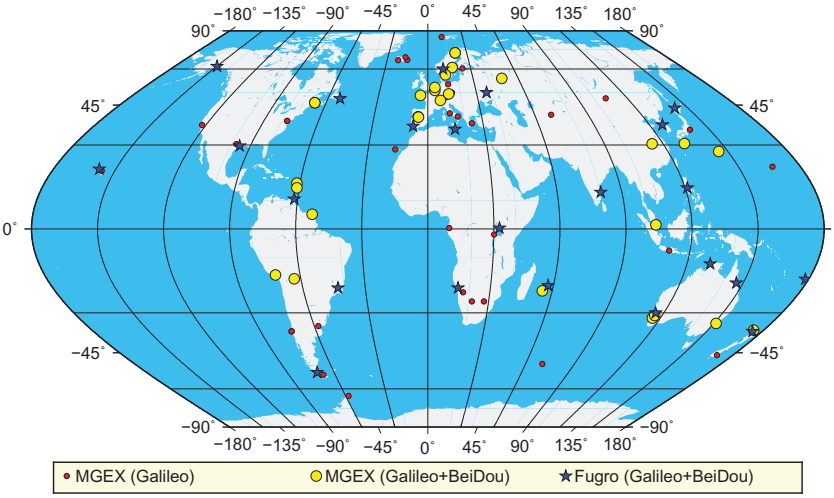

Fig. 6.1: Geographical distribution of MGEX and Fugro stations, indicating tracking capability for Galileo and BeiDou (August 2013).

which are out of the scope of this study. The reader is referred to [Melgard et al., 2013] for a study on interoperability of GPS and Galileo using E1/E5a in PPP.

All the Fugro stations, equipped with Trimble NETR9 receivers, are providing Galileo and BeiDou data in all frequencies. However, it has been found that, for MGEX stations, the signals availability depends on the receiver model, the firmware installed in each receiver and/or the way of generating Rinex3 files from raw data. Table 6.1 summarizes the number of stations per receiver type in the network, and the availability for Galileo and BeiDou tracking for each receiver type.

Tab. 6.1: Receiver type distribution in the MGEX network as per August 15th, 2013. Number of stations tracking each Galileo and BeiDou frequency are shown.

Receiver Brand	Model	Number of stations	Galileo				BeiDou		
			E1	E5a	E5b	E5a+b	B1	B2	B3
Javad	Delta G2T	3	3	3	0	0	0	0	0
	Delta G3T	23	23	23	1	1	1	1	0
Leica	GR10	4	4	4	4	4	0	0	0
	GR25	4	4	4	1	1	0	0	0
	GRX1200	5	5	5	5	5	0	0	0
Novatel	OEM6	1	1	1	0	0	0	0	0
Septentrio	AsteRx3	1	1	1	1	1	1	1	0
	PolaRx4	6	6	6	6	6	6	6	0
	PolaRx4TR	2	2	2	2	2	1	1	0
	PolaRxS	1	1	1	1	1	1	1	0
Trimble	NETR9	26	22	22	22	22	17	17	17
TOTAL		**78**	**72**	**72**	**43**	**43**	**27**	**27**	**17**

For instance, the majority of Javad G3T Delta receivers are tracking Galileo only on E1 and E5a frequencies. Actually only one Javad receiver (WTZZ, Wetzell, Germany), which is equipped with the most modern receiver board and firmware, is also tracking E5b and E5a+b signals, as well as BeiDou B1 and B2 signals.

Septentrio receivers are generally not able to track the BeiDou B3 signals, due to a limitation in the current receiver firmware. Some other stations equipped with Trimble NETR9 receivers are not providing any Galileo or BeiDou measurements, probably due to the way these receivers are configured by the station operators.

In order to maximize data availability with the existing observations, Galileo E1 and E5a, as well as BeiDou B1 and B2 signals have been selected for the subsequent analysis. The observables are processed using the ionosphere-free linear combination, whose observation equations are detailed in the next section.

6.4 Observations equations

For this study, the GPS observation equations proposed by [Collins et al., 2008] have been extended for accommodating multi-GNSS observations, adding inter-systembias parameters between different constellations. The resulting ionosphere-free observations equations, for each GNSS, for pseudorange P and carrier-phase L, between station i and satellite j, are:

$$P_i^{j,GPS} = \rho_i^j + \upsilon^j \Gamma_i + c(\delta t_i - \delta t^j) + \varepsilon_{P_i}^j \quad (6.1)$$

$$L_i^{j,GPS} = \rho_i^j + \upsilon^j \Gamma_i + c(\delta t_i - \delta t^j) + a_i^j + \varepsilon_{L_j}^j \quad (6.2)$$

$$P_i^{j,GLO} = \rho_i^j + \upsilon^j \Gamma_i + c(\delta t_i - \delta t^j + ISB_i^{j,GLO}) + \varepsilon_{P_i}^j \quad (6.3)$$

$$L_i^{j,GLO} = \rho_i^j + \upsilon^j \Gamma_i + c(\delta t_i - \delta t^j + ISB_i^{j,GLO}) + a_i^j + \varepsilon_{L_i}^j \quad (6.4)$$

$$P_i^{j,GAL} = \rho_i^j + \upsilon^j \Gamma_i + c(\delta t_i - \delta t^j + ISB_i^{GAL}) + \varepsilon_{P_i}^j \quad (6.5)$$

$$L_i^{j,GAL} = \rho_i^j + \upsilon^j \Gamma_i + c(\delta t_i - \delta t^j + ISB_i^{GAL}) + a_i^j + \varepsilon_{L_i}^j \quad (6.6)$$

$$P_i^{j,BEI} = \rho_i^j + \upsilon^j \Gamma_i + c(\delta t_i - \delta t^j + ISB_i^{BEI}) + \varepsilon_{P_i}^j \quad (6.7)$$

$$L_i^{j,BEI} = \rho_i^j + \upsilon^j \Gamma_i + c(\delta t_i - \delta t^j + ISB_i^{BEI}) + a_i^j + \varepsilon_{L_i}^j \quad (6.8)$$

where:

- ρ_i^j is the geometric distance between station and satellite, assuming relevant corrections, such as antenna phase center corrections or phase wind-up, have been already accounted for.

- $\upsilon^j \Gamma_i$ is the wet tropospheric delay between station and satellite, where Γ_i is the tropospheric zenith delay and υ^j is the associated elevation-depending mapping function. The dry component of the tropospheric delay is removed from the observations using an a-priori model.

- δt_i and δt^j are the epoch-wise receiver and satellite clock offsets, respectively. Following this notation, it has been assumed that there is a single receiver clock common to all observables from different GNSS. GNSS-differences are accounted for in the intersystem-bias terms.

- c is the speed of light.

- $ISB_i^{j,GLO}$ is the GPS-Glonass intersystem-bias term. It is to be noted that this bias depends on each station i and satellite j, due to the Frequency Division Multiple Access (FDMA) scheme implemented by Glonass, which induces receiver- and satellite-dependent inter-channel biases. As shown in [Reussner and Wanninger, 2011], each frequency (satellite) encounters a slightly difference delay in the receiver.

- ISB_i^{GAL} and ISB_i^{BEI} are the GPS-Galileo and GPS-BeiDou intersystem-biases, respectively. Contrary to Glonass, it is to be noted that these are satellite-independent, as Galileo and BeiDou have adopted the Code Division Multiple Access (CDMA) scheme, meaning that all satellites from the same constellation use the same carrier-frequency. Significant biases appear though depending on the receiver model, but might depend also on the digital signal processing (firmware) happening inside the receiver. It needs to be mentioned that the new generation of Glonass satellites (Glonass-K) is expected to implement CDMA as well.

- a_i^j is the ambiguity term between station and satellite, associated to the carrier-phase measurements. For the ionosphere-free linear combination, this term is in general not integer, due to non-integer nature of the combination coefficients, and the presence of satellite and receiver hardware delays [Laurichesse et al., 2009].

- $\varepsilon_{P_i}^j$ and $\varepsilon_{L_i}^j$ are unmodelled effects, such as thermal noise and multipath, for pseudorange and carrier-phase, respectively. It is to be noted that, for GNSS measurements, $\varepsilon_{L_i}^j << \varepsilon_{P_i}^j$.

6.5 Orbit and clock estimation

6.5.1 Processing strategy

For estimation of orbit and clocks, NAPEOS [Springer and Dow, 2009] software package has been used. The software has been extended to process BeiDou, on top of the existing capabilities for GPS, Glonass and Galileo. The processing strategy, depicted in figure 6.2, will be described next.

In order to obtain an a-priori orbit, broadcast ephemeris can be used for GPS and Glonass. For Galileo, test ephemeris started in March 2013, but satellites are still unhealthy meaning that this data might not always be reliable. For BeiDou, MGEX stations are at the moment not providing any ephemeris. For these reasons, Two Line Elements (TLEs) are used , for both Galileo and BeiDou, in order to obtain an a-priori orbit initialization. The accuracy of this a-priori orbit is at sub-kilometer level. TLEs can be downloaded from www.space-track.org, which also includes the format description.

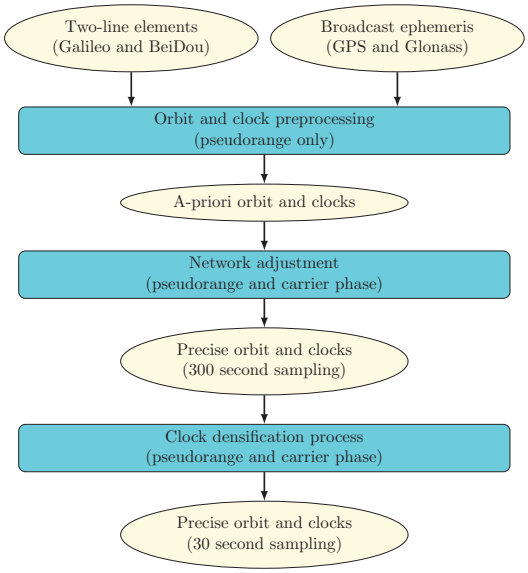

Fig. 6.2: Processing strategy for generation of orbit and clocks, including Galileo and BeiDou.

In a first processing step, a least-squares estimation using only pseudorange observations is performed, in order to improve the TLE-derived orbits and to obtain a-priori satellite clocks for Galileo and BeiDou. After this step, the orbit accuracy is around meter-level, similar to what is obtained for GPS and Glonass via broadcast ephemerides.

In a second step, both pseudorange and carrier-phase observations are used, in order to benefit from the precision of the carrier-phase measurements. Estimated parameters are the satellite state vectors, solar radiation pressure parameters, wet tropospheric delays, satellite and station clocks, intersystem-bias terms and carrier-phase ambiguities.

Finally, in order to obtain suitable clocks for PPP at 30 seconds sampling, a final clock densification process is performed. In this final step, only station and satellite clocks are estimated. All other parameters are kept fixed to the previous estimates.

6.5.2 Modeling for Galileo and BeiDou

A summary of the models being used for all constellations is presented in table 6.2. Being relatively new constellations, BeiDou and Galileo have a number of modeling limitations compared to more mature systems, such as GPS and Glonass. The impact of these limitations will be addressed in the current section.

Tab. 6.2: Summary of models used for multi-GNSS processing.

	GPS	Glonass	Galileo	BeiDou
Observation sampling	30 seconds			
Elevation cut-off	10 degrees			
Signal selection	L1/L2		E1/E5a	B1/B2
Antenna phase center corrections	IGS Antex file		A-priori values	
Tropospheric modeling	GPT/GMF [Boehm et al., 2007]			
Ionospheric modeling	First order removed by linear combination			
Solar Radiation Pressure	CODE Empirical Model with 5 parameters			

GPS and Glonass precise antenna phase center corrections [Schmid et al., 2007] have been made available as part of the IGS activities via the Antenna Exchange (ANTEX) format, both for transmitting and receiving antennas. These precise corrections are not yet available for neither Galileo nor BeiDou. For satellite antennas, the MGEX project has released approximate values for the distance between the satellite center of mass and the antenna phase center. These are [0.2, 0, 0.6] m for Galileo and [0.6, 0, 1.1] m for BeiDou, XYZ in the satellite body-fixed reference frame. It is expected that these values have an uncertainty around decimeter level. Nadir- or azimuth- dependent corrections are not available for these constellations so far.

On the receiving antennas, the phase center offset and azimuth- and elevation-dependent variations for Galileo and BeiDou frequencies are expected to be slightly different (up to few centimeters) to the ones used for GPS, due to the different frequencies used by Galileo and BeiDou. At the time of writing, there are no publicly available calibrations for the antennas used in MGEX stations. For this study, GPS calibrations have been used for Galileo and BeiDou, which introduces an additional uncertainty below decimeter level.

Satellite attitude modeling is not fully known for the new constellations. Under nominal attitude, yaw-steering mode has been assumed for Galileo and BeiDou, in the same way as for GPS [Kouba, 2008]. The behavior of the new satellites under eclipse seasons remains a topic for further research. A mismodelling of the satellite attitude in GNSS impacts the wind-up correction in carrier-phase measurements [Wu et al., 1993], due to the relative orientation between transmitting and receiving antennas.

In order to limit the impact of this uncertainty in PPP, the very same models have been applied in the orbit adjustment and in the precise point positioning estimation.

6.5.3 Orbit quality

For the orbit estimation, two different sets of daily solutions have been generated, in order to assess the impact of the orbit arc length on the orbit accuracy. The first solution is based on 24 hours arcs, while the second is based of 72 hours, where the central 24 hours are extracted as daily solutions.

In order to estimate the orbit quality for GPS and Glonass, a comparison with IGS Final products has been performed. For the 3-day arc orbits, the monthly RMS is 1.7 cm for GPS, 3.9 cm for Glonass.

Regarding BeiDou and Galileo satellites, the orbit precision can be assessed by measuring orbit differences between consecutive solutions at day boundaries. The monthly RMS values obtained for these day boundary differences, for both 1-day and 3-days arc solutions, for each Galileo and BeiDou satellite, are shown in table 6.3. Sample GPS and Glonass satellites have been included for reference.

It can be observed that the 3-day orbit solution improves significantly the orbit precision with respect to the 1-day solution, thanks to the better observability of the orbit dynamics over longer data arcs. Additionally, GEO orbit precision is typically lower than MEO and IGSO orbits, mainly on the along-track component. This could be explained by the fact that there is no geometry variation between the GEO satellites and the reference station network, which weakens the orbit estimation. Nevertheless, sub-decimeter level accuracy could still be achieved on the radial and cross-track components.

It is also interesting to note that the 3-day orbit solutions for IGSO satellites C07 and C10 are significantly worse than other IGSO satellites. The reason being that these satellites were under Earth eclipse periods during the first two weeks of August 2013. As mentioned earlier, precise attitude modeling for these satellites needs to be studied in order to obtain accurate orbits also during eclipse seasons.

For Precise Point Positioning, the 3-day orbit solution will be used, in order to achieve the highest possible accuracy. Additionally, the GEO satellites have been deweighted with a factor of 3 in PPP with respect to IGSO and MEO, in order to account for orbit uncertainty in these satellites.

Tab. 6.3: Orbit day-boundary differences (RMS), during August 2013, for 24 and 72 hours orbit arcs. All units are centimeters.

Satellite Type	PRN	1-day orbit arcs			3-day orbit arcs		
		Radial	Along-track	Cross-track	Radial	Along-track	Cross-track
GPS	G01	4.5	4.6	2.7	0.6	0.5	0.5
	G25	1.7	5.3	2.3	0.4	0.5	0.5
Glonass	R02	3.1	7.7	4.4	0.3	1.1	1.3
	R03	3.1	8.1	4.7	0.4	1.3	1.2
Galileo	E11	7.4	18.3	9.8	2.7	11.6	3.4
	E12	6.0	15.0	9.5	3.5	8.7	2.3
	E19	4.8	22.5	12.3	1.3	3.7	3.5
	E20	4.2	19.2	9.3	1.2	3.7	3.5
BeiDou GEO	C01	16.2	87.3	15.2	2.0	24.2	3.9
	C02	81.9	185.9	9.0	6.3	30.7	11.9
	C03	45.8	121.0	19.3	10.4	38.7	5.1
	C04	34.4	76.7	10.6	3.3	25.9	5.2
	C05	50.1	113.7	15.3	5.3	30.7	9.1
BeiDou IGSO	C06	58.9	22.4	16.9	3.0	4.3	2.7
	C07	24.7	22.1	24.3	15.4	60.5	11.8
	C08	22.8	12.8	16.6	1.8	4.7	2.5
	C09	17.0	10.9	10.2	1.0	2.2	1.8
	C10	24.6	15.3	17.6	13.1	35.1	9.6
BeiDou MEO	C11	4.5	44.8	11.5	1.2	6.6	2.6
	C12	4.2	54.3	10.6	1.4	7.3	2.8
	C13	5.0	48.5	16.2	0.9	7.9	4.8
	C14	5.2	50.2	17.7	0.9	8.2	5.2

6.6 Intersystem biases

When processing multi-GNSS observations, intersystem-biases need to be taken into account. For Glonass, these biases have been extensively analyzed in the literature [Chuang et al., 2013, Wanninger, 2012], and this study will mainly focus on Galileo and BeiDou. As described in section 6.4, a single parameter per station and system (either Galileo or BeiDou) is enough to account for intersystem biases, as all satellites are using the same carrier frequency.

Additionally, in order to define the clock datum, a zero-mean condition has been applied to all intersystem-biases in the orbit and clock estimation process, for each constellation. This approach allows to assess relative differences in intersystem-biases between different receivers in the network.

The daily intersystem biases for each constellation are depicted in figure 6.3. Generally, a strong receiver-type dependency can be observed, with all stations with the same receiver model showing similar biases. An exception has been found in receiver WTZZ (Javad Delta G3T), which shows significant differences with respect to other Javad receivers. One possible explanation is that this receiver has a different architecture that allows it to track also BeiDou. It is also to be noted that the BeiDou intersystem-bias for WTZZ is different by more than 100 ns compared to Trimble or Septentrio receivers, meaning the effect is significant enough and cannot be ignored for precise applications. Additionally, it is noticeable that there are

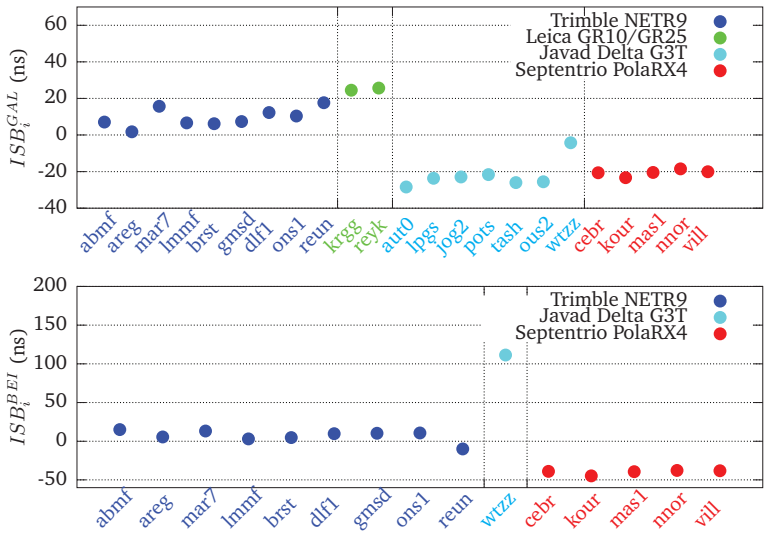

Fig. 6.3: Intersystem-bias estimates for several receivers in the MGEX network, for Galileo (top) and BeiDou (bottom).

still small remaining differences with stations equipped with the same receiver type. This might be due to antenna- or cable-induced delays, or thermal effects between hardware installations at different locations.

6.7 Precise Point Positioning assessment

For multi-constellation Precise Point Positioning, a new kinematic PPP algorithm has been implemented in NAPEOS, based on sequential least squares, following the guidelines given in [Kouba, 2009], and the observation equations described in section 6.4.

In order to assess the effect of multi-constellation precise point positioning, some reference stations from the MGEX network have been selected. These are KOUR (Kourou, French Guyana), BRST (Brest, France), NNOR (New Norcia, Australia) and JFNG (Jiufeng, China). The station locations are indicated in figure 6.4.

All stations are tracking GPS, Glonass, Galileo and BeiDou MEO. In addition, JFNG and NNOR are also tracking BeiDou IGSO and GEO satellites, thanks to their geographical location.

Figure 6.5 shows kinematic multi-GNSS PPP results for station NNOR on August 26th, 2013. The 95% position error quantiles are 1.74, 1.16 and 3.95 cm, in the East, North and Up components, respectively, after removing the first two hours of convergence period. It

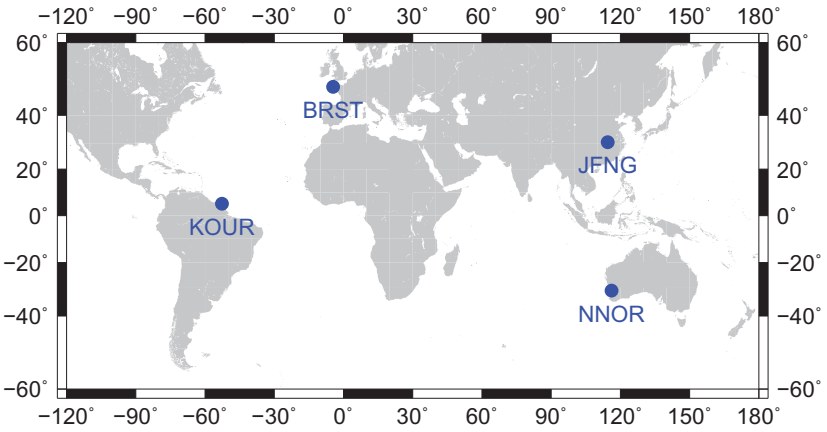

Fig. 6.4: MGEX stations selected for multi-GNSS PPP.

is interesting to notice the high number of satellites available for PPP when using all 4 constellations, resulting in a very stable geometry (Dilution of Precision - DOP).

In order to assess the benefits of multi-GNSS PPP, daily kinematic PPP results have been obtained for the month of August 2013, for all four stations, in different configurations: GPS only, GPS+Glonass, GPS+Glonass+Galileo and GPS+Glonass+Galileo+BeiDou. The monthly average of the daily 95% position error percentile is summarized in figure 6.6.

As shown in previous studies [Hesselbarth, 2011], the contribution of Glonass on top of GPS is quite significant in terms of kinematic positioning, thanks to the increased number of satellites available and improved geometry. For example, the NNOR vertical error is reduced by 36.3% when adding Glonass on top of GPS. Galileo further improves the vertical error by 3.5%, and the additional improvement with BeiDou is 6.7%. The contribution of Galileo on top of GPS and Glonass is relatively small, due to the small number of satellites available, which are visible from a station for a limited hours per day. The contribution of BeiDou is slightly more important, specially in JFNG and NNOR, where IGSO and GEO also contribute to the positioning solution in those locations.

Multi-constellation PPP is particularly suitable in situations with reduced sky visibility, where the increased number of satellites allows to obtain a significant higher availability and accuracy compared to standalone GPS. In order to simulate this scenario, the PPP engine has been run with several elevation cut-off angles from 0 (full sky visibility) to 35 (reduced sky visibility). The results for station NNOR are depicted in figure 6.7, in terms of positioning accuracy and average dilution of precision. It can be observed how the accuracy of the GPS-only solution degrades rapidly with partial sky visibility. The multi-GNSS solution behaves significantly better in this condition, in particular the one with all four constellations, where sub-decimeter level accuracy can still be obtained even in the 35 degrees cut-off scenario, mainly thanks to the increased number of satellites visible for BeiDou, on top of GPS, Glonass

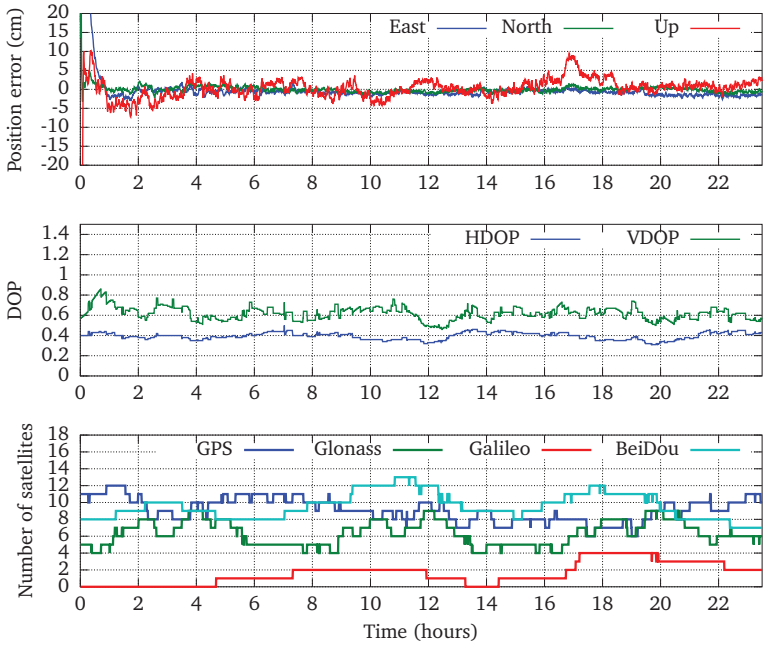

Fig. 6.5: PPP kinematic results for station NNOR on August 26th, 2013.

and Galileo. In this case, Galileo improves the vertical accuracy by 12.6%, and BeiDou brings an additional 33.1% improvement.

Regarding static PPP, it has been found that the addition of Galileo and BeiDou does not significantly improve the daily coordinate repeatability. The reason is that the quality of 24 hours GPS-only PPP is already at centimeter level, and the addition of new constellations does not improve significantly the accuracy. This was shown already for the case of GLONASS in [Hesselbarth, 2011].

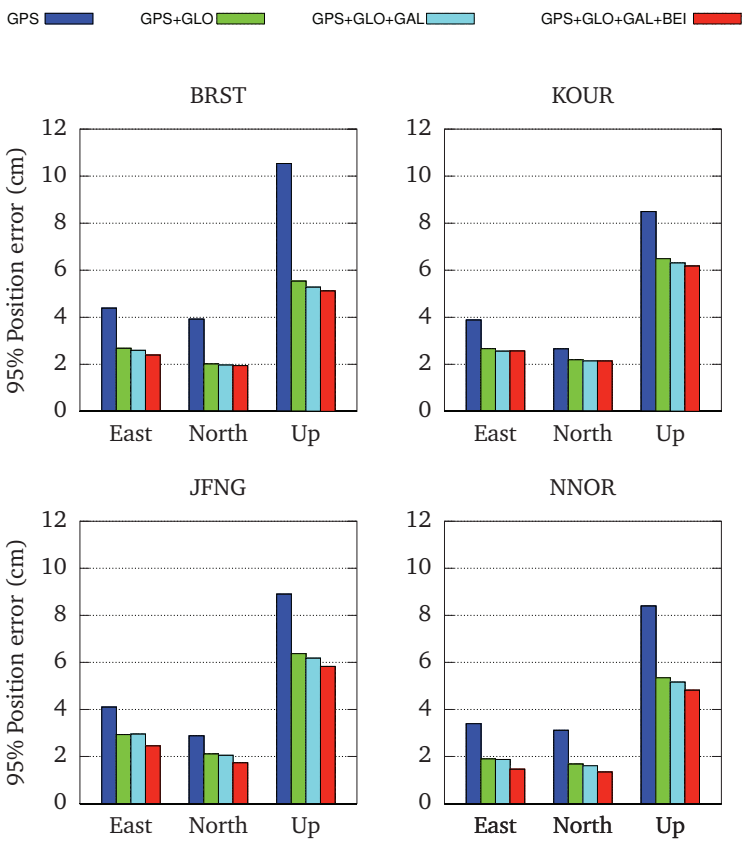

Fig. 6.6: Multi-constellation kinematic positioning statistics for several stations in MGEX.

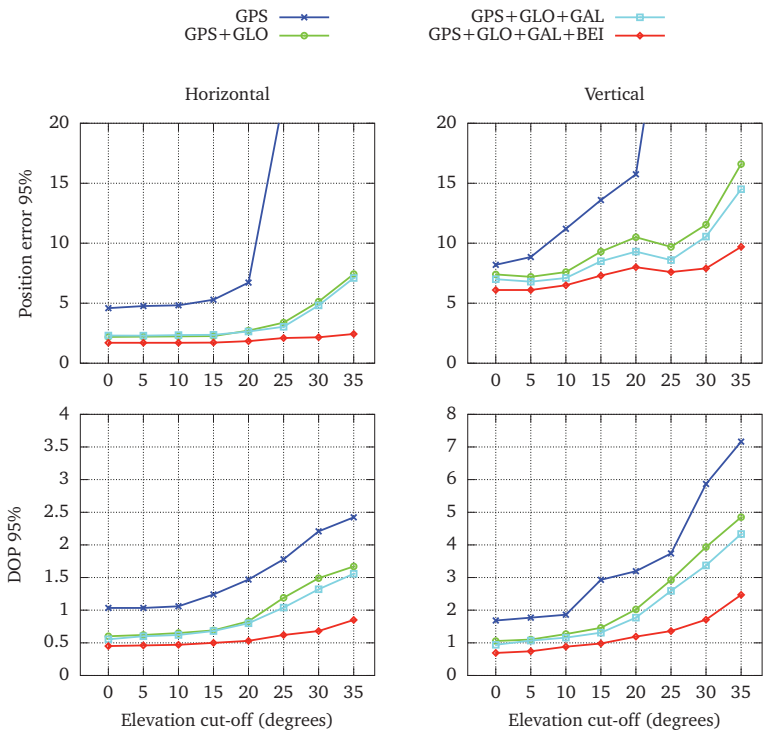

Fig. 6.7: Positioning statistics and Dilution of Precision (DOP), for different elevation cut-off angles, for station NNOR on August 26th, 2013.

6.8 Summary and Conclusions

The GNSS landscape is evolving rapidly, with the addition of emerging satellite systems on top of GPS and Glonass. In this study, precise orbit estimation results have been presented for Galileo and BeiDou. The achieved orbit precision is generally at sub-decimeter level for Galileo and BeiDou MEO and IGSO satellites. The orbit estimation for GEO satellites is challenging due to the lack of geometry variation with respect of the reference station network, and precision estimates are at few decimeter level. Satellite modeling remains an area for further research, in terms of antenna phase center corrections and precise attitude-modelling.

Significant intersystem-biases differences have been detected between different receiver brands, that cannot be neglected for precise applications. Extended observation equations have been presented to accommodate these biases, both in network adjustment and PPP solutions.

Multi-GNSS PPP results show enhanced accuracy when using all four satellite systems together. However, the accuracy improvement is relatively small compared to the GPS+Glonass case under good sky visibility. The improvement becomes more significant under reduced sky visibility conditions, where the increased number of satellites allows to obtain significantly higher accuracy and availability for the position solution. This is particularly visible in the Asia-Pacific area where BeiDou IGSO and GEO satellites are available for positioning. It can be expected that this level of performance will be extended worldwide with the further deployment of Galileo and BeiDou during this decade.

In this context, the data provided by the IGS MGEX campaign is highly valuable for the scientific community to get a better understanding of the new GNSS systems and signals. This study would not have been possible without such data. The authors are also grateful to Fugro for delivering the reference station data for scientific purposes.

7 Paper D: Estimation of Galileo Uncalibrated Hardware Delays for ambiguity-fixed Precise Point Positioning

Paper title: "Estimation of Uncalibrated Hardware Delays for ambiguity-fixed Precise Point Positioning"
Authors: Javier Tegedor, Xianglin Liu[1], Kees de Jong[1], Matthew Goode[1], Erik Vigen[2], Ola Øvstedal[3]
Peer-reviewed paper at the *International Technical Meeting of the Institute of Navigation (ION GNSS 2014)*
Manuscript Submitted: July 14, 2014
Manuscript Accepted: August 26, 2014

Contents

7.1 Abstract

Ambiguity fixing in Precise Point Positioning (PPP) has been extensively studied in recent years. The provision of Uncalibrated Hardware Delays (UHDs) to the PPP algorithm, on top of precise orbits and clocks, allows the recovery of the integer values of the carrier phase ambiguities. Experimental results show that integer ambiguity resolution increases the accuracy in the position domain. Most of the research so far has been done on GPS, where the wide- and narrow-lane approach for ambiguity resolution has proven successful.

[1]Fugro Intersite B.V., Leidschendam (The Netherlands)
[2]Fugro Satellite Positioning AS, Oslo (Norway)
[3]Norwegian University of Life Sciences, Department of Mathematical Sciences and Technology

In the context of multi-GNSS PPP, the aim of this study is to extend the method to Galileo. Initial results for UHD estimation for Galileo satellites are presented. The contribution of ambiguity-fixing to GPS+Galileo PPP is assessed.

7.2 Introduction

The Precise Point Positioning [Zumberge et al., 1997] technique enabled centimeter to decimeter accuracy without the need for local reference station observations, taking precise satellite orbits and clocks as input and precise observation modeling [Kouba and Héroux, 2001].

Traditional PPP is based on ionosphere-free linear combination of code and carrier phase observations, which does not preserve the integer nature of the carrier phase ambiguities. Therefore, without additional information, carrier phase ambiguities are estimated as real numbers, in what is commonly known as a *float solution*.

In order to increase PPP accuracy, *fixed solutions* shall be attempted, namely positioning estimates that are obtained after fixing of carrier phase ambiguities to their integer values. Studies during recent years have demonstrated the feasibility to resolve integer ambiguities in PPP using GPS, provided that additional code and carrier phase biases are provided as input to the PPP algorithm. Several approaches have been developed, such as the Decoupled Clock Model (NRCan, [Collins et al., 2008]), Integer Clock method (CNES, [Laurichesse et al., 2009]) and the Single-Difference approach (GFZ, [Ge et al., 2007]). The above-mentioned code and carrier phase biases are known in the existing literature as Uncalibrated Phase Delays (UPDs), Fractional Cycle Biases (FCBs) or Uncalibrated Hardware Delays (UHDs) [Geng, 2010].

It has been recently proven that all these approaches are equivalent [Shi and Gao, 2013]. Essentially, the ionosphere-free ambiguity is separated into a wide- and a narrow-lane ambiguity. Wide-lane ambiguity resolution is based on Melbourne-Wübbena geometry-free approach, while the narrow-lane ambiguity resolution is achieved via a geometry-based approach. Ambiguity-resolution in PPP then becomes then feasible when UHDs are estimated in a network adjustment and transferred to the end-user.

This method has been successful in increasing accuracy in GPS-based PPP. The aim of this study is to provide initial experimentation for the extension of the method to Galileo. There are currently[4] four In-Orbit Validation Satellites (IOV) in orbit, launched in October 2011 (E11 and E12) and October 2012 (E19 and E20). At the time of preparing this article (July 2014), no Full Operational Capability (FOC) satellites have been launched yet.

[4] As in July 2014

7.3 Ionosphere-free observation equations

The GNSS observation equations for pseudorange P and carrier phase L, between receiver r and satellite s, with nominal frequency i, can be written as:

$$P_i^{r,s} = \rho^{r,s} + T^{r,s} + I_i^{r,s} + c(\delta t^r - \delta t^s) + c(p_i^r - p_i^s) + \varepsilon_{P_i} \quad (7.1)$$

$$L_i^{r,s} = \rho^{r,s} + T^{r,s} - I_i^{r,s} + c(\delta t^r - \delta t^s) + c(l_i^r - l_i^s) + \lambda_i N_i^{r,s} + \varepsilon_{L_i} \quad (7.2)$$

where $\rho^{r,s}$ is geometric distance between satellite and receiver; $T^{r,s}$ is the tropospheric delay; $I_i^{r,s}$ is the frequency-dependent ionospheric delay; c is the speed of light; δt^r and δt^s are receiver and satellite clocks respectively; p_i^r and p_i^s are pseudorange delays for frequency f_i, for receiver and satellite respectively; l_i^r and l_i^s are carrier phase delays for frequency f_i, for receiver and satellite respectively; N_i is the integer carrier phase ambiguity with its associated wavelength $\lambda_i = c/f_i$; ε_{P_i} and ε_{L_i} are unmodelled effects, such as multipath and thermal noise.

The ionosphere-free (IF) linear combination between frequencies f_i and f_j is obtained as:

$$P_{IF}^{r,s} = \alpha P_i^{r,s} + \beta P_j^{r,s} \quad (7.3)$$

$$L_{IF}^{r,s} = \alpha L_i^{r,s} + \beta L_j^{r,s} \quad (7.4)$$

with $\alpha = f_i^2/(f_i^2 - f_j^2)$ and $\beta = 1 - \alpha$. Applying equations 7.3 and 7.4 to 7.1 and 7.2, the resulting observation equations for the ionosphere-free measurements are:

$$P_{IF}^{r,s} = \rho^{r,s} + c(\delta t_{IF}^r - \delta t_{IF}^s) + T^{r,s} + \varepsilon_{P_{IF}} \quad (7.5)$$

$$L_{IF}^{r,s} = \rho^{r,s} + c(\delta t_{IF}^r - \delta t_{IF}^s) + T^{r,s} + a_{IF}^{r,s} + \varepsilon_{L_{IF}} \quad (7.6)$$

where the ionosphere-free clocks also include the pseudorange hardware delay terms:

$$\delta t_{IF}^r = \delta t^r + \alpha p_i^r + \beta p_j^r \quad (7.7)$$

$$\delta t_{IF}^s = \delta t^s + \alpha p_i^s + \beta p_j^s \quad (7.8)$$

And the new ionosphere-free ambiguity term $a_{IF}^{r,s}$ reads:

$$a_{IF}^{r,s} = \alpha\lambda_i N_i^{r,s} + \beta\lambda_j N_j^{r,s} + b_{IF}^r - b_{IF}^s \quad (7.9)$$

The new hardware delays b_{IF}^r and b_{IF}^s are a combination of pseudorange and carrier phase delays, such that:

$$b_{IF}^r = c(\alpha l_i^r + \beta l_j^r - \alpha p_i^r - \beta p_j^r) \quad (7.10)$$

$$b_{IF}^s = c(\alpha l_i^s + \beta l_j^s - \alpha p_i^s - \beta p_j^s) \quad (7.11)$$

The hardware delays in 7.10 and 7.11 prevent the resolution of the integer ambiguities $N_i^{r,s}$ and $N_j^{r,s}$. Therefore, in traditional PPP, the ambiguity parameter $a_{IF}^{r,s}$ is estimated as a real valued number.

7.4 Derivation of UHDs

The wide and narrow lane approach described in section 7.2 is based on a the introduction of an integer wide-lane ambiguity N_w=N_i-N_j, so that the ambiguity term in 7.9 can be rewritten as:

$$a_{IF}^{r,s} = \frac{c}{f_i + f_j} N_i^{r,s} + \frac{f_j c}{f_i^2 - f_j^2} N_w^{r,s} + b_{IF}^r - b_{IF}^s \tag{7.12}$$

The wide-lane ambiguity $N_w^{r,s}$ can be resolved using the Melbourne-Wübbena linear combination [Melbourne, 1985, Wübbena, 1985] of code and carrier phase observations:

$$MW^{r,s} = \alpha_w L_i^{r,s} + \beta_w L_j^{r,s} - \alpha_n P_i^{r,s} - \beta_n P_j^{r,s} \tag{7.13}$$

Where the combination coefficients are:

$$\alpha_w = \frac{f_i}{f_i - f_j} \qquad \beta_w = 1 - \alpha_w \tag{7.14}$$

$$\alpha_n = \frac{f_i}{f_i + f_j} \qquad \beta_n = 1 - \alpha_n \tag{7.15}$$

Applying equation 7.13 to equations 7.1 and 7.4 results in:

$$MW^{r,s} = \frac{c}{f_i - f_j}(N_w^{r,s} + b_w^r - b_w^s) \tag{7.16}$$

Unmodelled effects are omitted from equation 7.16 for simplicity. b_w^r and b_w^s are the Wide-lane Uncalibrated Hardware Delays (WL-UHDs) for receiver and satellite respectively:

$$b_w^r = (f_i - f_j)(\alpha_w l_i^r + \beta_w l_j^r - \alpha_n p_i^r - \beta_n p_j^r) \tag{7.17}$$

$$b_w^s = (f_i - f_j)(\alpha_w l_i^s + \beta_w l_j^s - \alpha_n p_i^s - \beta_n p_j^s +) \tag{7.18}$$

Analogously, equation 7.12 can be rewritten as

$$a_{IF}^{r,s} = \frac{c}{f_i + f_j}(N_i^{r,s} + b_n^r - b_n^s) + \frac{f_j c}{f_i^2 - f_j^2} N_w^{r,s} \tag{7.19}$$

where b_n^r and b_n^s the Narrow-lane Uncalibrated Hardware Delays (NL-UHDs) for receiver and satellite, respectively, associated with the narrow-lane ambiguity $N_i^{r,s}$. Finally, the wide- and narrow-lane wavelengths are:

$$\lambda_w = \frac{c}{f_i - f_j} \qquad \lambda_n = \frac{c}{f_i + f_j} \tag{7.20}$$

The ambiguity resolution method is based on the estimation of satellite hardware delays b_w^s and b_n^s in a network adjustment, in a similar way as for orbit and clock estimation. Taking these as input, the PPP algorithm can resolve the integer wide- and narrow-lane ambiguities,

after the estimation of the receiver terms b_w^r and b_n^r. If between satellite single-differences are performed in the PPP solution then the receiver terms cancel out and the integer ambiguities can be recovered directly at single-difference level after applying the satellite UHDs.

Constellation	f_i/f_j	$\lambda_w(cm)$	$\lambda_n(cm)$
GPS	L1/L2	86.25	10.70
Galileo	E1/E5a	75.19	10.90
	E1/E5	78.20	10.84
	E1/E5b	81.46	10.78
	E1/E6	101.12	10.51
	E6/E5a	293.26	12.22
	E6/E5	345.01	12.14
	E6/E5b	418.94	12.07
	E5a/E5	1955.03	12.67
	E5b/E5	1955.03	12.51
	E5a/E5b	977.52	12.59

Tab. 7.1: Wide- and narrow-lane wavelengths for different signal combinations.

Table 7.1 shows the wide- and narrow-lane wavelengths for Galileo dual-frequency combinations, where GPS L1/L2 has been added as reference. Although no public tracking data on E6 exists at the moment, E6 combinations have been added for completeness. Although the extra wide-lane combinations such as E5a/E5 or E5b/E5 might appear attractive since the wide-lane ambiguity resolution can be done almost instantaneously thanks to the long wide-lane wavelength, narrow-lane ambiguity resolution becomes almost impossible due to the high-noise amplification factor of the corresponding ionosphere-free linear combination with small frequency separation. As an example, E5a/E5b ionosphere-free combination has an ionosphere-free noise amplification factor ($AF = \sqrt{\alpha^2 + \beta^2}$) of 27.4, compared to 3.0 for GPS L1/L2 or 2.6 for Galileo E1/E5a. In practice, only E1/E5 combinations are used, which show similar characteristics to the traditional GPS L1/L2 in terms of noise amplification.

An alternative approach is to process the original observations directly 7.1 and , instead of building the ionosphere-free linear combination. An example of this *raw* processing method was e.g. proposed in [Zhang et al., 2011]. In this case, ionosphere parameters $I^{r,s}$ have to be estimated, together with the UHDs in each frequency, i.e l_i^s. The benefit of this alternative approach is the additional MW step for deriving the WL-UHDs is not needed since the UHDs can be estimated directly from the original observations without the MW combination.

7.5 Orbit and clock estimation

WL-UHDs can be estimated directly from GNSS observations but the resolution of geometry-based NL-UHDs requires the availability of precise orbit and clock estimates. For this study, this is achieved by processing a global reference station network, using the data that is publicly available as part of the International GNSS Service (IGS) Multi-GNSS Experiment

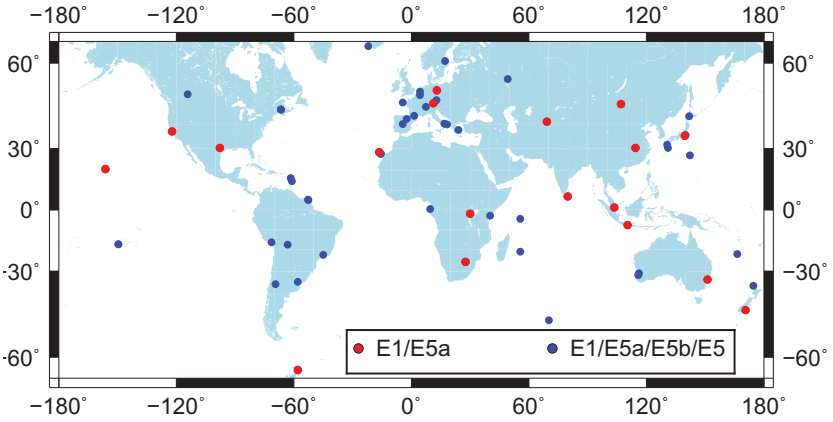

Fig. 7.1: Station network used for orbit and clock estimation, indicating Galileo signals availability.

(MGEX)[Montenbruck et al., 2014]. The station distribution is shown in figure 7.1. It has been noted that the majority of Javad receivers do not have observation data for Galileo signals E5b or the AltBOC signal E5. In order to maximize data availability, E1/E5a signals have been selected for this study, which are tracked from all the reference stations. Observation data is processed at a 30 second sampling interval. The orbit accuracy has a direct impact on the estimation of the geometry-based narrow-lane UHDs, as orbit errors will directly impact the satellite clock and NL-UHD estimates. In order to obtain a highly accurate orbit for Galileo satellites, 3-day orbits arcs are processed, where the central 24 hours is used for UHD estimation purposes. This ensures that the orbit accuracy is at the centimeter level. NAPEOS software package has been used for generating orbit and clocks for the Galileo satellites.

7.6 Consistency of Galileo Satellite UHDs

Since Galileo is a relatively new system, the consistency of the satellite UHDs estimated from different receiver brands needs to be assessed, namely the feasibility to estimate a consistent set of Galileo UHDs regardless of the receiver manufacturer and model. As shown in equations 7.16 and 7.19, the presence of satellite pseudorange or carrier phase biases will hamper ambiguity resolution, unless they are identical between receiver brands and can therefore be assimilated in the UHD terms. Typical examples of these biases are Differential Code Biases (DCBs), such as those existing for P and C/A tracking in GPS [Leandro et al., 2007b]. Regarding phase measurements, quarter cycle biases might appear when tracking different signal components, as I (In-phase) or Q (Quadrature) which have a quarter cycle difference that needs to be corrected at observation level. Any remaining uncorrected biases will impact the estimation of wide- and/or narrow-lane UHDs. As an example, ambiguity resolution when mixing GPS and Galileo signals on L1/E1 and L5/E5a is challenging, as already shown in [Melgard et al., 2013].

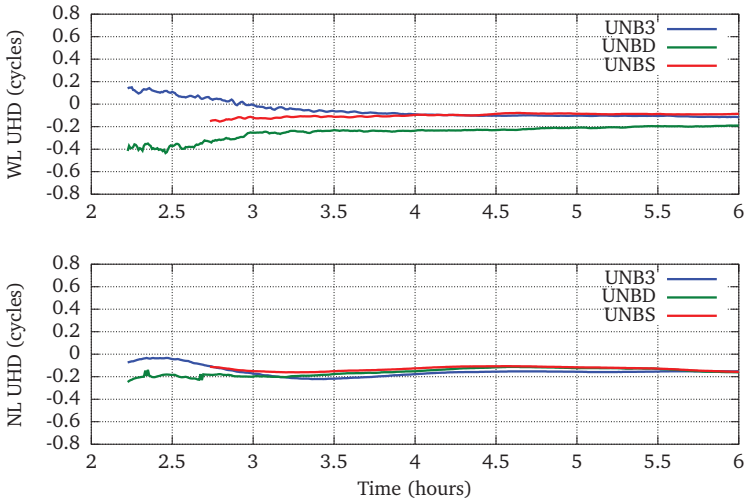

Fig. 7.2: Single difference UHDs for E12-E19, wide- (top) and narrow-lane (bottom), observed from New Brunswick on May 5th, 2014.

A zero-baseline setup is an adequate setup for assessing these biases, as all other errors are common between receivers connected to the same antenna [Bakker et al., 2012]. In particular, station data collected by the University of New Brunswick (Canada) has been analysed, where a Septentrio PolarRx4 (UNBS) and a Javad Delta G2T (UNBD) receivers are operated in a zero-baseline configuration, connected to a Trimble Zephyr Geodetic antenna. Additionally, there is a Trimble NETR9 receiver connected to a separated antenna located a few meters away, in a short baseline configuration. The data is being made available as part of the MGEX campaign. Figure 7.2 shows single-difference UHDs for E12 and E19, observed from these receivers on May 5th, 2014. The UHDs from different receiver brands show a good level of agreement, with the maximum difference of 0.1 cycles in the wide-lane component. This essentially means that a common set of satellite UHDs can be applied universally for ambiguity resolution by all receiver types, without the need of additional receiver-specific corrections. It is worth mentioning that the UHDs show some variations at the beginning of the pass, this is due to the noise introduced by pseudorange measurements, which are used in the Melbourne-Wübbena combination for the WL-UHD estimation. This is one of the main constraints of the method, as the measurements need to be averaged over a significant number of epochs (typically up to 30 minutes) before wide-lane ambiguity resolution can be successfully achieved. This is illustrated in figure 7.3, where the Melbourne-Wübbena observations from the three receivers for E20 satellite, have been plotted. It is interesting to note that the noise of the Javad receiver (UNBD) seems to be considerably higher than for Trimble (UNB3) or Septentrio (UNBS) receivers. Higher noise implies higher time needed for wide-lane ambiguity resolution, as the average time needs to be increased in order to get a reliable estimate for the wide lane ambiguity.

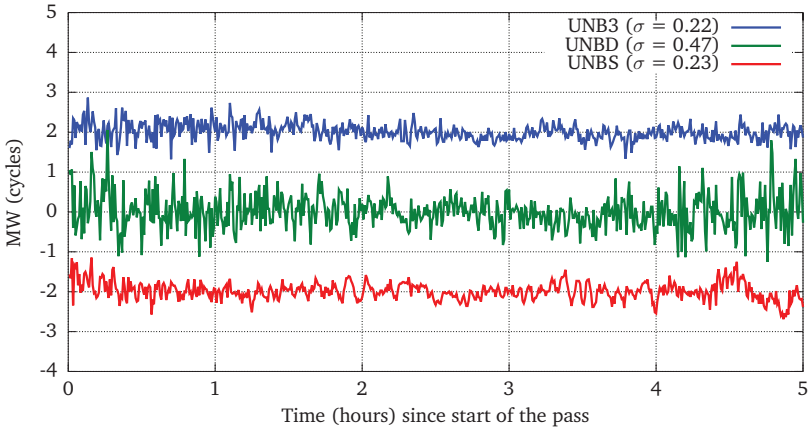

Fig. 7.3: Melbourne-Wübbena measurements for Galileo satellite E20, from three receivers in a zero-baseline configuration. For clarity, signals have been manually adjusted to have a 0 mean (UNBD), +2 (UNB3) and -2 (UNBS).

7.7 UHD estimation in network solution

The estimation of UHDs in a network adjustment is desirable in order to improve the accuracy of the estimates and consequently increase the reliability of ambiguity fixing in PPP. However, one of the main difficulties with the current Galileo constellation if global satellite observability, with few satellites available at the moment. The estimation of single-difference (between satellites) UHDs is challenging as it requires common visibility of (at least) two Galileo satellites from several stations, which was not always possible with the MGEX network shown in figure 7.1. In order to overcome this limitation, some additional regional stations from the European Permanent Network (EPN) are processed, together with global MGEX stations.

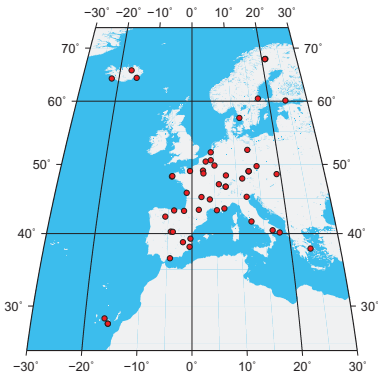

Fig. 7.4: EPN stations tracking Galileo signals.

Figure 7.4 shows the geographical distribution of EPN stations that have been selected for this study. All these stations are also tracking Galileo signals at the E1 and E5a frequencies. Figure 7.5 shows the epoch-wise estimated UHDs using this network, for a period where all satellites were visible simultaneously over Europe. Single-differenced satellite UHDs are depicted, using E20 as the reference satellite. It can be observed that, with a sufficient number of tracking stations, the UHDs can be reliably estimated and show a good temporal stability. The distribution of the residuals of the UHD estimation for Galileo is shown in figure 7.6. The concentration of the residuals around zero is an indication that the estimation has

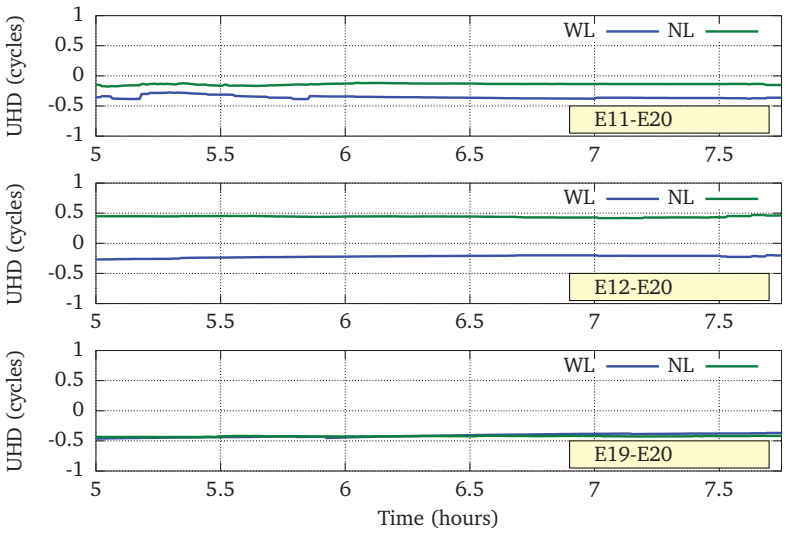

Fig. 7.5: Single difference UHDs for Galileo satellites on May 5th, 2014.

been done correctly. In order to evaluate the success of Galileo UHD estimation, compared to GPS, the cumulative distribution of residuals is depicted in figure 7.7. It can be observed that, both for GPS and Galileo, more than 80% of residuals are within 0.1 cycles, both for wide- and narrow-lane.

7.8 Ambiguity-fixed PPP results

In order to validate the estimated UHDs, the carrier phase ambiguities in a combined GPS/Galileo kinematic PPP solution are fixed to their integer values, after the network-estimated satellite UHDs are applied. In particular, three PPP scenarios are considered: 1) GPS float + Galileo float, 2) GPS float + Galileo fixed and 3) GPS fixed and Galileo fixed. For the latter, UHDs for GPS are obtained processing standard L1/L2 observations, as already shown in previous studies. The kinematic PPP results are summarized in table 7.2, where stations of different receiver types have been processed, using a common set of orbits, clocks and UHDs. The time span corresponds to a period when all Galileo satellites were visible over Europe, between 04 and 08 UTC, May 5th, 2014. It can be observed that fixing Galileo ambiguities allows improving the accuracy with respect to the float solution. However, the improvement is relatively small (10 % in average), mainly due to the small number of Galileo satellites currently available, compared to GPS. When GPS ambiguities are fixed, there is a more significant accuracy improvement (34 % improvement in average). It can be expected that the contribution of ambiguity-fixed Galileo PPP to the position accuracy improvement will increase following the further deployment of the constellation and more satellites are available for positioning.

Standalone Galileo PPP ambiguity resolution was also attempted in this study. However, this could not be achieved in a reliable manner as the quality of the float solution in Galileo-only PPP is relatively poor with only four satellites in view. The ambiguity success rates in this case were very low (25-30%), compared to over 99% in the case of combined GPS+Galileo.

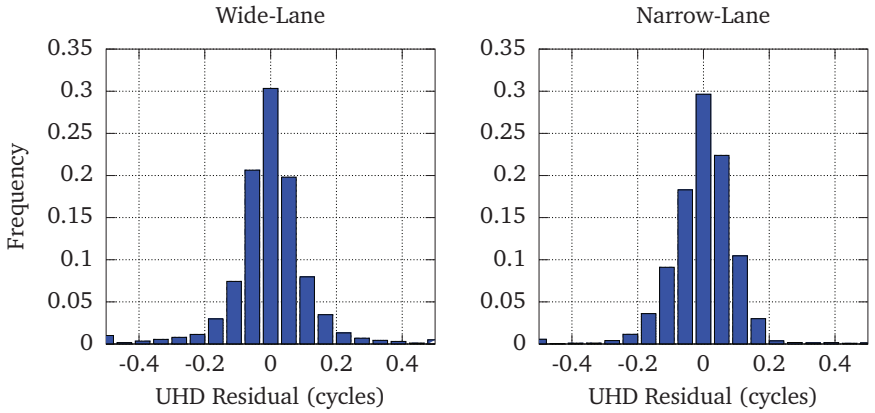

Fig. 7.6: Residuals distribution after UHD estimation, for Galileo satellites.

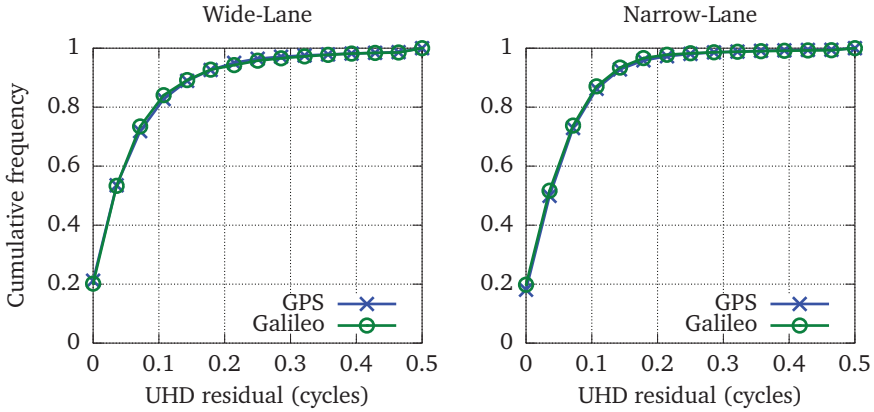

Fig. 7.7: Cumulative distribution of UHD residuals, both for GPS and Galileo.

	Trimble NETR9				Javad Delta G3T				Septentrio PolaRX4			
	BRST		ONS1		POTS		LLAG		CEBR		KIRU	
PPP Solution type	H	V	H	V	H	V	H	V	H	V	H	V
GPS (float) + Galileo (float)	2.6	6.0	3.3	6.3	3.0	6.3	3.1	3.5	2.2	4.6	3.3	5.8
GPS (float) + Galileo (fixed)	2.6	5.6	3.0	5.1	2.8	5.4	2.9	3.2	2.1	4.4	3.0	5.2
GPS (fixed) + Galileo (fixed)	2.0	4.1	2.0	4.1	1.4	2.6	1.3	2.7	0.9	3.6	2.0	4.5

Tab. 7.2: Kinematic PPP position errors (RMS) for different reference stations, horizontal (H) and vertical (V). All units are centimeters.

7.9 Conclusions

In this study, an initial estimation of Uncalibrated Hardware Delays for Galileo IOV satellites has been performed, using the wide- and narrow-lane approach and the E1 and E5a signals. A zero/short-baseline analysis reveals that a single set of Galileo satellite UHDs is valid for different receiver brands, including Javad, Septentrio and Trimble receivers. The UHDs can be estimated using a reference station network, but the small number of satellites available requires a relatively dense network in order to achieve sufficient observability for reliable estimation. The post-fit residuals show the expected distribution, similar to that obtained for GPS using the same approach.

In the position domain, the use of Galileo UHDs results in an increased positional accuracy with respect to the float solution, in combined GPS+Galileo PPP. The contribution of ambiguity-fixing for GPS is significantly higher, mainly due to the higher number of ambiguities that can be fixed thanks to the availability of more satellites.

Ambiguity-fixing in Galileo standalone PPP cannot be reliably achieved yet due to the suboptimal accuracy of the float solution, since only four Galileo satellites are available at the moment. Following further development of the constellation, the authors expect the contribution of Galileo to the improvement of position solution to increase.

8 Paper E: Comparison between multi-constellation ambiguity-fixed PPP and RTK for maritime precise navigation

Paper title: "Comparison between multi-constellation ambiguity-fixed PPP and RTK for maritime navigation"
Authors: Javier Tegedor, Xianglin Liu[1], Ole Ørpen[2], Niels Treffers[3], Matthew Goode[2], Ola Øvstedal[4]
Manuscript accepted for publication in the *Journal of Applied Geodesy*
Manuscript Submitted: December 29, 2014
Manuscript Accepted: April 7, 2015

Contents

8.1 Abstract

In order to achieve high-accuracy positioning, either Real-Time Kinematic (RTK) or Precise Point Positioning (PPP) techniques can be used. While RTK normally delivers higher-accuracy with shorter convergence times, PPP has been an attractive technology for maritime applications, as it delivers uniform positioning performance without direct need of a nearby reference station. Traditional PPP has been based on ambiguity-float solutions using GPS and Glonass constellations. However, the addition of new satellite systems, such as Galileo and BeiDou, and the possibility of fixing integer carrier-phase ambiguities (PPP-AR) allow

[1]Fugro Intersite B.V., Leidschendam (The Netherlands)
[2]Fugro Satellite Positioning AS, Oslo (Norway)
[3]Delft University of Technology (The Netherlands)
[4]Norwegian University of Life Sciences, Department of Mathematical Sciences and Technology

to increase PPP accuracy. In this article, a performance assessment has been done between RTK, PPP and PPP-AR, using GNSS data collected from two antennas installed on a ferry navigating in Oslo (Norway). RTK solutions have been generated using short, medium and long-baselines (up to 290 km). For the generation of PPP-AR solutions, Uncalibrated Hardware Delays (UHDs) for GPS, Galileo and BeiDou have been estimated using reference stations in Oslo and Onsala. The performance of RTK and multi-constellation PPP and PPP-AR are presented.

8.2 Introduction

High-accuracy GNSS-based positioning of a mobile receiver can be realized by means of absolute or relative positioning. Absolute positioning, as provided by the Precise Point Positioning (PPP) technique, can be obtained using precise orbit and clock products and accurate observation modeling, in order to compensate for or eliminate the errors impacting GNSS signals, such as ephemeris errors and atmospheric delays [Zumberge et al., 1997]. On the other hand, relative positioning, obtained by the Real-Time Kinematic (RTK) technique, makes use of a nearby reference station to take benefit of the temporal and spatial correlations of GNSS errors to compute the distance to the reference station with high accuracy [Remondi, 1985].

RTK has been extensively used in land-applications, as it delivers instantaneous real-time centimeter-level accuracy. One of the drawbacks of RTK is the need to keep a relatively dense station network, as accuracy degrades with the distance to the base station. Although techniques such as network-RTK or Virtual Reference Station (VRS) have been developed to increase robustness of RTK positioning [Vollath et al., 2002], the dense network infrastructure is still needed. As an example, the Norwegian Mapping Authority (NMA) is operating an RTK network in Norway (CPOS) consisting of more than 155 base stations. Average distance between stations is 70km. The communication between base station and rover is typically implemented by using radio frequency links in the UHF/VHF band, or mobile Internet, as demonstrated in [Hu et al., 2009]. For some applications, the need of being close to a base station is a significant constraint. A clear example is precise maritime navigation, where RTK can be used, but only near the coastline where the base stations can be located. For deep sea navigation, RTK is not a feasible positioning technology for high-accuracy.

The PPP technique appeared as a cost-effective alternative to RTK. Using a global station network, precise satellite and orbit clocks products can be computed to high-accuracy. A network of about 50 stations can be sufficient to estimate orbit/clock corrections with the desired accuracy. If these corrections are provided to users in the field, decimeter level accuracy can be achieved in real time. Commercial PPP service providers typically deliver precise orbit and clock corrections globally in the L-band by means of geostationary satellites [Melgard et al., 2010]. The main advantage of PPP is the provision of globally homogeneous accuracy, independent of the distance to the closest reference station that was used as part of the orbit and clock estimation process.

However, the accuracy obtained by standard PPP is generally worse than that achieved by RTK, and PPP still needs a relatively long period of convergence time (about 30 minutes)

before a decimeter level solution can be achieved. RTK delivers centimeter-level accuracy with negligible convergence time.

RTK can fully profit from the high-accuracy of the carrier-phase measurements by resolving the integer values of double-difference ambiguities between the base station and rover receivers. Traditional PPP does not have access to double-difference ambiguities (as no base station is directly involved in the position algorithm) and the zero-difference carrier-phase ambiguities are estimated as float numbers. However, recent research has proven that, if the fractional biases present in the zero-difference ambiguities are estimated, ambiguity-resolution can be achieved also in PPP [Ge et al., 2007, Collins et al., 2008, Laurichesse et al., 2009, Zhang et al., 2011]. The fractional biases have been known in the literature as Fractional Cycle Biases (FCBs), Uncalibrated Phase Delays (UPDs) or Uncalibrated Hardware Delays (UHDs) [Geng, 2010].

PPP with fixed ambiguities can improve accuracy with respect to the float solution. The term PPP-RTK has been used by the scientific community to denote PPP solution with fixed carrier phase ambiguities [Mervart et al., 2008, Geng et al., 2011], as well as PPP-AR (PPP with Ambiguity Resolution). GPS-based PPP-AR was first demonstrated in offshore marine platforms in [Geng et al., 2010], as a promising technique to increase PPP accuracy.

In parallel, the availability of new systems (such as Galileo and BeiDou), on top of the traditional GPS and Glonass, increases the number of satellites available for positioning. It is expected than multi-constellation PPP-AR solutions will improve the accuracy of absolute positioning and bring it closer to RTK performance. At the time of writing, BeiDou is composed of 5 Geostationary Orbit (GEO, PRNs C01-C05), 5 Inclined Geosynchronous Orbit (IGSO, PRNs C06-C10) and 4 Medium Earth Orbit (MEOs, PRNs C11-C14) satellites. Galileo constellation is made of the first In-Orbit Validation (IOV) satellites, assigned to PRN E11, E12, E19 and E20. E20 suffered a power problem at the end of May 2014 and stopped transmitting then L-band signals. For this reason, E20 could not be used for this research. The first two Full Operational Capability (FOC) satellites were launched on August 22nd 2014, but an anomaly in the launcher caused that they were delivered into a non-nominal elliptical orbit. At the time of writing this article, it is unclear whether these satellites will be part of the operational Galileo constellation.

The purpose of this study is to present an empirical comparison between RTK, PPP and PPP-AR using real dynamic data collected in a maritime environment, where multi-constellation GNSS data was collected on board a vessel navigating near Oslo (Norway).

8.3 Vessel setup

For this study, two Fugro 9205 multi-constellation GNSS receivers have been installed on board the *Baronen* vessel, a high-speed passenger ferry servicing the Oslo fjord. The receivers were connected to two Trimble GA810 antennas, approximately 16 meters apart, as shown in figure 8.1. The fixed antenna difference will be used as a reference for comparing the accuracies of RTK, PPP and PPP-AR. The receivers are also connected to an onboard computer for the storage of Rinex3 observation files that can be used for post-processing.

Fig. 8.1: Picture of the *Baronen* vessel navigating in the Oslo fjord, including a detail on one of the antennas on board.

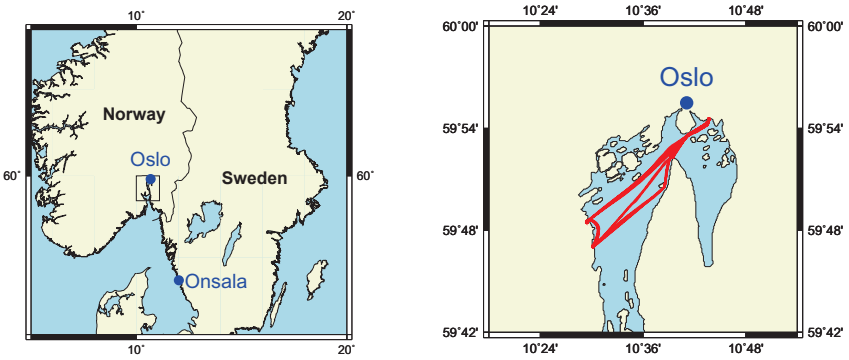

Fig. 8.2: Trajectory of the *Baronen* vessel on August 22nd, 2014. The vessel does short passenger trips around Oslo Fjord. The locations of the reference stations at Oslo and Onsala are also shown.

Observation data are stored in daily files at 5 seconds sampling. The vessel has a mobile Internet connection that allows the remote monitoring and configuration of the receivers and the download of the GNSS data.

In particular, GNSS data collected from 21st to 24th of August 2014 have been selected for this study, due to good visibility of both Galileo and BeiDou from Oslo on these days. The vessel was navigating during the first two days of the experiment, and was moored in harbor the last two days. The analysis of these data provides a good representation of PPP and RTK accuracies in both static and dynamic conditions. As an example, the trajectory of the vessel on August 22nd 2014 is depicted in figure 8.2.

The vessel dynamics are depicted in figure 8.3, where both GNSS-derived velocity and geodetic height are plotted, derived from antenna A on August 22nd. It can be observed that, for this particular day, the ferry is making short trips between 4 and 7 UTC, and between

13 and 19 UTC. The rest of the time the vessel is static. The average cruising speed is 27.1 knots (13.9 m/s).

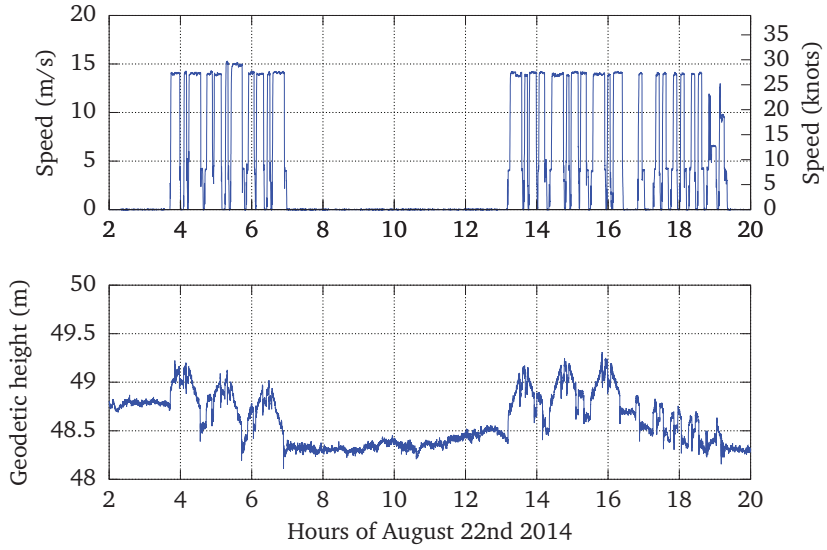

Fig. 8.3: Vessel speed (top) and geodetic height (bottom), derived from GNSS data collected on antenna A, on August 22nd 2014.

The number of GNSS satellites visible from Oslo is plotted in figure 8.4. Apart of GPS and Glonass, three Galileo In-Orbit Validation (IOV) satellites were tracked on the day under analysis. For BeiDou, all 5 Inclined Geosynchronous Orbit (IGSO) satellites and 4 Medium Earth Orbit (MEO) satellites were tracked. BeiDou GEO satellite C05 is also visible from Oslo, but only at 10 degrees elevation and therefore not included in this study, due to the high noise and multipath in the measurements at low elevation. The same applies to QZSS satellite J01 which is visible from Oslo but at a maximum 12 degrees elevation.

8.4 PPP and PPP-AR processing

A prerequisite for PPP estimation is the availability of precise satellite orbits and clocks. These have been estimated using NAPEOS (Navigation Package for Earth Orbiting Satellites) and a combination of reference stations from the Fugro proprietary network and the publicly available Multi-GNSS Experiment (MGEX) data. MGEX is a campaign by the International GNSS Service (IGS) for the provision of multi-constellation GNSS data for scientific purposes [Rizos et al., 2013]. In this case, dual-frequency pseudorange and carrier-phase measurements on L1 and L2 frequencies have been used for GPS and Glonass, E1 and E5a for Galileo and B1 and B2 for BeiDou. A study of the methodology for orbit and clock estimation and the obtained accuracy has already been presented in [Tegedor et al., 2014], and therefore will not be repeated here for simplicity.

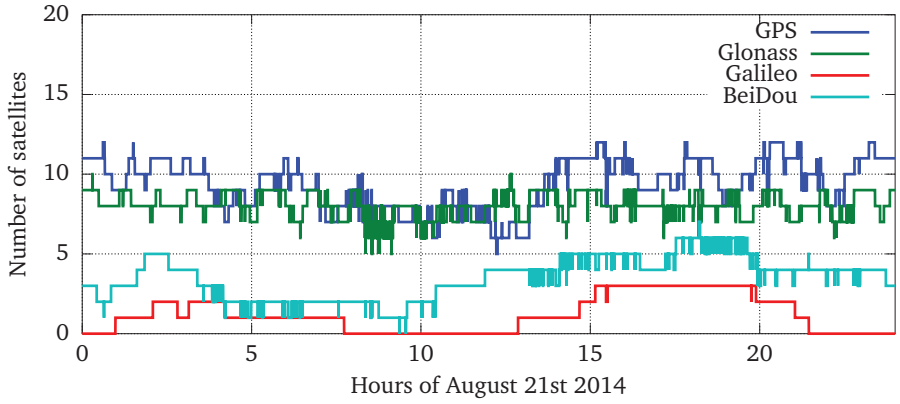

Fig. 8.4: Number of GNSS satellites visible from Oslo on August 21st 2014

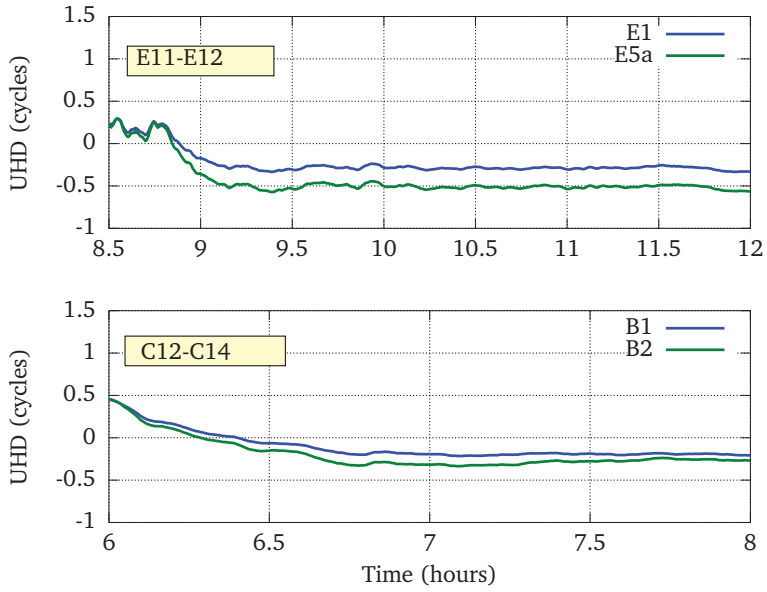

Fig. 8.5: Single differenced Uncalibrated Hardware Delays (UHDs) for Galileo satellites E11-E12 (top) and BeiDou C12-C14 (bottom), on August 23rd 2014

PPP-AR solutions need the additional availability of Uncalibrated Hardware Delays. For this study, these are derived independently from two different locations. In the first place, the Fugro reference station located in downtown Oslo has been used to generate UHDs. The station is equipped with a Trimble NETR9 receiver connected to a Trimble Zephyr Geodetic antenna (depicted in figure 8.6). In addition, the reference station ONS1, located in Onsala (Sweden) (figure 8.2), is used. The ONS1 station is operated by the Swedish Mapping Authority (Lantmateriet) at the Onsala Space Observatory. The data are publicly available as part of the MGEX campaign. ONS1 station consists of a Trimble NETR9 receiver connected to a Leica AR25 antenna.

For both Onsala and Oslo, using the known antenna coordinates and satellite orbits and clocks as input, UHDs have been estimated for GPS, Galileo and BeiDou, following the undifferenced approach proposed by [Zhang et al., 2011]. In this case, the satellite UHDs are estimated as the fractional part of the carrier-phase ambiguities, which are estimated in PPP-mode with fixed antenna coordinates. The receiver UHDs can be eliminated by forming between satellite single differences. The estimated hardware delays are used later on in the kinematic PPP solutions for resolving the integer carrier-phase ambiguities. Glonass UHDs have not been estimated, due to the presence of frequency-dependent biases that make ambiguity-resolution challenging.

Figure 8.5 shows epoch-wise single-differenced hardware delays for Galileo E11-E12 and BeiDou C12-C14 satellites, derived from the reference station at Oslo. It can be observed that the delays are quite stable, but there are some variations in the estimated parameters at the beginning of the pass while satellites are at low elevation and the carrier-phase ambiguity has not fully converged yet.

Fig. 8.6: Oslo reference station antenna used for UHD estimation and short- and medium-baseline RTK

In addition, the processing of the dynamic data in Precise Point Positioning has some challenges that will be described next. For the Trimble GA810 antennas used, there is no antenna calibration information, meaning that azimuthal- and elevation-dependent variations are ignored in the PPP estimation. These phase variations are assumed to be relatively small for these high-end antennas, and therefore the lack of modeling has no

significant impact in the results of this study. Furthermore, the phase windup [Wu et al., 1993] needs to be modeled in PPP, which requires the knowledge of the orientation of the vessel antennas. For this study, the phase wind-up correction has been applied assuming non-rotating receiving antennas. This is valid due to the fact that the mismodelling can be absorbed in the estimated receiver phase-clock term, as the effect is common to all satellites in view.

Fugro proprietary software has been used to generate the PPP solutions, generating epoch-wise positions in ITRF08 reference frame for each on-board antenna. The elevation cut-off is 10 degrees. Equal stochastic parameters are given to all constellations. In terms of ambiguity-fixing performance, more than 98% of epochs have 6 or more ambiguities fixed. Time to first fix oscillates between 10 and 20 minutes depending on the satellite geometry at PPP initialization and the convergence of the float solution.

8.5 RTK processing

In order to have a reference solution for PPP, an additional RTK solution has been performed for the antennas on-board, also using Fugro proprietary software. Unlike PPP, RTK does not need precise orbits and clocks, as it is based on the usage of double-differenced observations between the mobile antenna and the base antenna, in order to obtain the baseline length between both. As the RTK performance depends on baseline length, three different scenarios have been considered, including short, medium and long baseline.

For the short baseline scenario, antenna A has been considered the reference antenna and antenna B the mobile antenna. The RTK processing estimates directly the distance between the two on-board antennas. In this short baseline scenario, all GNSS errors are effectively cancelled out and the GPS double-difference carrier-phase ambiguities can be fixed to the integer values.

For the medium baseline scenario, the reference station in Oslo has been used as base station. The baseline varies in this case between 2 and 20 km, depending on the vessel position. In this medium baseline scenario, GNSS errors are cancelled out to a large extent (but not completely), and it is still possible to fix carrier-phase ambiguities.

Finally, for the long baseline scenario, the station ONS1 has been used as a base station. In this long baseline scenario, the baseline lengths varies between 278 and 288 km. In this case, double-difference ambiguity-resolution cannot be reliably achieved due to the fact that significant residual GNSS errors remain at observation level due to the large baseline length.

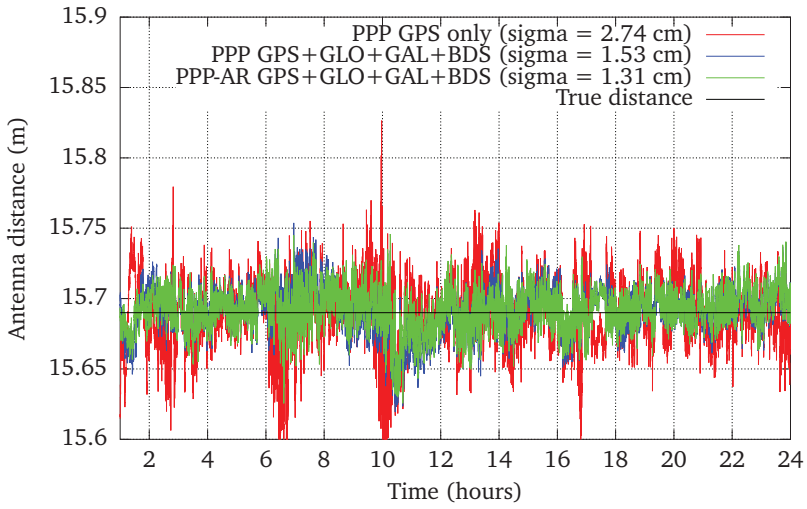

Fig. 8.7: Distance between antennas for August 21st 2014, using GPS-only PPP (red) and multi-constellation PPP (blue), including GPS, Glonass (GLO), Galileo (GAL) and BeiDou (BDS).

		Dynamic vessel		Static vessel	
		Aug 21	Aug 22	Aug 23	Aug 24
RTK GPS+GLO	Long baseline (Onsala base station)	2.28	3.31	3.08	3.55
	Medium baseline (Oslo base station)	1.04	0.85	0.67	0.70
	Short baseline	0.89	0.79	0.52	0.66
PPP (float)	GPS	2.74	2.26	2.76	2.54
	GPS+GLO	1.55	1.58	1.69	1.66
	GPS+GLO+GAL	1.54	1.57	1.63	1.63
	GPS+GLO+GAL+BDS	1.53	1.56	1.58	1.61
PPP-AR (fixed, UHDs from Oslo)	GPS	2.29	2.11	2.58	2.47
	GPS+GLO	1.33	1.41	1.50	1.57
	GPS+GLO+GAL	1.31	1.40	1.48	1.54
	GPS+GLO+GAL+BDS	1.31	1.39	1.42	1.51
PPP-AR (fixed, UHDs from Onsala)	GPS	2.12	2.23	2.60	2.53
	GPS+GLO	1.43	1.43	1.53	1.59
	GPS+GLO+GAL	1.40	1.42	1.52	1.56
	GPS+GLO+GAL+BDS	1.29	1.39	1.45	1.53

Tab. 8.1: RMS of GNSS-based distance between on-board antennas in, for RTK, PPP and PPP-AR, from August 21st to August 24th. All units are centimeters.

8.6 Processing results

In order to compare PPP and RTK performances, the distance between the two antennas on board is used as reference. The *true* antenna distance is derived as an average over 24 hours for the epoch-wise baseline estimates in the short-baseline RTK scenario. This results in an antenna distance of 15.69 meters. Then the same antenna distance is derived

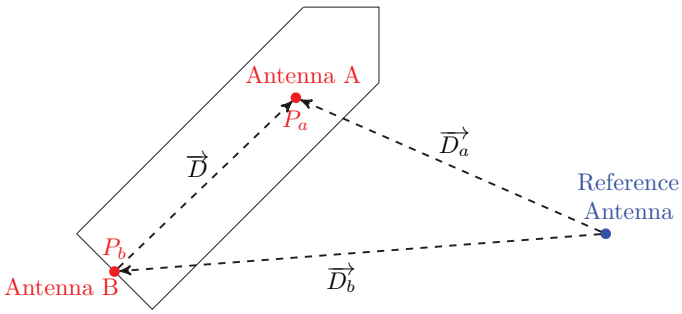

Fig. 8.8: Diagram of the PPP and RTK solutions for the estimation of the antenna distance

from the epoch-wise PPP and RTK processing described in previous sections. As shown in figure 8.8, PPP estimates directly the absolute position of each antenna P_a and P_b, and the computation of the antenna distance can be easily done as $d = \|\overrightarrow{D}\| = \|P_a - P_b\|$. As an example, epoch-wise distance between antennas is depicted in figure 8.7, using GPS-only PPP and a multi-constellation solution, including GPS, Glonass, Galileo and BeiDou, both with float (PPP) and fixed ambiguities (PPP-AR).

In the case of RTK, the distances $\overrightarrow{D_a}$ and $\overrightarrow{D_b}$ from each antenna to the base station are computed, and the distance can be computed as $d = \|\overrightarrow{D}\| = \|\overrightarrow{D_a} - \overrightarrow{D_b}\|$. It is to be noted that the coordinates of the reference station antenna are not needed in order to compute the distance between the on-board antennas.

The accuracy statistics for all scenarios for each day are summarized in table 8.1, which includes the daily RMS errors from the true antenna distance, for each RTK and PPP configuration. These results will be discussed in next section.

8.7 Discussion and conclusions

In this study, an accuracy assessment has been performed between RTK and PPP, both with float and fixed ambiguities (PPP-AR), using the distance of two moving antennas as reference. As expected, the results indicate that the best performance is obtained by short-baseline RTK, and that the RTK performance degrades with the distance to the base station. In average,

the long-baseline RTK solution is 4.5 times worse than the short-baseline RTK solution. The medium-baseline RTK solution is only 15% worse than the short baseline solution.

In terms of float PPP performance, a significant improvements comes from multi-constellation PPP solutions. The solution including all GNSS systems is in average 40% better than the GPS-only solution. The contribution of Galileo and BeiDou is relatively small due to the few satellites available at the moment. Ambiguity resolution in PPP brings an average improvement of 10% with respect to the float solutions, even when UHDs are derived from a single station. An interesting outcome is that, contrary to RTK, PPP-AR results are very similar regardless of which station is used to generate the UHDs, either Oslo or Onsala, despite the relatively large distance between them.

In terms of PPP versus RTK performance, RTK performance is still better in short and medium-baseline scenarios, but PPP accuracy is better than RTK in the long-baseline scenario, specially when multi-constellation PPP is used.

Regarding the difference between the static and dynamic scenarios, it is relevant to observe that the results obtained in the dynamic scenario are generally more accurate than in the static one. In the static case, the vessel is moored in harbor and GNSS tracking is slightly suboptimal, due to the increased multipath and partial sky obstruction, due to presence of nearby buildings. In the dynamic scenario, while the vessel navigates in Oslo fjord, tracking conditions are better, due to open sky visibility.

As mentioned earlier, ambiguity-fixed PPP delivers the best point positioning accuracy, but cannot replace short and medium-baseline RTK accuracy yet. The most likely reason is that RTK is able to remove residual errors (such as atmospheric and ephemeris errors) to a very large extent, but these are still present in PPP solutions, despite the availability of precise orbits and clocks. However, the development of new systems, such as Galileo and BeiDou, and the modeling improvements for these satellites will likely allow an increase in PPP accuracy and bring it even closer to RTK.

PPP-AR relies heavily on satellite availability and visibility for fixing single-difference ambiguities. Therefore it can be also expected that the performance of PPP-AR with Galileo and BeiDou will also improve when there will be more satellites available from these constellations, in the same way as for GPS today.

9 Conclusions

The work presented in this thesis has been focused on the usage of multi-frequency multi-constellation Precise Point Positioning for geodetic applications. The research was motivated by the on-going innovations in GNSS, due to new systems, satellites and signals being made available by the service providers.

In particular, the usage of the new GPS frequency L5 revealed that the time-dependent interfrequency biases need to be handled appropriately, in order to fully benefit from the new signals. The current L1/L2-based clock products are insufficient to adequately accommodate L5 observations in point positioning. In this research, a new set of L1/L5-based clocks has been generated to apply to L5 observations.

In the context of multi-constellation PPP, orbit and clock products for Galileo and BeiDou needed to be generated before point positioning could be achieved. The generation of these products is somehow limited by the amount of tracking data available, as not all geodetic receivers are tracking all the new signals and frequencies yet. Additionally, intersystem biases need to be taken into account in the orbit and clock estimation process. Contrary to Glonass, a single intersystem bias per receiver is enough to account for system-time differences and internal receiver delays. The results indicate a strong receiver-type dependency for these intersystem biases.

The orbit determination results indicate that the orbit accuracy for Galileo and BeiDou is lower compared to more mature systems like GPS and Glonass. This suggests that further research is needed in order to improve the orbit model for the new constellations. In particular, models for solar radiation pressure and attitude (specially during eclipses) need to be developed and further improved in order to increase orbit accuracy. Precise antenna phase center offsets and variations need to be estimated or calibrated, both for satellite and receiver antennas, to fully benefit from the precision of the phase measurements. Finally, ambiguity-resolution in network solutions is a promising way to increase orbit accuracy.

Additionally, for the case of BeiDou, it is the first time that dual-frequency GEO satellites could be used in precise point positioning. However, the orbit determination for these satellites is specially challenging, due to lack of varying geometry from the reference station network. The orbit accuracy for this satellites is significantly worse than for IGSO and MEO satellites. In precise point positioning, stochastic models for GEO satellites need to be tuned in order to account for this suboptimal orbit accuracy.

The contribution of Galileo and BeiDou to PPP is significant in terms of availability, specially in difficult tracking conditions. The additional number of satellites can be of special benefit in

scenarios with partial-sky obstruction, scintillation or interference. Additionally, multi-GNSS positioning is likely to be less sensitive to single-GNSS failure, thanks to the large number of satellites available. Under ideal satellite visibility, the accuracy results improve slightly with the addition of Galileo and BeiDou, but the contribution is still reduced due to the modeling limitations mentioned above.

BeiDou system is particularly interesting for PPP, as the current constellation configuration allows to obtain continuous positioning in the Asia-Pacific area using BeiDou-standalone. The performance of BeiDou PPP has been demonstrated, both in real-time and post-processing, in this research.

In previous studies, ambiguity resolution for GPS had been used to increased positional accuracy. During this research, the method has been extended to be able to estimate Uncalibrated Hardware Delays for the new systems Galileo and BeiDou, enabling ambiguity resolution in multi-GNSS PPP.

All the above concepts have been demonstrated in a field experiment, in which a vessel was equipped with two multi-constellation receivers and two antennas. The results indicate that the best absolute positioning accuracy was obtained when combining all GNSS systems and fixing carrier phase ambiguities. However, the accuracy is still less than medium RTK positioning (with 20 kilometer baseline). It is expected that the availability of more GNSS satellites and the orbit and position models will allow to bring PPP positioning accuracy closer to RTK.

In summary, this thesis has presented the initial results in Precise Point Positioning combining several global navigation systems. The further deployment of Galileo and BeiDou, and the constant improvements in network tracking and modeling efforts, will allow a better understanding of the new systems, allowing higher accuracy in PPP in particular, and in satellite geodesy in general.

10 Additional publications during the PhD program

Non peer-review papers

1. Melgard T, **Tegedor J**, de Jong K, Lapucha D, Lachapelle, G. "Interchangeable Integration of GPS and Galileo by Using a Common System Clock in PPP". Conference paper at ION GNSS 2013, Nashville (USA) 16-20 September 2013.

2. de Jong K, **Tegedor J**, Goode M, Guo, Liu X, Wang . "Precise Point Positioning with BeiDou and Galileo - initial results". Conference paper at IMCA Annual Seminar 2013, 6-7 November 2013.

3. Vigen E, Melgard T, Ørpen O, Strandli R, Lapucha D, **Tegedor J**. "Real-time PPP with Galileo". Conference paper at European Navigation Conference, Vienna (Austria), 23-25 April 2013.

Oral presentations

1. **Tegedor J**. "Estimation of Uncalibrated Phase Delays for single-difference ambiguity resolution". GNSS Bias Workshop, Zurich (Switzerland), 18-19 January 2012.

2. **Tegedor J**. "New prospects for precise navigation: towards multi-frequency multi-GNSS PPP". Geodesidagene, Stavanger (Norway), 6-7 November 2012.

3. **Tegedor J**, Melgard T, Øvstedal O, Vigen E. "Multi-constellation Precise Point Positioning including GPS, GLONASS, Galileo and BeiDou". PPP workshop: reaching new Potential. Ottawa (Canada), 12-14 June 2013.

4. **Tegedor J**, de Jong K, Liu X, Vigen E, Øvstedal O. "Real-time Precise Point Positioning using BeiDou". IAG Scientific Assembly, Potsdam (Germany), 2-6 September 2013.

5. Liu X, **Tegedor J**, de Jong K. "Towards Real-Time PPP and PPP-RTK by adding BeiDou and Galileo". China Satellite Navigation Conference (CSNC), Nanjing (China), 21-23 May 2014.

6. **Tegedor J**, "Improving kinematic accuracy by means of multi-constellation PPP-RTK", Geodesidagene, Stavanger (Norway), 12-13 December 2014.

Posters

1. **Tegedor J**, Melgard T, Vigen E, Øvstedal O. "Precise Point Positioning for characterization of L5 biases using MGEX data". IGS workshop, Olsztyn (Poland), 23-27 November 2012.

Bibliography

[Altamimi et al., 2011] Altamimi, Z., Collilieux, X., and Métivier, L. (2011). ITRF2008: an improved solution of the international terrestrial reference frame. *Journal of Geodesy*, 85(8):457–473, doi:10.1007/s00190-011-0444-4.

[Bakker et al., 2012] Bakker, P. F., Tiberius, C. C. J. M., Marel, H., and Bree, R. J. P. (2012). Short and zero baseline analysis of GPS L1 C/A, L5Q, GIOVE E1B, and E5aQ signals. *GPS Solutions*, 16(1):53–64, doi:10.1007/s10291-011-0202-3.

[Bar-Sever et al., 1998] Bar-Sever, Y. E., Kroger, P. M., and Borjesson, J. a. (1998). Estimating horizontal gradients of tropospheric path delay with a single GPS receiver. *Journal of Geophysical Research*, 103(B3):5019–5035, doi:10.1029/97JB03534.

[Beutler et al., 2005] Beutler, G., Hugentobler, U., Ploner, M., Meindl, M., Schildknecht, T., and Urschl, C. (2005). Determining the orbits of EGNOS satellites based on optical or microwave observations. *Advances in Space Research*, 36(3):392–401, doi:10.1016/j.asr.2004.11.015.

[Bisnath and Gao, 2009] Bisnath, S. and Gao, Y. (2009). Current state of precise point positioning and future prospects and limitations. *Observing our Changing Earth. International Association of Geodesy Symposia 133*, pages 615–623.

[Boehm, 2004] Boehm, J. (2004). Vienna mapping functions in VLBI analyses. *Geophysical Research Letters*, 31(1):L01603, doi:10.1029/2003GL018984.

[Boehm et al., 2007] Boehm, J., Heinkelmann, R., and Schuh, H. (2007). Short Note: A global model of pressure and temperature for geodetic applications. *Journal of Geodesy*, 81(10):679–683, doi:10.1007/s00190-007-0135-3.

[Boehm et al., 2006] Boehm, J., Niell, A., Tregoning, P., and Schuh, H. (2006). Global Mapping Function (GMF): A new empirical mapping function based on numerical weather model data. *Geophysical Research Letters*, 33(7):L07304, doi:10.1029/2005GL025546.

[Bree and Tiberius, 2011] Bree, R. J. P. and Tiberius, C. C. J. M. (2011). Real-time single-frequency precise point positioning: accuracy assessment. *GPS Solutions*, 16(2):259–266, doi:10.1007/s10291-011-0228-6.

[Bruyninx, 2006] Bruyninx, C. (2006). Comparing GPS only with GPS+GLONASS positioning in a regional permanent GNSS network. *GPS Solutions*, 11(2):97–106, doi:10.1007/s10291-006-0041-9.

[Caissy et al., 2012] Caissy, M., Agrotis, L., Weber, G., Hernandez-Pajares, M., and Hugentobler, U. (2012). The International GNSS Real-time Service. *GPS World*, June 2012.

[Chen and Gao, 2005] Chen, K. and Gao, Y. (2005). Real-time precise point positioning using single frequency data. In *Proceedings of the 18th International Technical Meeting of the Satelite Division of the Institute of Navigation (ION GNSS 2005)*, pages 1514–1523.

[Chen et al., 2011] Chen, X., Allison, T., Cao, W., and Ferguson, K. (2011). Trimble RTX, an innovative new approach for network RTK. In *Proceedings of the 24th International Technical Meeting of the Satellite Division of the Institute of Navigation (ION GNSS 2011)*, pages 2214–2219.

[Chuang et al., 2013] Chuang, S., Wenting, Y., Weiwei, S., Yidong, L., and Rui, Z. (2013). GLONASS pseudorange inter-channel biases and their effects on combined GPS/GLONASS precise point positioning. *GPS solutions*, 17:439–451, doi:10.1007/s10291-013-0332-x.

[Cocard et al., 2008] Cocard, M., Bourgon, S., Kamali, O., and Collins, P. (2008). A systematic investigation of optimal carrier-phase combinations for modernized triple-frequency GPS. *Journal of Geodesy*, 82(9):555–564, doi:10.1007/s00190-007-0201-x.

[Collins et al., 2008] Collins, P., Bisnath, S., Lahaye, F., and Héroux, P. (2008). Undifferenced GPS Ambiguity Resolution using the Decoupled Clock Model and Ambiguity Datum Fixing. In *Proceedings of the 21st International Technical Meeting of the Satellite Division of The Institute of Navigation (ION GNSS 2008)*, pages 1315–1322.

[CSNO, 2012] CSNO (2012). BeiDou Navigation Satellite System. Signal In Space Interface Control Document. Open Service Signal B1I. BDS-SIS-ICD-1.0. China Satellite Navigation Office.

[Defraigne et al., 2008] Defraigne, P., Guyennon, N., and Bruyninx, C. (2008). GPS Time and Frequency Transfer: PPP and Phase-Only Analysis. *International Journal of Navigation and Observation*, (Article ID 175468, 7 pages, 2008), doi:10.1155/2008/175468.

[Diessongo et al., 2012] Diessongo, H., Bock, H., Schuler, T., Junker, S., and Kiroe, A. (2012). Exploiting the Galileo E5 Wideband Signal. *Inside GNSS*, 2012(September/October):64–73.

[Dow et al., 2009] Dow, J., Neilan, R., and Rizos, C. (2009). The International GNSS Service in a changing landscape of global navigation satellite systems. *Journal of Geodesy*, 83(3):191–198.

[Droz and Mosset, 2006] Droz, F. and Mosset, P. (2006). The on-board Galileo clocks: Rubidium standard and Passive Hydrogen Maser-current status and performance. In *Proceedings of the 20th European Frequency and Timing Forum (EFTF)*, pages 420–426.

[Dupuis et al., 2008] Dupuis, R., Lynch, T., and Vaccaro, J. (2008). Rubidium frequency standard for the GPS IIF program and modifications for the RAFSMOD program. In *Frequency Control Symposium*, pages 655–660. IEEE.

[European Commision, 2010] European Commision (2010). European GNSS (Galileo) Open Service Signal in Space Interface Control Document. OS SIS ICD, Issue 1.1, September 2010.

[Feng, 2003] Feng, Y. (2003). Combined Galileo and GPS: a technical perspective. *Journal of Global Positioning Systems*, 2(1):67–72, doi:10.5081/jgps.2.1.67.

[Gao et al., 2009] Gao, G. X., Chen, A., Lo, S., Lorenzo, D. D., Walter, T., and Enge, P. (2009). Compass-M1 Broadcast Codes in E2. *IEEE Journal of Selected Topics in Signal Processing*, 3(4):599–612.

[Ge et al., 2005] Ge, M., Gendt, G., Dick, G., and Zhang, F. P. (2005). Improving carrier-phase ambiguity resolution in global GPS network solutions. *Journal of Geodesy*, 79(1-3):103–110.

[Ge et al., 2007] Ge, M., Gendt, G., Rothacher, M., Shi, C., and Liu, J. (2007). Resolution of GPS carrier-phase ambiguities in Precise Point Positioning (PPP) with daily observations. *Journal of Geodesy*, 82(7):389–399.

[Geng, 2010] Geng, J. (2010). *Rapid Integer Ambiguity Resolution in GPS Precise Point Positioning*. PhD thesis, University of Notthingham.

[Geng et al., 2010] Geng, J., Teferle, F., Meng, X., and Dodson, A. (2010). Kinematic precise point positioning at remote marine platforms. *GPS Solutions*, 14(4):343–350, doi:10.1007/s10291-009-0157-9.

[Geng et al., 2011] Geng, J., Teferle, F., Meng, X., and Dodson, A. (2011). Towards PPP-RTK: Ambiguity resolution in real-time precise point positioning. *Advances in Space Research*, 47(10):1664–1673, doi:10.1016/j.asr.2010.03.030.

[Geng et al., 2009] Geng, J., Teferle, F. N., Shi, C., Meng, X., Dodson, a. H., and Liu, J. (2009). Ambiguity resolution in precise point positioning with hourly data. *GPS Solutions*, 13(4):263–270, doi:10.1007/s10291-009-0119-2.

[Ghoddousi-Fard et al., 2009] Ghoddousi-Fard, R., Dare, P., and Langley, R. B. (2009). Tropospheric delay gradients from numerical weather prediction models: effects on GPS estimated parameters. *GPS Solutions*, 13(4):281–291, doi:10.1007/s10291-009-0121-8.

[GPS Directorate, 2007] GPS Directorate (2007). Global Positioning System Precise Positioning Service (PPS) Performace Standard. February 2007.

[GPS Directorate, 2008] GPS Directorate (2008). GPS Standard Positioning Service (SPS) Performance Standard. September 2008.

[GPS Directorate, 2011a] GPS Directorate (2011a). Interface Specification GPS-705B. Navstar GPS Space Segment/User Segment L5 interfaces. September 2011.

[GPS Directorate, 2011b] GPS Directorate (2011b). Interface Specification IS-GPS-200. Navstar GPS Space Segment/User Segment Interfaces. September 2011.

[GPS Directorate, 2012] GPS Directorate (2012). Interface Specification IS-GPS-800. Navstar GPS Space Segment/User Segment L1C Interface. September 2012. Technical report.

[Grelier, 2007] Grelier, T. (2007). Initial Observations and analysis of Compass MEO Satellite Signals. *Inside GNSS*, 2007(May/June):39–42.

[Gurtner and Estey, 2009] Gurtner, W. and Estey, L. (2009). Rinex (The Receiver Independent Exchange Format) Version 3.01. Available at ftp://igs.org/pub/data/format/rinex301.pdf.

[Hatch et al., 2006] Hatch, R., Sharpe, T., and Galyean, P. (2006). StarFire : A Global High Accuracy Differential GPS System. In *Proceedings of the 19th International Technical Meeting of the Satellite Division of The Institute of Navigation (ION GNSS 2006)*, pages 2286–2296.

[Hauschild et al., 2011a] Hauschild, A., Montenbruck, O., Sleewaegen, J.-M., Huisman, L., and Teunissen, P. J. G. (2011a). Characterization of Compass M-1 signals. *GPS Solutions*, 16(1):117–126, doi:10.1007/s10291-011-0210-3.

[Hauschild et al., 2011b] Hauschild, A., Steigenberger, P., and Rodriguez-Solano, C. (2011b). Signal, orbit and attitude analysis of Japan's first QZSS satellite Michibiki. *GPS Solutions*, 16(1):127–133, doi:10.1007/s10291-011-0245-5.

[Hauschild et al., 2012] Hauschild, a., Steigenberger, P., and Rodriguez-Solano, C. (2012). QZS-1 Yaw Attitude Estimation Based on Measurements from the CONGO Network. *Navigation*, 59(3):237–248, doi:10.1002/navi.18.

[He et al., 2013a] He, H., Li, J., Yang, Y., Xu, J., Guo, H., and Wang, A. (2013a). Performance assessment of single- and dual-frequency BeiDou/GPS single-epoch kinematic positioning. *GPS Solutions*, 18(3):393–403, doi:10.1007/s10291-013-0339-3.

[He et al., 2013b] He, L., Ge, M., Wang, J., Wickert, J., and Schuh, H. (2013b). Experimental study on the precise orbit determination of the BeiDou navigation satellite system. *Sensors*, 13(3):2911–28, doi:10.3390/s130302911.

[Hernandez-Pajares et al., 2007] Hernandez-Pajares, M., Juan, J. M., Sanz, J., and Oru, R. (2007). Second-order ionospheric term in GPS : Implementation and impact on geodetic estimates. *Journal of Geophysical Research*, 112(B08417):1–16, doi:10.1029/2006JB004707.

[Hernández-Pajares et al., 2009] Hernández-Pajares, M., Juan, J. M., Sanz, J., Orus, R., Garcia-Rigo, a., Feltens, J., Komjathy, a., Schaer, S. C., and Krankowski, a. (2009). The IGS VTEC maps: a reliable source of ionospheric information since 1998. *Journal of Geodesy*, 83(3-4):263–275, doi:10.1007/s00190-008-0266-1.

[Herring, 1999] Herring, T. (1999). Geodetic applications of GPS. *Proceedings of the IEEE*, 87(1):92–110, doi:10.1109/5.736344.

[Hesselbarth, 2011] Hesselbarth, A. (2011). *Statische und kinematische GNSS-Auswertung mittels Precise Point Positioning (PPP)*. PhD thesis, Technischen Universitat Dresden.

[Hesselbarth and Wanninger, 2012] Hesselbarth, A. and Wanninger, L. (2012). SBAS orbit and satellite clock corrections for precise point positioning. *GPS Solutions*, 17(4):465–473, doi:10.1007/s10291-012-0292-6.

[Hu et al., 2009] Hu, G., Khoo, V., Goh, P., and Law, C. (2009). Internet-based GPS VRS RTK positioning with a multiple reference station network. *Journal of Global Positioning Systems*, 1(2):113–120.

[IGS and RTCM-SC104, 2013] IGS and RTCM-SC104 (2013). Rinex (The Receiver Independent Exchange Format) Version 3.02. Available at ftp://igs.org/pub/data/format/rinex302.pdf.

[Inaba et al., 2009] Inaba, N., Matsumoto, A., Hase, H., Kogure, S., Sawabe, M., and Terada, K. (2009). Design concept of Quasi Zenith Satellite System. *Acta Astronautica*, 65(7-8):1068–1075, doi:10.1016/j.actaastro.2009.03.068.

[Ishijima et al., 2009] Ishijima, Y., Inaba, N., Matsumoto, A., and Terada, K. (2009). Design and development of the first Quasi-Zenith Satellite attitude and orbit control system. *2009 IEEE Aerospace conference*, pages 1–8, doi:10.1109/AERO.2009.4839537.

[ISRO, 2014] ISRO (2014). Indian Space Reseach Organization. Indian Regional Navigation Satellite Sytem. Signal in Space ICD for Standard Positioning Service. Version 1.0, June 2014.

[Jan, 2010] Jan, S.-S. (2010). Vertical guidance performance analysis of the L1-L5 dual-frequency GPS/WAAS user avionics sensor. *Sensors*, 10(4):2609–25, doi:10.3390/s100402609.

[JAXA, 2013] JAXA (2013). Interface Specification for QZSS (IS-QZSS) V1.5. Japan Aerospace Exploration Agency.

[Juan et al., 2012] Juan, J. M., Sanz, J., Orús, R., Ochieng, W., Feng, S., Jofre, M., Coutinho, P., Samson, J., and Tossaint, M. (2012). Enhanced Precise Point Positioning for GNSS users. *IEEE Transactions on Geoscience and Remote Sensing*, 50(10):4213 – 4222, doi:10.1109/TGRS.2012.2189888.

[Kanzaki et al., 2011] Kanzaki, M., Matsushita, Y., and Kakimoto, H. (2011). GNSS Positioning of Ocean Buoys in Japan for Disaster Prevention. In *Proceedings of the 24th tInternational Technical Meeting of the Satellite Division of the Institute of Navigation (ION GNSS 2011)*, pages 717–723.

[Kjørsvik et al., 2006] Kjørsvik, N., Gjevestad, J., and Øvstedal, O. (2006). Handling of the tropospheric delay in kinematic precise point positioning. In *Proceedings of the 19th International Technical Meeting of the Satelite Division of the Institute of Navigation (ION GNSS 2006)*, pages 2279–2285.

[Kouba, 2008] Kouba, J. (2008). A simplified yaw-attitude model for eclipsing GPS satellites. *GPS Solutions*, 13(1):1–12, doi:10.1007/s10291-008-0092-1.

[Kouba, 2009] Kouba, J. (2009). A guide to using International GNSS Service (IGS) products. Available at http://igscb.jpl.nasa. gov/components/usage.html.

[Kouba and Héroux, 2001] Kouba, J. and Héroux, P. (2001). GPS Precise Point Positioning using IGS orbit products. *GPS solutions*, 5(2):12–28.

[Kursinski and Hajj, 1997] Kursinski, E. and Hajj, G. (1997). Observing Earth's atmosphere with radio occultation measurements using the Global Positioning System. *Journal of Geophysical Research*, 102(97):429–465.

[Larson et al., 2008] Larson, K. M., Small, E. E., Gutmann, E. D., Bilich, A. L., Braun, J. J., and Zavorotny, V. U. (2008). Use of GPS receivers as a soil moisture network for water cycle studies. *Geophysical Research Letters*, 35(L24405), doi:10.1029/2008GL036013.

[Laurichesse et al., 2009] Laurichesse, D., Mercier, F., Berthias, J., and Broca, P. (2009). Integer ambiguity resolution on undifferenced GPS phase measurements and its application to PPP and satellite precise orbit determination. *Navigation*, 56(2):135–149.

[Le and Tiberius, 2006] Le, A. Q. and Tiberius, C. (2006). Single-frequency precise point positioning with optimal filtering. *GPS Solutions*, 11(1):61–69, doi:10.1007/s10291-006-0033-9.

[Leandro et al., 2011] Leandro, R., Landau, H., and Nitschke, M. (2011). RTX Positioning: The Next Generation of cm-accurate Real-Time GNSS Positioning. In *Proceedings of the 24th International Technical Meeting of The Satellite Division of the Institute of Navigation (ION GNSS 2011)*, pages 1460 – 1475.

[Leandro et al., 2007a] Leandro, R., Santos, M., and Langley, R. (2007a). PPP-based ionospheric activity monitoring. In *Proceedings of the 20th International Technical Meeting of the Satellite Division of The Institute of Navigation (ION GNSS 2007)*, pages 2849–2853.

[Leandro et al., 2010] Leandro, R., Santos, M., and Langley, R. (2010). Analyzing GNSS data in precise point positioning software. *GPS Solutions*, 15(1):1–13, doi:10.1007/s10291-010-0173-9.

[Leandro et al., 2008] Leandro, R., Thirumurthi, T., Sukeova, L., Langley, R., and Santos, M. (2008). Analysis of GPS L2C Signal Quality and its Impact on PPP Performance. In *Proceedings of the 21st International Technical Meeting of The Institute of Navigation (ION GNSS 2008)*, pages 1020–1031.

[Leandro et al., 2007b] Leandro, R. F., Langley, R. B., and Santos, M. C. (2007b). Estimation of P2-C2 Biases by Means of Precise Point Positioning. *Proceedings of the 63rd Annual Meeting of the Institute of Navigation*, pages 225–231.

[Lewandowski, 2008] Lewandowski, A. (2008). Performance evaluation of satellite-based search and rescue services: Galileo vs. Cospas-Sarsat. In *Proceedings of the 68th IEEE Vehicular Technology Conference, Calgary, September 2008.*

[Li and Zhang, 2013] Li, P. and Zhang, X. (2013). Integrating GPS and GLONASS to accelerate convergence and initialization times of precise point positioning. *GPS Solutions*, 18(3):461–471, doi:10.1007/s10291-013-0345-5.

[Li et al., 2013] Li, X., Ge, M., Zhang, H., and Wickert, J. (2013). A method for improving uncalibrated phase delay estimation and ambiguity-fixing in real-time precise point positioning. *Journal of Geodesy*, 87(5):405–416, doi:10.1007/s00190-013-0611-x.

[Lou et al., 2014] Lou, Y., Liu, Y., Shi, C., Yao, X., and Zheng, F. (2014). Precise orbit determination of BeiDou constellation based on BETS and MGEX network. *Scientific reports*, 4(4692):1–10, doi:10.1038/srep04692.

[Melbourne, 1985] Melbourne, W. (1985). The case for ranging in GPS-based geodetic systems. In *Proceedings of the 1st International Symposium on Precise Positioning with GPS, Rockville, Maryland*.

[Melgard et al., 2013] Melgard, T., Tegedor, J., de Jong, K., Lapucha, D., and Lachapelle, G. (2013). Interchangeable Integration of GPS and Galileo by Using a Common System Clock in PPP. In *Proceedings of the 26th International Technical Meeting of the Satellite Division of the Institute of Navigation (ION GNSS 2013)*, pages 1198–1206.

[Melgard et al., 2009] Melgard, T., Vigen, E., de Jong, K., and Oerpen, O. (2009). G2 - The First Real-Time GPS and GLONASS Precise Orbit and Clock Service. In *Proceedings of the 22nd International Technical Meeting of the Satellite Division of the Institute of Navigation (ION GNSS 2009)*, pages 1885–1891.

[Melgard et al., 2010] Melgard, T., Vigen, E., and Ø rpen, O. (2010). Pulling in All Signals PPP with GPS and GLONASS : The New G2. *GPS World*, 2012(March).

[Mervart et al., 2008] Mervart, L., Zdenek Lukes, Christian Rocken, and Tetsuya Iwabuchi (2008). Precise Point Positioning With Ambiguity fixing in Real-Time. In *Proceedings of the ION GNSS 2008, Savannah, Georgia*, Savannah, Georgia.

[Montenbruck et al., 2005] Montenbruck, O., Gill, E., and Kroes, R. (2005). Rapid orbit determination of LEO satellites using IGS clock and ephemeris products. *GPS Solutions*, 9(3):226–235, doi:10.1007/s10291-005-0131-0.

[Montenbruck et al., 2010] Montenbruck, O., Hauschild, A., and Hessels, U. (2010). Characterization of GPS/GIOVE sensor stations in the CONGO network. *GPS Solutions*, 15(3):193–205, doi:10.1007/s10291-010-0182-8.

[Montenbruck et al., 2012] Montenbruck, O., Hauschild, A., Steigenberger, P., Hugentobler, U., Teunissen, P., and Nakamura, S. (2012). Initial assessment of the COMPASS/BeiDou-2 regional navigation satellite system. *GPS Solutions*, 17(2):211–222, doi:10.1007/s10291-012-0272-x.

[Montenbruck et al., 2011] Montenbruck, O., Hugentobler, U., Dach, R., Steigenberger, P., and Hauschild, A. (2011). Apparent clock variations of the Block IIF-1 (SVN62) GPS satellite. *GPS Solutions*, 16(3):303–313, doi:10.1007/s10291-011-0232-x.

[Montenbruck et al., 2014] Montenbruck, O., Steigenberger, P., Khachikyan, R., G, W., Langley, R., Mervart, L., and Hugentobler, U. (2014). IGS-MGEX: Preparing the ground for multi-GNSS science. *Inside GNSS*, 2014(January/February):42–49.

[Nadarajah et al., 2014] Nadarajah, N., Teunissen, P. J. G., Sleewaegen, J.-M., and Montenbruck, O. (2014). The mixed-receiver BeiDou inter-satellite-type bias and its impact on RTK positioning. *GPS Solutions*, 2014, doi:10.1007/s10291-014-0392-6.

[Niell, 1996] Niell, A. E. (1996). Global mapping functions for the atmosphere delay at radio wavelengths. *Journal of Geophysical Research*, 101(B2):3227, doi:10.1029/95JB03048.

[Øvstedal, 2002] Øvstedal, O. (2002). Absolute positioning with single-frequency GPS receivers. *GPS Solutions*, 5(4):33–44.

[Odijk, 2003] Odijk, D. (2003). Ionosphere-Free Phase Combinations for Modernized GPS. *Journal of Surveying Engineering*, 129(4):165–173.

[Oliveira and Tiberius, 2008] Oliveira, J. and Tiberius, I. (2008). EGNOS performance for landing. *European Journal of Navigation*, 6(2):2–7.

[Remondi, 1985] Remondi, B. (1985). Global Positioning System carrier phase: description and use. *Bulletin géodésique*, 59:361–377.

[Reussner and Wanninger, 2011] Reussner, N. and Wanninger, L. (2011). GLONASS Interfrequency Biases and Their Effects on RTK and PPP Carrier-phase Ambiguity Resolution. In *Proceedings of the 24th International Technical Meeting of The Satellite Division of the Institute of Navigation (ION GNSS 2011)*, pages 712–716.

[Rizos et al., 2012] Rizos, C., Janssen, V., Roberts, C., and Grinter, T. (2012). Precise Point Positioning : Is the Era of Differential GNSS Positioning Drawing to an End ? In *FIG Working Week 2012*, pages 1–17.

[Rizos et al., 2013] Rizos, C., Montenbruck, O., Weber, R., Weber, G., Neilan, R., and Hugentobler, U. (2013). The IGS MGEX Experiment as a Milestone for a Comprehensive Multi-GNSS Servicele. In *Proceedings of the ION 2013 Pacific PNT Meeting, Honolulu, Hawaii*, pages 289–295.

[Rocken et al., 2011] Rocken, C., Mervart, L., Johnson, J., Lukes, Z., Springer, T., and Iwabuchi, T. (2011). A New Real-Time Global GPS and GLONASS Precise Positioning Correction Service : Apex. In *Proceedings of the 24th International Technical Meeting of The Satellite Division of the Institute of Navigation (ION GNSS 2011)*, pages 1825–1838.

[Russian Institute of Space Device Engineering, 2008] Russian Institute of Space Device Engineering (2008). Glonass Interface Control Document v5.1.

[Saastamoinen, 1972] Saastamoinen, J. (1972). Atmospheric correction for the troposphere and stratosphere in radio ranging satellites. *Geophysical Monograph Series*, 15:247–251, doi:10.1029/GM015p0247.

[Sakai et al., 2009] Sakai, T., Fukushima, S., and Ito, K. (2009). Development of QZSS L1-SAIF augmentation signal. *ICCAS-SICE, 2009*, pages 4462–4467.

[Schmid et al., 2005] Schmid, R., Rothacher, M., Thaller, D., and Steigenberger, P. (2005). Absolute phase center corrections of satellite and receiver antennas. *GPS solutions*, 9(4):283–293, doi:10.1007/s10291-005-0134-x.

[Schmid et al., 2007] Schmid, R., Steigenberger, P., Gendt, G., Ge, M., and Rothacher, M. (2007). Generation of a consistent absolute phase-center correction model for GPS receiver and satellite antennas. *Journal of Geodesy*, 81(12):781–798, doi:10.1007/s00190-007-0148-y.

[Schönemann et al., 2011] Schönemann, E., Becker, M., and Springer, T. (2011). A new Approach for GNSS Analysis in a Multi-GNSS and Multi-Signal Environment. *Journal of Geodetic Science*, 1(3):204–214.

[Shi et al., 2012] Shi, C., Zhao, Q., Hu, Z., and Liu, J. (2012). Precise relative positioning using real tracking data from COMPASS GEO and IGSO satellites. *GPS Solutions*, 17(1):103–119, doi:10.1007/s10291-012-0264-x.

[Shi and Gao, 2013] Shi, J. and Gao, Y. (2013). A comparison of three PPP integer ambiguity resolution methods. *GPS Solutions*, 2013, doi:10.1007/s10291-013-0348-2.

[Springer and Dilssner, 2009] Springer, T. and Dilssner, F. (2009). SVN49 and other GPS anomalies. *Inside GNSS*, 2009(July-August):32–36.

[Springer and Dow, 2009] Springer, T. and Dow, J. (2009). NAPEOS Mathematical Models and Algorithms 1.0. *European Space Agency, DOPS-SYS-TN-0100-OPS-GN*.

[Steigenberger et al., 2013] Steigenberger, P., Hugentobler, U., Hauschild, A., and Montenbruck, O. (2013). Orbit and clock analysis of Compass GEO and IGSO satellites. *Journal of Geodesy*, 87(6):515–525, doi:10.1007/s00190-013-0625-4.

[Tegedor et al., 2014] Tegedor, J., Ø vstedal, O., and Vigen, E. (2014). Precise orbit determination and point positioning using GPS, Glonass, Galileo and BeiDou. *Journal of Geodetic Science*, 4(1):65–73, doi:10.2478/jogs-2014-0008.

[Teke et al., 2011] Teke, K., Böhm, J., Nilsson, T., Schuh, H., Steigenberger, P., Dach, R., Heinkelmann, R., Willis, P., Haas, R., García-Espada, S., Hobiger, T., Ichikawa, R., and Shimizu, S. (2011). Multi-technique comparison of troposphere zenith delays and gradients during CONT08. *Journal of Geodesy*, 85(7):395–413, doi:10.1007/s00190-010-0434-y.

[Teunissen and Kleusberg, 1996] Teunissen, P. and Kleusberg, A. (1996). *GPS for Geodesy*. Springer-Verlag.

[Teunissen et al., 2013] Teunissen, P. J. G., Odolinski, R., and Odijk, D. (2013). Instantaneous BeiDou+GPS RTK positioning with high cut-off elevation angles. *Journal of Geodesy*, 88(4):335–350, doi:10.1007/s00190-013-0686-4.

[Thoelert et al., 2013] Thoelert, S., Montenbruck, O., and Meurer, M. (2013). IRNSS-1A: signal and clock characterization of the Indian regional navigation system. *GPS Solutions*, 18(1):147–152, doi:10.1007/s10291-013-0351-7.

[Urlichich et al., 2011] Urlichich, Y., Subbotin, V., Stupak, G., Dvorkin., V., Povalyaev., A., Karutin, S., and Bakitko, R. (2011). GLONASS Modernization. *GPS World*, 2011(November/December).

[Vollath et al., 2002] Vollath, U., Landau, H., and Chen, X. (2002). Network RTK versus single base RTK: understanding the error characteristics. In *Proceedings of the 15th International Technical Meeting of the Satellite Division of The Institute of Navigation (ION GPS 2002)*, pages 2774–2781.

[Wanninger, 2012] Wanninger, L. (2012). Carrier-phase inter-frequency biases of GLONASS receivers. *Journal of Geodesy*, 86(2):139–148.

[Warren and Raquet, 2003] Warren, D. L. M. and Raquet, J. F. (2003). Broadcast vs. precise GPS ephemerides: a historical perspective. *GPS Solutions*, 7(3):151–156, doi:10.1007/s10291-003-0065-3.

[Weber and Springer, 2001] Weber, R. and Springer, T. a. (2001). The international GLONASS experiment: products, progress and prospects. *Journal of Geodesy*, 75(11):559–568, doi:10.1007/s001900100199.

[Wert et al., 2004] Wert, T., Establishment, C., and Defence, N. (2004). Tidal Height Retrieval Using Globally Corrected GPS in the Amundsen Gulf Region of the Canadian Arctic. In *Proceedings of the 17th International Technical Meeting of the Satellite Division of The Institute of Navigation (ION GNSS 2004)*, pages 1246–1255.

[Wilde et al., 2007] Wilde, W. D. E., Boon, F., Sleewaegen, J.-M., and Wilms, F. (2007). More Compass Points tracking China's MEO satellite. *Inside GNSS*, 2007(July/August):44–48.

[Willems and Sleewaegen, 2011] Willems, T. and Sleewaegen, J.-M. (2011). Septentrio's AsteRx3 Tracks First Glonass CDMA Signal on L3. News release.

[Wu et al., 1993] Wu, J., Wu, S., Hajj, G., Bertiguer, W., and Lichten, S. (1993). Effects of Antenna Orientation on GPS Carrier Phase Measurements. *Manuscripta Geodaetica*, 18:91–98.

[Wübbena, 1985] Wübbena, G. (1985). Software developments for geodetic positioning with GPS using TI 4100 code and carrier measurements. In *Proceedings of First International Symposium on Precise Position with GPS, Rockville, Maryland*, pages 403–412.

[Yao et al., 2013] Yao, Y., Zhang, R., Song, W., Shi, C., and Lou, Y. (2013). An improved approach to model regional ionosphere and accelerate convergence for precise point positioning. *Advances in Space Research*, 52(8):1406–1415, doi:10.1016/j.asr.2013.07.020.

[Zhang et al., 2011] Zhang, B., Teunissen, P. J., and Odijk, D. (2011). A Novel Un-differenced PPP-RTK Concept. *Navigation*, 64(S1):S180–S191, doi:10.1017/S0373463311000361.

[Zhang et al., 2013] Zhang, H., Gao, Z., Ge, M., Niu, X., Huang, L., Tu, R., and Li, X. (2013). On the convergence of ionospheric constrained precise point positioning (IC-PPP) based on undifferential uncombined raw GNSS observations. *Sensors*, 13(11):15708–25, doi:10.3390/s131115708.

[Zumberge et al., 1997] Zumberge, J. F., Heflin, M. B., Jefferson, D. C., and Watkins, M. M. (1997). Precise point positioning for the efficient and robust analysis of GPS data from large networks. *Journal of Geophysical Research*, 102(1):5005–5017.

List of Figures

Chapter 6

Chapter 7

List of Tables

Chapter 7

Acronyms

AltBOC	Alternate Binary Offset Carrier
ARNS	Aeronautical Radionavigation Service
CDDIS	Crustal Dynamics Data Information System
CDMA	Code Division Multiple Access
DORIS	Doppler Orbitography and Radiopositioning Integrated by Satellite
EGNOS	European Geostationary Navigation Overlay System
EPN	European Permanent Network
FCB	Fractional Cycle Bias
FDMA	Frequency Division Multiple Access
GAGAN	GPS Aided Geo-Augmented Navigation
GEO	Geostationary Orbit
GMF	Global Mapping Function
GNSS	Global Navigation Satellite System
GPS	Global Positioning System
GPT	Global Pressure and Temperature
IGS	International GNSS Service
IGSO	Inclined Geosynchronous Orbit
IOV	In Orbit Validation
IRNSS	Indian Regional Navigation Satellite System
ISRO	Indian Space Research Organisation
ITRF	International Terrestrial Reference Frame
ITRS	International Terrestrial Reference System
JAXA	Japanese Aerospace Exploration Agency
LEO	Low Earth Orbit

LOD	Length of Day
LRA	Laser Retroreflector Array
MEO	Medium Earth Orbit
MGEX	Multi-GNSS EXperiment
MSAS	Multi-functional Satellite Augmentation System
MW	Melbourne-Wübbena
NAVSTAR	Navigation System Using Timing And Ranging
NDGPS	Nationwide Differential GPS
NMF	Niell Mapping Function
OCX	Next Generation Operational Control System
PHM	Passive Hydrogen Maser
PNT	Position, Navigation and Timing
PPP	Precise Point Positioning
QZO	Quasi Zenith Orbits
QZSS	Quasi Zenith Satellite System
RAFS	Rubidium Atomic Frequency Standard
RTK	Real-Time Kinematic
SAR	Search And Rescue
SBAS	Satellite-Based Augmentation Systems
SDCM	System for Differential Corrections and Monitoring
SPS	Standard Positioning Service
TECU	Total Electron Content Unit
TLE	Two Line Element
UHD	Uncalibrated Hardware Delay
UPD	Uncalibrated Phase Delay
VLBI	Very Large Baseline Interferometry
VMF	Vienna Mapping Function
WAAS	Wide Area Augmentation System

Acknowledgements

The research presented in this thesis would not have been possible without a number of people and institutions. First and foremost, I would like to thank my supervisors, Ola Øvstedal and Erik Vigen for their support and guidance during the PhD program, and their help in producing and publishing my first peer-reviewed papers.

I would like to thank the Norwegian Research Council for sponsoring this research, and Fugro Satellite Positioning for the valuable and productive cooperation during these years, and the freedom I have been given to explore new fields in satellite positioning.

A number of individuals have been instrumental during the research, and I would like to thank them in particular. Tor Egil Melgård deserves credit for the lengthy discussions about different aspects of GNSS, and for reviewing the thesis in detail. I want to thank Xianglin Liu for the fruitful cooperation during the research and for sharing with me his wide knowledge on precise positioning. Kees de Jong was always a source of inspiration and I am convinced he would have been happy of seeing the completion of this thesis. I would like to thank the other co-authors of the papers presented in this thesis, Matthew Goode, Niels Treffers and Ole Ørpen for their valuable contributions.

At a more personal level, I would like to give a warm thank to my parents and my sister, for their unconditional support during whole my life and for teaching me the values of perseverance and hard work that have made this research possible.

I will never be grateful enough for my wife Agnieszka, for her constant encouragement, motivation and support all these years. She is an important contributor to this work, and deserves big credit for that. My final thanks go to my children Anna and Wiktor, for the unforgettable moments you give me every day. While doing this research, I have seen you be born, take your first steps and say "papá" for the first time. Every single moment with you has helped me to overcome the difficulties and work harder to complete this thesis. I hope you can once read these words and realize how proud I am of you both.

Javier Tegedor
Oslo, April 2015